Experimental and Numerical Study of Thermal Performance of a Self-Contained Drum Motor Drive System (SCDMDS)

Experimental and Numerical Study of Thermal Performance of a Self-Contained Drum Motor Drive System (SCDMDS)

By Ahmed M. Teamah, M.Sc., B.Sc., Mechanical Engineering

Alexandria University

A Thesis Submitted to the School of Graduate Studies in Partial Fulfillment of the Requirements for the Degree

Doctor of Philosophy

in Mechanical Engineering

McMaster University

Doctor of Philosophy (2023) McMaster University

Mechanical Engineering Hamilton, Ontario

TITLE: Experimental and Numerical Study of Thermal Performance of a Self-Contained Drum Motor Drive System (SCDMDS)

AUTHOR: Ahmed M. Teamah
B.Sc. (Alexandria University)
M.Sc. (Alexandria University)

SUPERVISORS: Dr. Mohamed S. Hamed, Professor, Department of Mechanical Engineering

NUMBER OF PAGES: xxiv, 201

Lay Abstract

This study is focused on investigating heat transfer and fluid flow inside a self-contained drum motor drive system (SCDMDS). The problem of interest involves multiple heat sources enclosed inside a tight space of the rotating drum. There is an electrical motor, gearbox and a multiphase (oil/air) flow inside the rotating drum of the SCDMDS. In this thesis, experimental test rigs were constructed to investigate the effect of a number of operating and geometrical parameters. In addition, numerical analysis of the multiphase oil/air flow was carried out using Ansys - CFX. The KISSsoft and KISSsys software packages were used to determine various types of heat losses within the geartrain. Due to the presence of multiple heat sources inside a confined space, overheating of a number of SCDMDS has been reported. The overheating problem worsened even more when rubber lagging is used to increase traction between the drive drum and the belt. Several correlations have been developed for various heat transfer mechanisms governing the overall thermal performance of the entire SCDMDS. An analytical model (a digital twin) has been developed using Visual Basics and Excel. The digital twin estimates the temperature distribution and the amount of heat generated and dissipated inside the SCDMDS. It has been validated against many case studies provided by the industrial partner. The model identifies the possibility of overheating and provides the user with several potential modifications to resolve it. Hence, the model can be used as a performance and design tool of various models of SCDMDS.

Abstract

The main focus of this work is to investigate thermal performance of self-contained drum motor drive systems (SCDMDS). All components of a SCDMDS are contained inside a rotating drum including the electric motor, gearbox, and an air/oil multiphase flow. A considerable amount of heat is generated within the SCDMDS from various sources, namely, the electric motor losses, the oil viscous dissipation and the gearbox losses. In meantime, a limited amount of heat is dissipated through the surface of the rotating drum and the side flanges. Therefore, a SCDMDS sometimes encounters a serious overheating problem, which often results in electric motor failure.

The different heat generation and dissipation mechanisms as well as the two-phase flow within the SCDMDS have been studied experimentally and numerically under different operating parameters, namely, the oil level (OV), the drum rotational speed (N), the torque (ζ), the number of motor poles (n) and the electric motor dimensions. The effects of rubber lagging material and thickness as well as the use of rubber belts have been investigated as well.

The numerical part of the present study has been carried out using Ansys-CFX and was validated using experimental data. Results showed that the optimum oil level (OV) for the best thermal performance is about 65%. The increase in the rotational speed (N) enhanced the heat transfer within the SCDMDS due to the improved oil splashing.

Viscous dissipation (VD) between the motor stator and the rotating drive drum was found to be almost negligible. However, oil viscous dissipation within the gap between the motor rotor and stator was found to have an important effect on the thermal performance. An analytical model has been developed and implemented using MATLAB to estimate VD within the motor.

The losses from the gearbox were studied experimentally and numerically considering planetary and co-axial gear trains. The numerical work was carried out using the KISSsoft and KISSsys software. Results showed that, the increase in the drum rotational speed (N) or the drum torque (ζ) increased the gearbox losses. In the planetary gearbox, any increase in the OV increases the churning losses, however, the increase in OV increased the losses in the co-axial gearbox up to OV = 31% beyond which the losses remained constant.

After understanding the complex interplay between all the heat generating and dissipating mechanisms within the SCDMDS, a number of possible modifications have been proposed in order to resolve the overheating problem. The effect of cooling the electric motor by using an axial air flow has been investigated. The effect of adding fins along the inner surface of the outer rotating drum has also been studied.

Correlations of the various contributing mechanisms have been developed. Based on a thermal resistance network, a SCDMDS sizing and performance assessment computer software tool in the form of a digital twin (DT) has been developed. A user-friendly interface has been developed using Visual Basics and Excel. The DT estimates temperature distribution and the amount of heat generated and dissipated from each component within the SCDMDS and hence it identifies whether the case is considered safe to operate or overheating is expected. In overheated cases, the DT also suggests several possible modifications the user could consider resolving the overheating problem. The DT has been validated against several experimental case studies and found to be very reasonably accurate.

<u>Dedication</u>

This Thesis is dedicated to the following special people in my life:

To my late mother **Esmat Mohamed**, Mum, I wish you were here to be proud of your son. I miss you each and every day, and you always believed in me. Your endless love, guidance, and the good you instilled in me continue to bless my life. O Allah forgive and have mercy upon her, excuse her and pardon her, make honorable his reception, and grant her paradise, next to your beloved prophet Muhammad (Peace be upon him).

To my father **Mohamed Teamah**, Dad, I owe you my life, I can't imagine my life without you. I will never be able to fulfill your rights upon me. Dad, you have always been there for me in time of need. You gave me the most precious feeling in the world, you MOTIVATED me. You are a great example of hard work, patience, and kindness above all. You are always my inspiration; I wish that I can be a perfect father and a great professor like you.

My sister, **Heba**, you have helped me a lot in my carreer. You always give me guidance to achieve my dreams. My sister, **Asmaa**, I miss your great push towards going to amusement parks like Dream Park. My brother, **Abdelfatah**, I miss your discussions about new technologies regarding smart phones and speed tests.

My world, my wife, **Esraa**, no words can describe what I want to say about you. You are really the best wife in the whole world. The apple of my eye, my son, **Mohamed**, you just came before my Ph.D. defense. I wish I can make you proud of your father in your entire life.

Love You All!!

Acknowledgments

In the name of Allah, the Most Gracious and the Most Merciful, all praise is due to Allah alone for blessing me with patience, knowledge, and strength to complete this work and granting me everything in my life.

I would like to express my gratitude to my supervisor, Dr. Mohamed S. Hamed. No words can describe my gratitude toward Dr. Hamed. His critically organized way of thinking and revision throughout this program was the key to having the work in its present form. Dr. Hamed is a great leader, his suggestions and fruitful discussions were a motivation throughout the course of this work. Thanks a lot Dr. Hamed for your great help and support all the time. I would never have accomplished this without the mentorship of Dr. Hamed.

I am also grateful to my supervisory committee members, Dr. Lightstone and Dr. Cotton, for their suggestions and comments during our annual meetings.

Special thanks to Eng. Hany Gafar, the engineering manager of the industrial partner, for helping me in constructing the experimental test rigs at Vander Graaf.

Thank you to Mechanical Engineering administrators, Nicole, Lily, and Leslie. Whenever I ask for help you instantly do your best to help, you always make it easy for us.

Thank you to my lab friends Mahmoud Amer, Remon, and Nikhil, I had a wonderful time with you that I will never forget.

Special thanks to my dear friend Safy, you always make everything easy for me, you are a very helpful person. Thank you for helping me from the instance I entered Canada.

Special thanks to my dear friend Ahmed Saber, I always loved our online meetings in the Halaqa messenger group. You are a great friend that I am glad to have. Thanks for helping me a lot while moving to my new address.

Special thanks to my dear friend Hassan, I always loved our gatherings. You are a great friend that I am glad to have. Thanks for helping me, especially in my last year.

Thanks to my friends in Canada: Abdelrahman Amr, Hammouda, Waleed, Waraky, Mostafa Mohsen, Mohamed Abdelnabi, Ahmed Ali, Mohamed Ibrahim, Omar Bahaa, and Ahmed Tarek.

Thanks to my lifetime friends; Ahmed Abdelrahman, Abanoub, Essam Nabil, Taha, Abdallah Elabd and Bassem Sobih.

Table of Contents

List of Tables

List of Figures

Notations and Abbreviations

Nomenclature

A	Lateral surface area, πDL, m^2.
b	Face width, m.
Br	Brinkman number, $\mu(\omega^* r_{i,oc})^2 / \lambda\ (T_{ic}-T_{oc})$.
$C_{1,2}$	Factors in calculating gear churning losses.
C_{Sp}	Splash oil factor.
D	Diameter, m.
d_m	Mean bearing diameter, m.
D_h	Hydraulic diameter, m.
e	Annular gap, m.
$f_{0,1}$	Coefficients for bearing losses.
F_{bt}	Tooth normal force, N.
g	Gravitational acceleration, 9.81 m/sec^2.
Gr	Grashof number, $\frac{g\beta(T_{w,oc}-T_{amb})D_{o,oc}{}^3}{\nu^2}$
h	Heat transfer coefficient, W/m^2.°C.

$\bar{h}$ Normalized oil height, defined to be:

Oil vertical height from lowest point of gears [m] / Gear radius [m]

h_{ov} Height of oil inside the gear train from the bottom, m.

h_{tot} Specific total enthalpy, J/kg.

H_V Gear loss factor.

k Thermal conductivity, W/m.°C.

L Drum axial length, m.

N Rotational speed, rpm.

Nu Nusselt number, h D_h/ k.

OPTR Optimized Thermal Rating Results.

OV Oil volume percentage inside the annular area, %.

p_1 Bearing load, N.

p Static pressure, Pa.

P Slot width, m.

P_B Bearing load dependent losses, W.

P_L Load dependent losses, W.

P_M Gear meshing losses, W.

P_N Load independent losses, W.

P_Q Heat dissipation, W.

Pr Prandtl number, ν/α.

Ps Normalized power loss, (Total power losses)/300[W].

P_V Heat generated, W.

P_W Gear churning losses, W.

P_{WB} Bearing load independent losses, W.

q” Amount of heat per unit surface area, W/m^2

Q Amount of heat, W.

R Radius, m.

Rri Inner radius of rotor, m.

Rro Outer radius of rotor, m.

Rsi Inner radius of stator, m.

Rso Outer radius of stator, m.

r* Dimensionless radius, $(r-r_{o,ic})/(r_{i,oc}-r_{o,ic})$.

Re_a	Axial Reynolds number, $V_a D_h/\upsilon$.
Re	Reynolds number at RR=0.21, $\frac{\pi N r_{oc}^{2}}{30\nu}$
Re_{RR}	Reynolds number at any Radius Ratio, $\frac{\omega R_{is,oc}(R_{is,oc}-R_{os,ic})}{\nu}$
Re_o	Outside Reynolds number, $\frac{\omega D_{Lag}^{2}}{2\nu}$
$(Re_r)_{cr}$	Critical Reynolds number.
Re_r	Rotational Reynolds number, $V_t D_h/\ \upsilon$.
RR	Radius ratio, $R_{os,ic}/R_{is,oc}$
SCDMDS	Self-Contained Drum Motor Drive System.
t	Time, Second.
Ta	Taylor number, $\omega^2 Rro(D_h/2)^3/\ \upsilon^2$
T	Temperature, °C.
T*	Dimensionless temperature, $(T-T_{o,ic})/(T_{i,oc}-T_{o,ic})$
T_H	Hydraulic loss torque, N.m.
TC	Taylor-Couette Flow
TCP	Taylor-Couette-Poiseuille Flow

TRUI Thermal Rating based on User-Inputs.

u Fluctuating velocity component in turbulent flow, m/sec.

U Velocity vector, m/sec.

$u_{\theta,r,z}$ Velocity components in circumferential, radial and axial, m/sec.

V_a Mean axial velocity at entrance, m/sec.

V_t Mean tangential velocity, ω*Rro, m/sec.

V_{tl} Pitch line velocity, m/sec.

X Reynolds number ratio, Re_a/Re_r

z Number of teeth.

Z Axial axis, m.

Greek symbols

α Thermal diffusivity, m^2/sec.

β Thermal expansion coefficient, 1/K.

δ Lagging thickness, mm.

ε Surface emissivity.

ζ Torque, N.m.

η	place holder for any parameter.
θ	Angle, °
λ	Turbulence kinetic energy per unit mass, J/kg.
μ	Dynamic viscosity, kg/m.s.
μ_m	Mean coefficient of friction in gear mesh.
ν	Kinematic viscosity, m^2/s.
ρ	Density, kg/m^3
σ	Stefan Boltzmann constant, $5.67*10^{-8}$ W/ ($m^2.K^4$).
τ	Shear stress tensor, N/m^2
ω	Angular speed, rad/sec.
Ψ	Specific turbulence dissipation rate, 1/sec.

Subscript

amb	Ambient
av	Average
as	Annular space
conv	convective

Lag	Lagging
oc	Outer cylinder
is	Inner surface
m	Mean
max	Maximum value
ic	Inner cylinder
os	Outer surface
rotor	Rotor of the electric motor
slot	Rotor slots
Stator	Stator of the electric motor
w	Wall

Chapter 1

Introduction

1.1 Background

Materials handling via conveyor belts are vastly used in many industries. Some industries, like the food and pharmaceutical industries require a clean environment. The conventional open conveyor drive systems have an electric motor, gearbox, chain, and sprockets running in the open air. These conventional conveyors could spread contamination to the surrounding environment from its grease and/or lubricating oil. This contamination problem can be avoided by using Self-Contained Drum Motor Drive Systems (SCDMDS). In the SCDMDS all components are enclosed inside the rotating drum including the lubricating oil. Figure 1.1 shows the components of a typical SCDMDS.

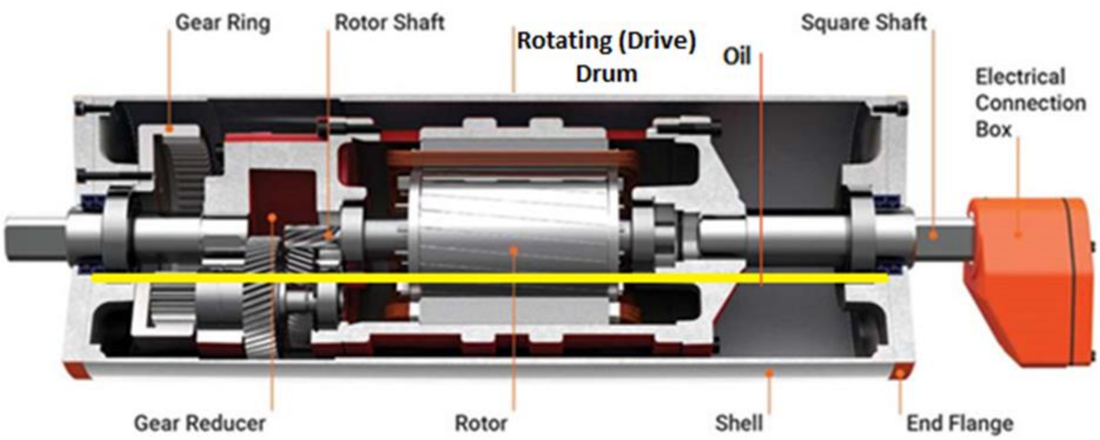

Figure 1.1 Components of a typical SCDMDS [1]

The SCDMDS is susceptible to overheating. The reason behind that comes from the fact that there are multiple heat sources inside the rotating drive drum with a limited heat dissipation area to the ambient. The heat sources present inside the SCDMDS are the motor, the gearbox and oil viscous dissipation. The motor used is an electrical motor which produces heat from the coil resistance and the viscous dissipation of oil trapped between the rotor and the stator.

The gearbox also contributes to the heat generation through two types of thermal losses according to its dependency on the conveyor power (load). Losses are classified as load-dependent and load-independent. The load-dependent losses are the meshing losses (gear contact) and bearings losses, studied by Changenet, et al. [2] and Terauchi, et al. [3]. The load-independent losses are the oil squeezing (pocketing) and the windage (churning) losses,

studied by Concli and Gorla [4] and Liu, et al. [5]. The squeezing losses, as the name implies, arise from lubricant being squeezed between the mating gears or having pockets of oil of volume changing with rotation as in Figure 1.2.

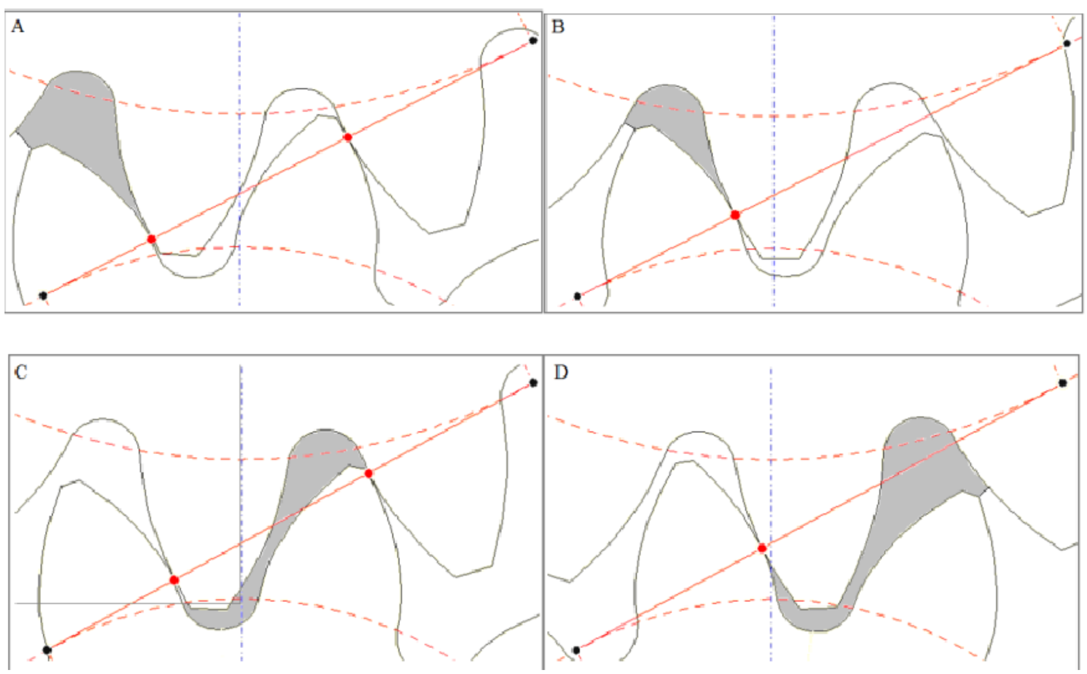

Figure 1.2 Oil squeezing or pocketing phenomena by Concli and Gorla [4]

The multiphase oil/air flow inside the rotating outer drum has also viscous dissipation in the gap between the motor casing and the outer rotating drum. The flow enclosed between two concentric cylinders is called Taylor-Couette (TC) flow. The TC flow has been investigated by many researchers as Andereck, et al. [6], Naseem, et al. [7] and Rüdiger, et al. [8]. Previous researchers found that the increase in the rotational speed enhances the heat transfer inside the gap between the two cylinders. The TC flow published studies were mainly focused on single-phase flows. The TC flow is subjected to instability as discussed by Dong [9] especially when the inner cylinder is rotating at high speeds with Reynolds (Re) number reaching 8000.

On some occasions, the TC flow can be superimposed with axial flow namely Taylor-Couette-Poiseuille (TCP) flow. The axial flow added to the TC flow improves the heat transfer as reported by Seghir-Ouali, et al. [10]. A deep review by Fénot, et al. [11] has been summarized for the effect of different parameters in TC and TCP flows on the heat transfer inside the gap. They discussed the effect of gap thickness, inner and outer cylinder rotational speeds, and axial flow rate on the fluid flow and heat transfer. They showed that decreasing the gap thickness, adding slots on the inner or outer cylinder surface or on both, increasing the rotational speed of the inner or the outer cylinder, and increasing the axial flow rate all resulted in an increase in the rate of heat transfer within the gap.

Some published articles studied the modifications to TC flow by adding ribs to the inner or outer cylinder. Enhancement of up to 140% has been achieved by Jeng, et al. [12] by adding longitudinal ribs over the inner rotating cylinder. Others like Nouri-Borujerdi and Nakhchi [13] implemented inner grooves in the inner surface of the outer fixed cylinder. The groove aspect ratio of 1.5 gave the highest enhancement of 115% compared to the case with no grooves.

The heat is dissipated by convection and radiation from the outer rotating drum and the flanges. The heat dissipation is restricted to the available surface area of the drum and the flanges. The convective heat transfer coefficient from the outer surface to the ambient is affected by the rotational speed as studied by Ma, et al. [14] and Elghnam [15]. The increase in the rotational speed of the cylinder enhances the heat transfer coefficient to the ambient as indicated by Özerdem [16]. The current problem is that the rotational speed in the SCDMDS is one of the operating parameters required by the production line and cannot be changed.

The previous overview has shown that there is a high possibility of overheating that can occur in SCDMDS. Careful investigation of different parameters and operating conditions needs to be undertaken. This aids in figuring out the root causes of overheating and hence proposing modifications to mitigate them. This will be reflected on operational stability of SCDMDS.

1.2 Motivation

The SCDMDS overheating problem is a common problem. The SCDMDS failure leads to an unfavorable stoppage of the production lines. Even short interruptions are not acceptable and lead to significant delays and loss of production. Thus, the overheating issue must be solved in order to achieve reliable operations of the SCDMDS. The SCDMDS thermal performance is challenging as it has complicated multiphase flow beside the interplay of various components and mechanisms. To date, most studies focused on single phase Taylor-Couette (TC) flows. A limited number of studies investigated the multiphase TC flow. Just two recent studies, Chatterjee, et al. [17] and Chatterjee, et al. [18], considered an axial water flow within a rotating horizontal cylinder. In addition, all the previously published articles which included studies of gearboxes were conducted for a stationary outer casing. The multiphase TC flow and gearbox losses in a rotating outer case is rare in the literature. Such a complex matrix of different parameters and operating conditions motivated the main objectives of the current study as described in the next subsection.

1.3 Research objectives

The main objectives and contributions of the current research are to:

i. Develop a good understanding of the interplay and the effect of various mechanisms on the thermal performance of SCDMDS,

ii. Propose and assess possible design modifications to address the overheating problem frequently encountered in these systems.

iii. Develop a tool, in terms of an analytical model, that can be used to design and assess expected thermal performance of various types of SCDMDS.

The proposed research includes numerical and experimental components. It focuses on investigating fluid flow and rate of heat transfer of a TC flow inside SCDMDS. Operating parameters considered in the current work are the drum rotational speed, oil level, power losses, and geometry, etc. It is worth noting that the problem of interest doesn't include any Taylor-Couette flow instability. The problem of interest has been divided into several sub-problems, each representing a research objective, as follows:

a. Multiphase, free-surface flow of air/oil inside the SCDMDS

The main objective of this study is to understand the nature of the multiphase, free surface, flow of air/oil in the annular space between the electric motor casing and the rotating drum. This objective considers the effect of oil level, rotational speed, viscous dissipation and radius ratio on flow and heat transfer inside the SCDMDS. This study was carried out both experimentally and numerically using ANSYS-CFX software. The experimental part involved the design and construction of a test rig at the Thermal Processing Laboratory (TPL).

Experimental data were used to validate numerical results. The computational tool was used to expand the range and scope of the intended parametric analysis.

b. Heat Loss from the Gear Train

The objective is to investigate the rate of heat transfer of oil/air surrounding the internal, and planetary gear train used in the SCDMDS. The main focus of this objective is to determine the amount of heat generated within the gear train as function of various operating parameters, such as: speed, oil level and torque. It is carried out using the KISSsys and KISSsoft computational software beside experiments on a test rig at VDG facility.

c. Rate of Heat Transfer from the Drum

Lagging material is sometimes applied on the outer drum to increase its traction with the belt. Lagging is mostly made from rubber, which is a poor conductor of heat. The effect of lagging material, and belt speed on the rate of heat transfer of the outer drum is investigated. This study was conducted experimentally at the industrial partner facility. The lagging addition was studied numerically using ANSYS-CFX software.

d. Develop an Analytical Model of the Entire SCDMDS

Correlations of the rate of heat transfer of the entire SCDMDS as function of its operating parameters is developed using data obtained from the studies described above. An analytical model of the entire SCDMDS is developed using the thermal resistance network approach. The analytical model allows the industrial partner to determine acceptable operating conditions under which system overheating can be avoided.

e. SCDMDS Modifications

After understanding the role of various sources of heat generation and heat dissipation within the SCDMDS, modifications were proposed. Its effect on thermal management of the SCDMDS is determined numerically using ANSYS-CFX.

1.4 Thesis outline

Overall, the main results of this thesis have been prepared into five journal articles, in which three articles are already published, and the other two articles are submitted to a peer-review journal. The thesis is divided into the following chapters:

Chapter (1) introduces the background, motivation, and objectives of the research, to frame the scope of the thesis.

Chapter (2) is the first published journal article; it covers the fluid flow and heat transfer of the multiphase flow between two concentric cylinders (Taylor-Couette flow) at constant radius ratio (RR) and different oil levels (OV) and drum rotational speeds (N). A correlation has been developed in terms of the OV and Reynolds number (Re) in order to estimate the Nusselt number inside the gap.

Chapter (3) is the second journal article; it provides a wide investigation of TC flow at various RR, Re and OV in addition to the effect of lagging and surface emissivity. Correlations of the Nusselt number at various RR, Re and OV have been developed. A Thermal resistance network approach has been introduced to the system and applied to a case study.

Chapter (4) is the third journal article; it covers the thermal losses from the gearbox at different drum rotational speeds, torque, and oil levels. This paper shows the effect of various operating parameters on the heat losses from gearbox system. The heat losses from both dependent on load and independent on load losses has been investigated clearly.

Chapter (5) is the fourth journal article; it provides a way to cool down electrical motors by axial air flow. The radius ratio inside the motor was constant of 0.65. Different axial Reynolds numbers and rotational Reynolds numbers have been studied to show their effects on the Nusselt number.

Chapter (6) is the fifth journal article; it widens the study of chapter (5) by considering cooling of electrical motors at different radius ratio reaching 0.85. Correlation as a function of the radius ratio, rotational and axial Reynolds number has been developed.

Chapter (7) is the digital twin (DT) program; it shows the main construction of the DT, inputs, outputs, and solution methods. In addition to showing the solution technique, validation, and a case study.

Chapter (8) summarizes the main conclusions and contribution of the thesis, highlights the strengths, and presents some suggestions for future work. Finally, it defines the contribution of this thesis to the previous literature.

1.5 References

[1] *Van der Graaf Drum Motors*. Available: https://www.vandergraaf.com/

[2] C. Changenet, X. Oviedo-Marlot, and P. Velex, "Power Loss Predictions in Geared Transmissions Using Thermal Networks-Applications to a Six-Speed Manual Gearbox," *Journal of Mechanical Design,* vol. 128, no. 3, pp. 618-625, 2005.

[3] Y. Terauchi, K. Nagamura, and K. Ikejo, "Study on Friction Loss of Internal Gear Drives : Intluence of Pinion Surface Finishing, Gear Speed and Torque," *JSME international journal. Ser. 3, Vibration, control engineering, engineering for industry*, vol. 34, no. 1, pp. 106-113, 1991.

[4] F. Concli and C. Gorla, "Analysis of the Oil Squeezing Power Losses of a Spur Gear Pair by Mean of CFD Simulations," in *ASME 2012 11th Biennial Conference on Engineering Systems Design and Analysis*, 2012, vol. Volume 2: Applied Fluid Mechanics; Electromechanical Systems and Mechatronics; Advanced Energy Systems; Thermal Engineering; Human Factors and Cognitive Engineering, pp. 177-184.

[5] H. Liu, T. Jurkschat, T. Lohner, and K. Stahl, "Determination of oil distribution and churning power loss of gearboxes by finite volume CFD method," *Tribology International*, vol. 109, pp. 346-354, 2017/05/01/ 2017.

[6] C. D. Andereck, S. S. Liu, and H. L. Swinney, "Flow regimes in a circular Couette system with independently rotating cylinders," *Journal of Fluid Mechanics*, vol. 164, pp. 155-183, 1986.

[7] U. Naseem, M. B. Awan, B. Saeed, N. Abbas, S. Nawaz, and M. Hussain, "Experimental investigation of flow instabilities in a wide gap turbulent rotating Taylor-Couette flow," *Case Studies in Thermal Engineering*, vol. 14, p. 100449, 2019/09/01/ 2019.

[8] G. Rüdiger, M. Gellert, R. Hollerbach, M. Schultz, and F. Stefani, "Stability and instability of hydromagnetic Taylor–Couette flows," *Physics Reports*, vol. 741, pp. 1-89, 2018/04/26/ 2018.

[9] S. Dong, "Direct numerical simulation of turbulent Taylor–Couette flow," *Journal of Fluid Mechanics,* vol. 587, pp. 373-393, 2007.

[10] S. Seghir-Ouali, D. Saury, S. Harmand, O. Phillipart, and D. Laloy, "Convective heat transfer inside a rotating cylinder with an axial air flow," *International Journal of Thermal Sciences,* vol. 45, no. 12, pp. 1166-1178, 2006/12/01/ 2006.

[11] M. Fénot, Y. Bertin, E. Dorignac, and G. Lalizel, "A review of heat transfer between concentric rotating cylinders with or without axial flow," *International Journal of Thermal Sciences,* vol. 50, no. 7, pp. 1138-1155, 2011/07/01/ 2011.

[12] T.-M. Jeng, S.-C. Tzeng, and C.-H. Lin, "Heat transfer enhancement of Taylor–Couette–Poiseuille flow in an annulus by mounting longitudinal ribs on the rotating inner cylinder," *International Journal of Heat and Mass Transfer,* vol. 50, no. 1, pp. 381-390, 2007/01/01/ 2007.

[13] A. Nouri-Borujerdi and M. E. Nakhchi, "Optimization of the heat transfer coefficient and pressure drop of Taylor-Couette-Poiseuille flows between an inner rotating cylinder and an outer grooved stationary cylinder," *International Journal of Heat and Mass Transfer,* vol. 108, pp. 1449-1459, 2017/05/01/ 2017.

[14] H. Ma *et al.*, "Experimental investigation on the steady, external laminar mixed convection heat transfer characteristics around a large diameter horizontal rotating cylinder," *International Communications in Heat and Mass Transfer,* vol. 57, pp. 239-246, 2014/10/01/ 2014.

[15] R. I. Elghnam, "Experimental and numerical investigation of heat transfer from a heated horizontal cylinder rotating in still air around its axis," *Ain Shams Engineering Journal,* vol. 5, no. 1, pp. 177-185, 2014/03/01/ 2014.

[16] B. Özerdem, "Measurement of convective heat transfer coefficient for a horizontal cylinder rotating in quiescent air," *International Communications in Heat and Mass Transfer,* vol. 27, no. 3, pp. 389-395, 2000/04/01/ 2000.

[17] S. Chatterjee, G. Sugilal, and S. V. Prabhu, "Heat transfer in a partially filled rotating pipe with single phase flow," *International Journal of Thermal Sciences,* vol. 125, pp. 132-141, 2018/03/01/ 2018.

[18] S. Chatterjee, G. Sugilal, and S. V. Prabhu, "Impact of inclination on single phase heat transfer in a partially filled rotating pipe," *International Journal of Heat and Mass Transfer,* vol. 123, pp. 867-878, 2018/08/01/ 2018.

Chapter 2

Investigation of Transient Multiphase Taylor-Couette Flow

Chapter 2

Investigation of Transient Multiphase Taylor-Couette Flow

Complete Citation:

A. M. Teamah and M. S. Hamed, "Investigation of transient multiphase Taylor-Couette flow," Alexandria Engineering Journal, vol. 61, no. 4, pp. 2723-2738, 2022/04/01/ 2022.

Copyright:

Relative Contributions:

Ahmed M. Teamah: Wrote the first draft of the manuscript.

Mohamed S. Hamed: Revised and edited the manuscript.

Investigation of Transient Multiphase Taylor-Couette Flow

Ahmed M. Teamah* and Mohamed S. Hamed

Thermal Processing Laboratory, Department of Mechanical Engineering,

McMaster University, Hamilton, Ontario, Canada

*Corresponding Author: teamaha@mcmaster.ca, Tel: +1 905-920-6960

Abstract

A multiphase, transient, horizontal, Taylor-Couette flow has been investigated numerically. This flow governs thermal performance of self-contained drum motor (SCDM) drive systems. These drive systems are extensively used with conveyor belt systems, employed in many industrial and commercial applications. Thermal performance of the SCDM drive system is governed by heat transfer within multiphase flow of air and oil. This flow is confined within a horizontal annular space between two concentric cylinders. The outer cylinder is the drum. It rotates and rejects heat to the atmosphere. The inner cylinder is the outer surface of the motor. It is stationary and subjected to a constant heat flux. This heat is generated within the electric motor, gearbox, and oil viscous dissipation. Numerical simulations have been carried out using ANSYS-CFX. Transient flow and thermal fields have been investigated, starting from an initial stationary state until a quasi-steady state is reached. The effect of drum rotational speed and oil level on thermal performance of the SCDM drive system has been investigated. The study covers a range of rotational speeds from 0 to 150 rpm, oil level from 0%, (i.e., 100% air-filled) to 100%. Numerical results have been validated using experimental data. The optimum oil

level has been determined which gives the lowest possible overall maximum SCDM system temperatures. This optimum oil level depends on the drum rotational speed. Results indicated that the 100% oil-filled case does not provide the best thermal performance. The Nusselt number around the inner cylinder has been correlated as a function of rotational Reynolds number and oil level. The developed correlation can be used as a design tool. This tool is to optimize system thermal performance by determining the optimum oil level at a given rotational speed.

Keywords: Multiphase Taylor-Couette flow, Self-contained Drum Motor Drive System, Thermal Performance, Rotating Cylinders.

Nomenclature

Br	Brinkman number, $\mu(\omega^* r_{i,oc})^2/ \lambda\ (T_{ic}-T_{oc})$
D	Diameter, m
g	Gravitational acceleration, 9.81 m/sec^2.
Gr	Grashof number, $\frac{g\beta(T_{w,oc}-T_{amb})D_{o,oc}{}^3}{\nu^2}$
h	Heat transfer coefficient, W/m^2.°C
h_{tot}	Specific total enthalpy, J/kg
k	Turbulence kinetic energy per unit mass, J/kg
N	Rotational speed, rpm
Nu	Nusselt number, h D_{ic}/ λ

OV Oil volume percentage inside the annular area, %

p Static pressure, Pa

Pr Prandtl number, ν/α

r Radius, m

r* Dimensionless radius, $(r-r_{o,ic})/(r_{i,oc}-r_{o,ic})$

Re Rotational Reynolds number, $\frac{\pi N {r_{oc}}^2}{30\nu}$

$(Re_r)_{cr}$ Critical rotational Reynolds number.

RR Radius ratio, $r_{o,ic}/r_{i,oc}$

t Time, Second

T Temperature, °C

T* Dimensionless temperature, $(T-T_{o,ic})/(T_{i,oc}-T_{o,ic})$

u Fluctuating velocity component in turbulent flow, m/sec

U Velocity vector, m/sec

Greek symbols

α Thermal diffusivity, m^2/sec.

β Thermal expansion coefficient, 1/K.

η place holder for any parameter.

θ	Angle, °
λ	Thermal conductivity, W/m.°C
μ	Dynamic viscosity, kg/m.s
ν	Kinematic viscosity, m^2/s
ρ	Density, kg/m^3
τ	Shear stress tensor, N/m^2
ω	Angular speed, rad/sec
ω	Specific turbulence dissipation rate, 1/sec.

Subscript

amb	Ambient
av	Average
as	Annular space
oc	Outer cylinder
i	Inner surface
max	Maximum value
ic	Inner cylinder
o	Outer surface
w	Wall

2.1 Introduction

Components of a typical belt conveyor drive system are placed inside the outer drum of the Self-contained drum motor (SCDM) drive system, as shown in Figure 2.1. Lubrication oil is confined within the annular space inside the drum. This makes the SCDM drive systems more suitable for the pharmaceutical and food industries due to their compact design and cleaner environment, which is an important requirement for these industries. However, failure due to overheating, at some operating conditions, has been experienced in many SCDM drive systems. The overheating problem arises from the, relatively, limited heat dissipation capability and the large heat generation taking place within the SCDM drive system. Heat is dissipated to ambient air only through the drum outer surface area. While a significant amount of heat is generated within the SCDM drum from a number of sources. Such as, energy losses within the electric motor, within the gearbox and due to viscous dissipation within oil. Understanding the interplay and effect of these parameters on the thermal performance of a SCDM drive system is essential. So that, we can address and propose solutions for the overheating problem.

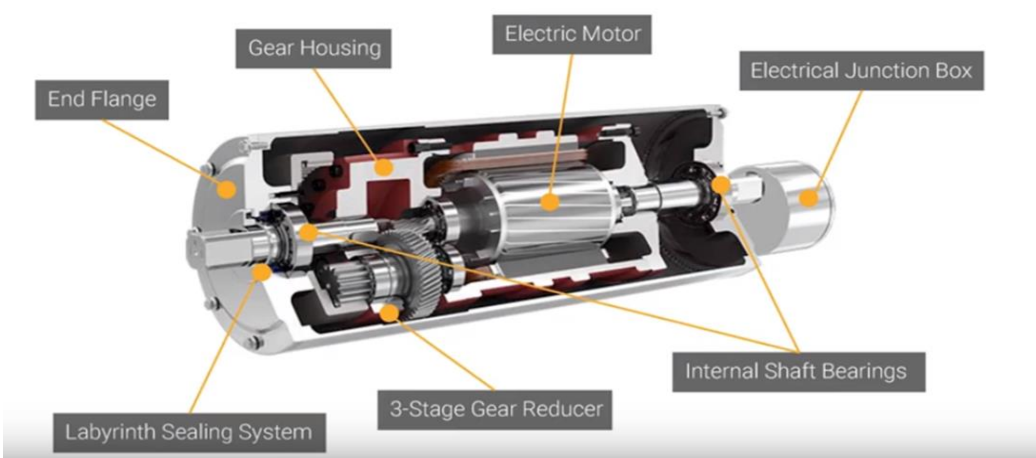

Figure 2.1 Main components of a SCDM drive system [1]

The following literature review summarizes previous studies addressing the effect of some of these parameters on fluid flow and heat transfer within the SCDM drive system.

The effect of rotational speed on heat transfer from a horizontal heated cylinder placed in a quiescent air was studied experimentally by Özerdem [2]. Özerdem showed that the rate of heat transfer depended significantly on the rotational speed. A correlation of the average Nusselt number, as a function of the rotational Reynolds number in the range of 2000-40,000, was developed. Ma, et al. [3] investigated, experimentally, the effect of rotational speed on heat transfer from a rotating horizontal heated cylinder. They considered the effect of mixed convection. Similar to what was reported in Özerdem [2], they found that the rate of heat transfer was directly proportional to the rotational speed.

Anderson, et al. [4] studied, experimentally, the effect of rotational speed on the rate of heat transfer from a horizontal rotating cylinder placed in stagnant air. Their study focused on a low range of Reynolds (Re) number, where natural convection was dominant. Their study considered the effect of surrounding air pressure, up to 4 atmospheres. They found that the average Nusselt number was independent of the rotational Reynolds number until Re number reached a critical value. This critical value equals to $1.09 \times Gr^{1/2}$, above which the effect of the rotational speed became more dominant.

Multiple researchers studied the effect of rotational speed on the rate of heat transfer from horizontal heated cylinders placed in still air or subjected to axial airflow. For example, Chiou and Lee [5], Morales, et al. [6], Farouk and Ball [7], Yan and Zu [8], Morgan [9] and Van Der Hegge Zijnen [10]. All these researchers confirmed that the rotational speed has a significant effect on the rate of heat transfer from the rotating cylinders.

Andereck, et al. [11] investigated, experimentally, flow regimes of an isothermal Taylor-Couette flow within an annular space between two rotating cylinders. They identified various flow regimes and different instabilities. Marcus [12] carried out a numerical study of a single-phase flow of a viscous fluid confined in an annular space between a fixed outer cylinder and a rotating inner cylinder. The study was carried out within the wavy vortex flow regime. He solved Navier-Stokes equations by using a pseudo-spectral method. He calculated the torque required to rotate the inner cylinder at different speeds. Hsu [13] studied, numerically, fluid flow and heat transfer within a single-phase Taylor-Couette flow. The main objective of his study was to develop an inverse approach to calculate fluid viscosity and rate of heat transfer.

Hasan and Sanghi [14] carried out a numerical study of natural convection of air inside a horizontal rotating cylinder subjected to periodic temperature distribution. They investigated the effect of centrifugal and Coriolis forces on a natural convection driven flow. They considered a constant gravitational Rayleigh number of 10^5. While varying the rotational Rayleigh number from 10^2 to 10^7. Their results showed that the gravitational force was dominant when the rotational Rayleigh number was below 386. However, the centrifugal force became dominant when the rotational Rayleigh number was above 1900.

A numerical study of airflow and heat transfer within an annular space between a horizontal fixed inner cylinder and a rotating outer cylinder was carried out by Yoo [15]. The two cylinders were kept at different constant temperatures. The inner cylinder was kept at a higher temperature than the outer cylinder. The study was focused on low rotational speeds, corresponding to rotational Reynolds number less than 1500. They identified three flow patterns as function of Reynolds number: (1) a two-eddy flow pattern at extremely low

Reynolds numbers, (2) a one-eddy pattern at slightly higher Reynolds number reaching 300, and (3) a no-eddy pattern at higher Reynolds numbers between 500 and 1500.

Paghdar, et al. [16] numerically investigated stability of a Taylor-Couette flow within an annular space between two counter-rotating cylinders. They considered very high Reynolds numbers, in the range of 8000 to 16000. They also considered the effect of eccentricity of the inner cylinder with respect to the outer cylinder. Their results showed that flow within the smaller gap, formed due to the eccentricity, contained a larger number of vortex structures than those formed within the larger gap region.

Many other researchers studied Taylor-Couette flow, with and without an imposed axial flow. For example, Alshahrani and Zeitoun [17], Fusegi, et al. [18], Tachibana, et al. [19], and Moukalled and Acharya [20]. Other researchers, such as Jangili, et al. [21], Sheikholeslami, et al. [22], and Sheikholeslami, et al. [23], investigated different ways to enhance the rate of heat transfer within Taylor-Couette flows, such as the use of nano-particles and magnetic fields.

Chatterjee, et al. [24] studied, experimentally, an axial water flow within a rotating horizontal cylinder. The cylinder was partially filled with water and subjected to a constant heat flux. They considered the effects of rotational speed in the range of 5 to 300 rpm, heat flux from 799 to 12522 W/m^2 and water flow rate from 6 to 80 L/h; on the developed flow and thermal fields. They concluded that all three parameters have a positive effect on the rate of heat transfer. They presented a correlation of the average Nusselt number. This correlation is a function of the axial Reynolds number, the rotational Reynolds number, and the dimensionless heat flux.

Nouri-Borujerdi and Nakhchi [25] investigated a method to enhance the rate of heat transfer in a Taylor-Couette flow. They placed grooves on the inner side of the outer cylinder, which was fixed, while the inner cylinder was rotating. Taylor number, groove aspect ratio, number of grooves, and wall temperature were varied from 0 to 8.36×10^6, 0 to 2.0, 0 to 20.0, and 50 to 90 °C, respectively. The best enhancement in the rate of heat transfer was achieved at the highest groove aspect ratio of 2. They also found that increasing the rotational speed and the number of grooves resulted in an enhancement of the rate of heat transfer.

The previous literature review clearly indicates that, although many investigations have been carried out considering a number of Taylor-Couette flows. But the exact configuration of the Taylor-Couette flow that takes place inside the SCDM drive system has not been investigated before. The flow considered in the present study involves a multiphase Taylor-Couette flow of air and oil inside an annular space. This annular space is between a fixed, heated, inner cylinder (representing the motor) and a rotating outer cylinder (representing the drum), subjected to ambient air. The main focus of the present work is to investigate the effect of oil level and drum rotational speed on the heat transfer of the flow within the SCDM drive system.

2.2 Problem Definition

The length to the annular gap ratio of the SCDM drive system is about 10. Therefore, flow and heat transfer within the SCDM drive system considered in this study can be investigated using the two-dimensional model shown in Figure 2.2. The inner cylinder is fixed and subjected to a constant heat flux of 1900 W/m^2. This heat flux is due to energy losses within the electric motor and gear train. The outer cylinder (drum) is rotating and exposed to ambient air. The drum rotational speed has been varied between 0 and 150 rpm. The selected values of the heat flux and the rotational speed correspond to the operating conditions of the SCDM drive systems of interest. The outside heat transfer coefficient of the surrounding air as function of drum rotational speed has been calculated using the correlation reported by Etemad [26], given in equation (1).

$$\overline{Nu} = 0.11 * ((0.5 * Re^2 + Gr) * \mathrm{Pr})^{0.35} \tag{1}$$

The annular space is filled with air and oil. The type of oil used is Enduratex-EP 150. Oil properties, including its viscosity as function of temperature, have been obtained from manufacturer's data [27]. Table 2-1 provides correlations of oil properties as function of temperature.

Table 2-1 Oil Enduratex-EP 150 properties as a function of temperature

Oil Property	Values from manufacturer's data[27]	Correlations developed by authors for the oil Enduratex-EP 150 properties
Density (ρ) [kg/m³]	856 kg/m³ @40°C 818 kg/m³ @100°C	$\rho(\mathrm{T}) = 880 - 0.44 * T - 0.0061 * T^2 + 6.398 * 10^{-5} * T^3 - 2.08817 * 10^{-7} * T^4$
Dynamic viscosity (μ) [Pa.s]	0.1284 Pa.s @40°C 0.01217 Pa.s @100°C	$\mu(\mathrm{T}) = 0.0146 + 2.6254 * e^{(-0.102338T)} + 9.7258 * 10^{-4} * T^2 * e^{(-0.077355T)} - 7.0317 * 10^{-5} * T$
Thermal conductivity (λ) [W/m.°C]	0.14 W/m.°C	-

Five oil levels (OV) equal to 0, 42, 64, 86 and 100% have been considered in this study. Where, OV is the percentage of oil volume to the annular space volume.

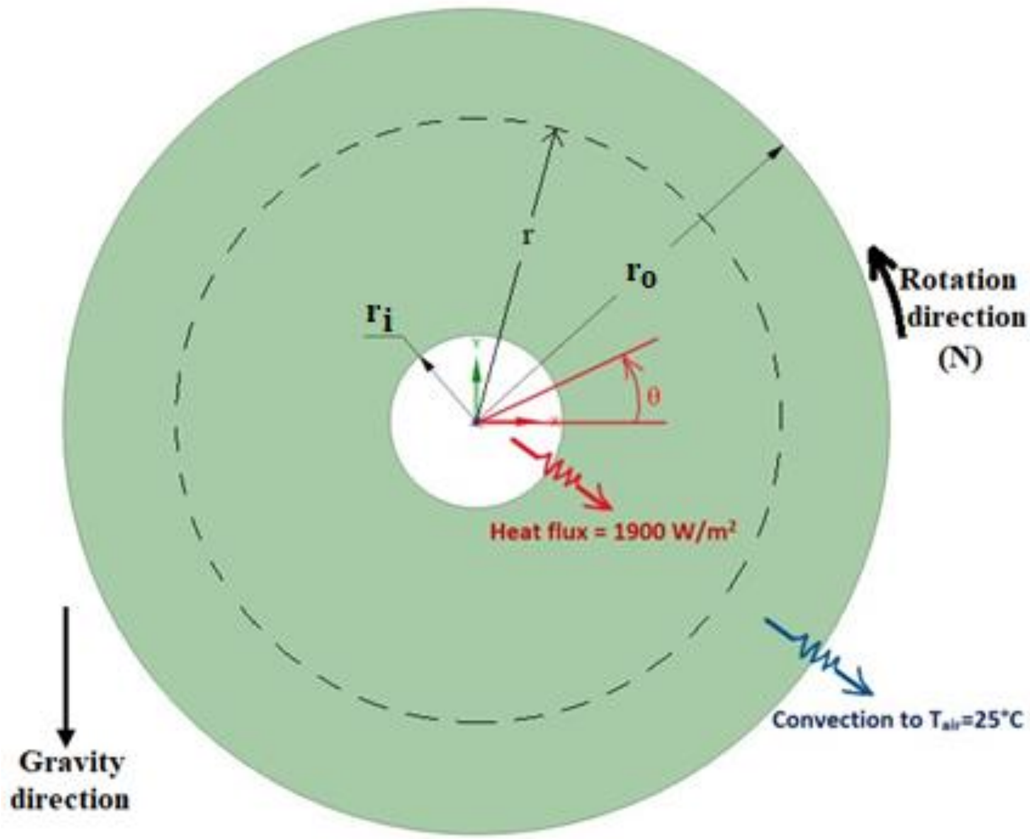

Figure 2.2 Schematic diagram of the problem of interest.

2.3 The Mathematical Model

2.3.1. The Governing Equations

The following set of conservation equations of mass, momentum and energy has been solved using ANSYS [28]:

$$\frac{\partial \rho}{\partial t} + \nabla \cdot (\rho U) = 0 \tag{2}$$

$$\frac{\partial(\rho U)}{\partial t} + \nabla \cdot (\rho U \otimes U) = -\nabla p + \nabla \cdot \tau \tag{3}$$

$$\frac{\partial(\rho h_{tot})}{\partial t} - \frac{\partial p}{\partial t} + \nabla \cdot (\rho U h_{tot}) = \nabla \cdot (\lambda \nabla T) + \nabla \cdot (U \cdot \tau) \tag{4}$$

Heat due to oil viscous dissipation has been taken into account, which is presented by the last term in the energy equation (4). The shear stress tensor and total enthalpy in equations (3) and (4) are represented by expressions given in equations (5) and (6).

$$\tau = \mu\left(\nabla U + (\nabla U)^T - \frac{2}{3}\delta \nabla \cdot U\right) \tag{5}$$

$$h_{tot} = enthalpy + \frac{1}{2}U^2 \tag{6}$$

The Shear Stress Transport (SST) turbulence model has been chosen because it is able to capture the viscous sublayer, which is required to clearly identify the point of oil separation from the rotating drum. The following additional transport equations have been solved.

$$\frac{\partial(\rho k)}{\partial t} + \frac{\partial(\rho u_j k)}{\partial x_j} = P - \beta^* \rho \omega k + \frac{\partial}{\partial x_j}[(\mu + \sigma_k \mu_t)\frac{\partial k}{\partial x_j}] \tag{7}$$

$$\frac{\partial(\rho \omega)}{\partial t} + \frac{\partial(\rho u_j \omega)}{\partial x_j} = \frac{\gamma}{\nu_t}P - \beta \rho \omega^2 + \frac{\partial}{\partial x_j}[(\mu + \sigma_\omega \mu_t)\frac{\partial \omega}{\partial x_j}] + 2(1 - F_1)\frac{\rho \sigma_{\omega 2}}{\omega}\frac{\partial k}{\partial x_j}\frac{\partial \omega}{\partial x_j} \tag{8}$$

The variables appeared in equations (7) and (8) of the turbulence model are defined in equations (9) to (18).

$$P = \tau_{ij}\frac{\partial u_i}{\partial x_j} \tag{9}$$

$$\tau_{ij} = \mu_t(2S_{ij} - \frac{2}{3}\frac{\partial u_k}{\partial x_k}\delta_{ij}) - \frac{2}{3}\rho k\delta_{ij} \quad (10)$$

$$S_{ij} = \frac{1}{2}(\frac{\partial u_i}{\partial x_j} + \frac{\partial u_j}{\partial x_i}) \quad (11)$$

$$\mu_t = \frac{\rho a_1 k}{max(a_1\omega, \Omega F_2)} \quad (12)$$

$$\phi = F_1\phi_1 + (1 - F_1)\phi_2 \quad (13)$$

$$F_1 = \tanh(\mathrm{arg}_1^4) \quad (14)$$

$$\mathrm{arg}_1 = min[max(\frac{\sqrt{k}}{\beta^*\omega d}, \frac{500\nu}{d^2\omega}), \frac{4\rho\sigma_{\omega 2}k}{\mathrm{CD}_{k\omega}d^2}] \quad (15)$$

$$\mathrm{CD}_{k\omega} = max(2\rho\sigma_{\omega 2}\frac{1}{\omega}\frac{\partial k}{\partial x_j}\frac{\partial \omega}{\partial x_j}, 10^{-20}) \quad (16)$$

$$F_2 = \tanh(\mathrm{arg}_2^2) \quad (17)$$

$$\mathrm{arg}_2 = max(2\frac{\sqrt{k}}{\beta^*\omega d}, \frac{500\nu}{d^2\omega}) \quad (18)$$

2.3.2. The Boundary Conditions

As shown in Figure 2.2, the governing equations are subjected to the following boundary conditions.

At r=r_i U=0 and $q'' = constant = 1900\ W/m^2$. (19)

At r=r_o $u_\Theta = \omega r_o$, $u_r = u_z = 0$ and $q''_{cond} = q''_{conv}$ so that

$$h(T_{w,oc} - T_{amb}) = -\lambda \frac{\partial T}{\partial r}\Big|_{r=r_o} \quad (20)$$

At z = 0 and L, a symmetry boundary condition is used, i.e., $\frac{\partial \eta}{\partial z} = 0$ (21)

Where, η is a place holder for any parameter, e.g., velocity component, temperature, pressure, etc.

In the multiphase flow, the Volume of Fluid (VOF) method has been used to resolve the free oil-air interface.

2.3.3. Solution Procedure

The ANSYS CFX solver discretized and solved the governing equations using the finite volume method. The solver used a transient scheme employing the implicit method. The time step was selected according to the maximum value of Courant number of 1.

i. Grid Independence Test

A grid independence test has been carried out until the optimum number of elements that gave an acceptable level of accuracy of the estimated average fluid temperature was obtained. Results of the grid independence test are shown in Figure 2.3. A mesh of 519,142 elements was deemed sufficient. The selected mesh is shown in Figure 2.4, where the finer grids are placed near the solid boundaries, where significant gradients are expected. The selected mesh has a maximum aspect ratio of 10 and an average skewness of 0.21.

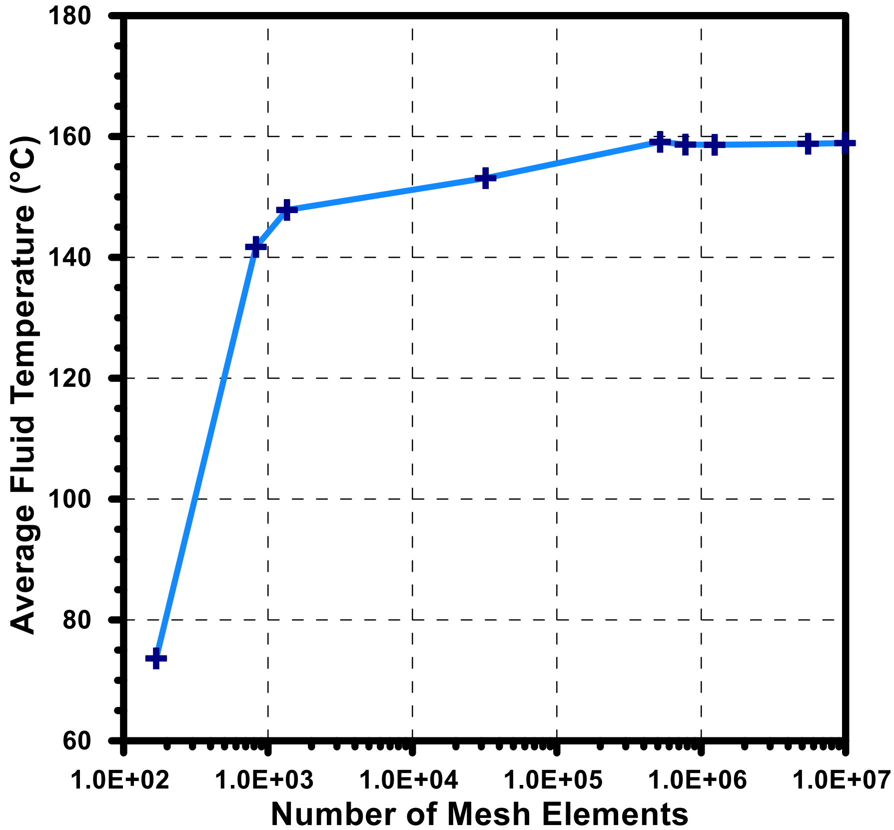

Figure 2.3 Grid independence test results.

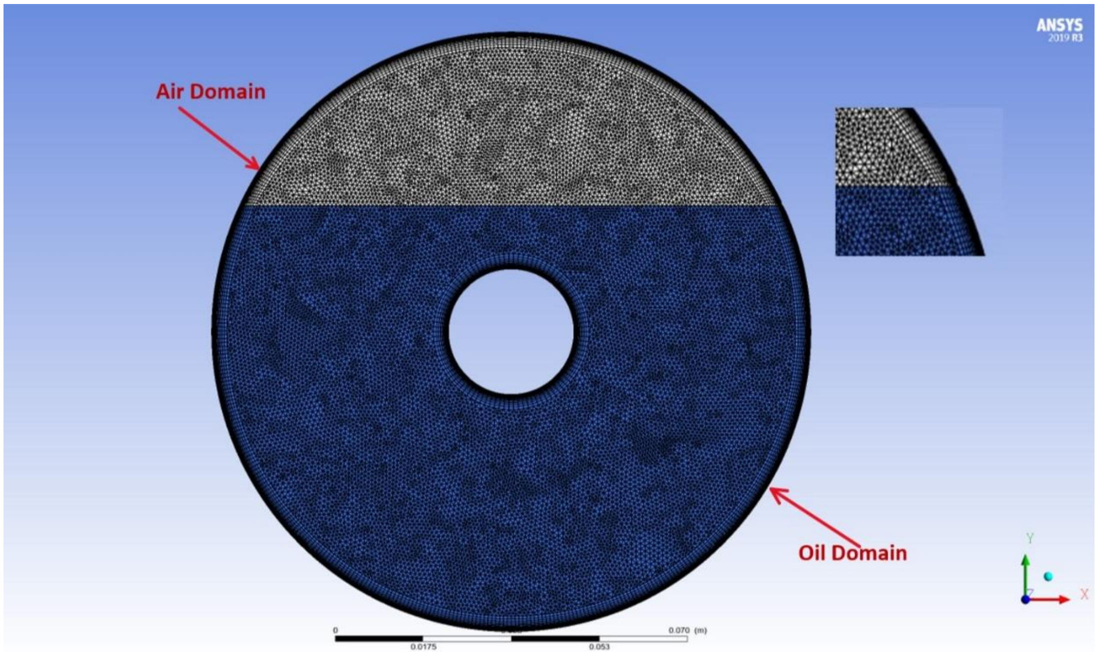

Figure 2.4 Grid distribution using the selected mesh

2.4 Validation of Numerical Results

The multiphase flow confined in a horizontal annular space has not studied before. Validation of current numerical results for single phase cases has been carried out using published data. Validation of the multiphase cases has been carried out using experimental results obtained from the industrial partner.

2.4.1. Single Phase Comparison

Validation of the present numerical results has been carried out for a single-phase case. The fixed inner cylinder (r_i = 12.5 mm) and the outer rotating cylinder (r_o = 59.5 mm) were kept at constant temperatures of 90°C and 35°C, respectively. The outer cylinder rotational speed was kept at 150 rpm. These conditions were selected so that numerical results obtained for this case can be compared with analytical results available in Kundu and Cohen [29] and White and Corfield [30]. Viscous dissipation was taken into consideration in this validation but with neglecting the gravitational forces. The analytical velocity and temperature distributions are given by equations (22) and (23). Figure 2.5 shows a comparison between present numerical results and analytical velocity and temperature distributions inside the gap. The maximum deviation is about 6.7%.

$$V_\theta = r_0\omega_0 \frac{\frac{r_i}{r} - \frac{r}{r_i}}{\frac{r_i}{r_0} - \frac{r_0}{r_i}} + r_i\omega_i \frac{\frac{r}{r_0} - \frac{r_0}{r}}{\frac{r_i}{r_0} - \frac{r_0}{r_i}} \tag{22}$$

$$\frac{T - T_0}{T_i - T_0} = \frac{Br * r_i^4}{(r_i^2 - r_0^2)^2}\left[\left(1 - \frac{r_0^2}{r^2}\right) - \left(1 - \frac{r_0^2}{r_i^2}\right)\frac{ln\left(\frac{r}{r_0}\right)}{ln\left(\frac{r_i}{r_0}\right)}\right] + \frac{ln\left(\frac{r}{r_0}\right)}{ln\left(\frac{r_i}{r_0}\right)} \tag{23}$$

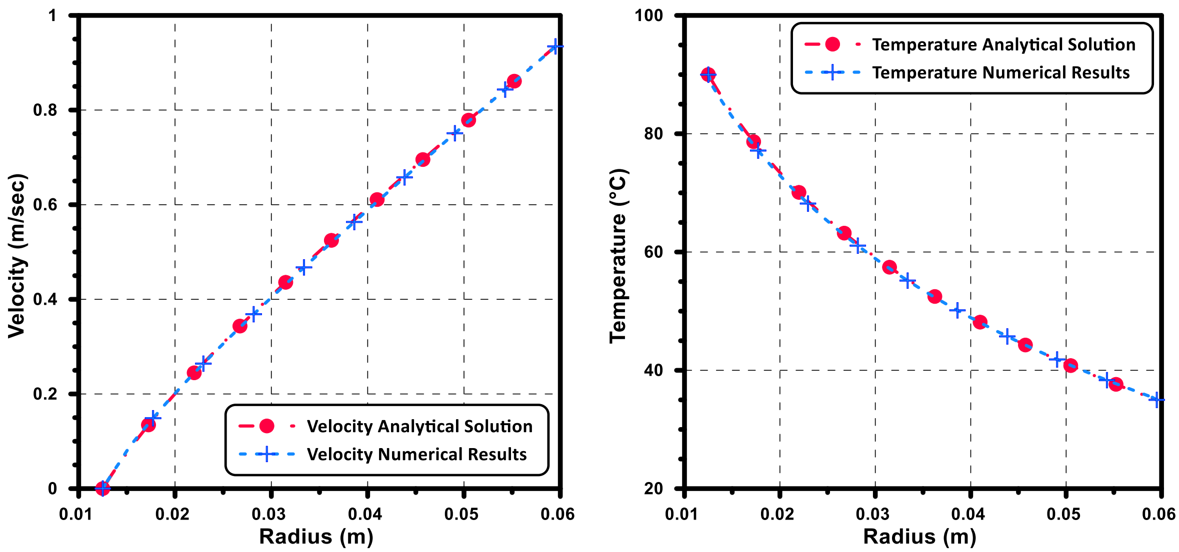

(a) (b)

Figure 2.5 Comparison of numerical and analytical results,

(a)Velocity distribution (b)Temperature distribution

Another validation case was carried out considering mixed convection heat transfer results reported by Yoo [15] for an inner diameter-gap width ratio of 2, Rayleigh number of 10^4, and rotational Reynolds number between 100 and 500. Figure 2.6 shows a comparison of present numerical results and those reported by Yoo [15]. At a low Reynolds number below 300, two eddies formed on the right and left sides of the annular space. Increasing Reynolds number to 300, only one eddy was present. At a higher Reynolds number reaching 500 no eddies were observed.

From Figure 2.6, it is seen a good agreement between present results and Yoo [15] results.

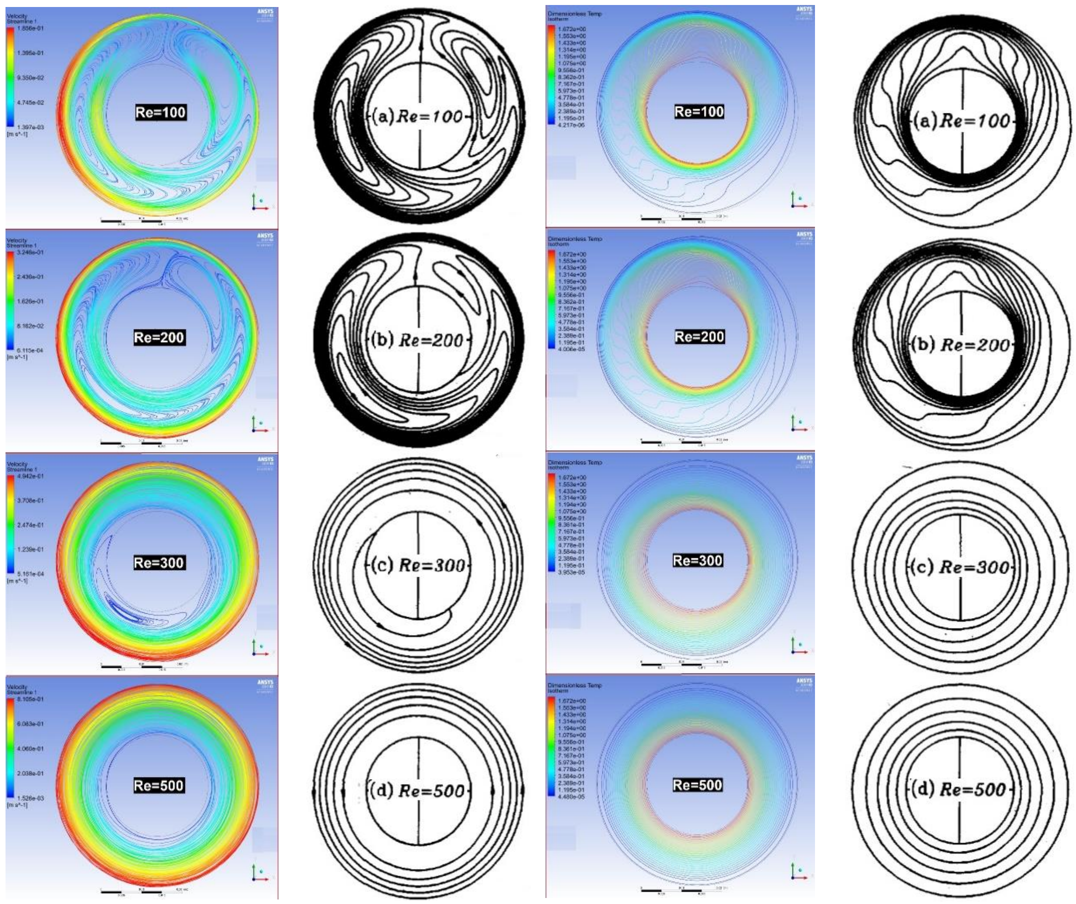

(a) Streamline (b) Streamline (c) Isotherms (d) Isotherms

Figure 2.6 Comparison of present numerical results (a) and (c) and results reported in Yoo [15] (b) and (d)

2.4.2. Multiphase Comparison

A set of experiments were carried out considering an actual SCDM drive system. The drum diameter and the inner cylinder diameter was 217 and 176 mm, respectively. During the test, drum rotational speed was kept at 45 rpm, oil volume ratio and heat loss due to electric motor and gearbox were 32% and 200 W, respectively. A photograph of the experimental test setup is shown in Figure 2.7. Three thermocouples were placed circumferentially on the motor surface measuring temperatures at three angular positions at $\theta = 50^o$, 90^o, and -90^o. Numerical simulations of this SCDM drive system were carried out considering same conditions.

Figure 2.8 shows simulation results of the same configuration considered in the experimental setup shown on Figure 2.7. Figure 2.8 a, b and c show oil distribution, velocity vector and temperature contours, respectively. The red and blue regions in Figure 2.8a represent oil and air, respectively. The velocity vectors shown in Figure 2.8b clearly indicate oil splashing over the motor surface at $-8^o \leq \theta \leq 21^o$. So, in this region the temperature over the motor decreased due to the additional forced convection cooling, as shown in Figure 2.8c and Figure 2.8d.

For the bottom section of $-137^o \leq \theta \leq -42^o$, the motor surface is surrounded by stagnant oil which provides better cooling than the remaining circumference of the motor surface, $21^o \leq \theta \leq 180^o$ and $-180^o \leq \theta \leq -137^o$, which is cooled by air, causing the highest surface temperatures.

Figure 2.8d shows a comparison of the present numerical results of temperature distribution along the entire motor surface and the experimental data. A reasonable agreement, with a maximum deviation of about 4%, has been observed.

Figure 2.7 Test rig of the experiment

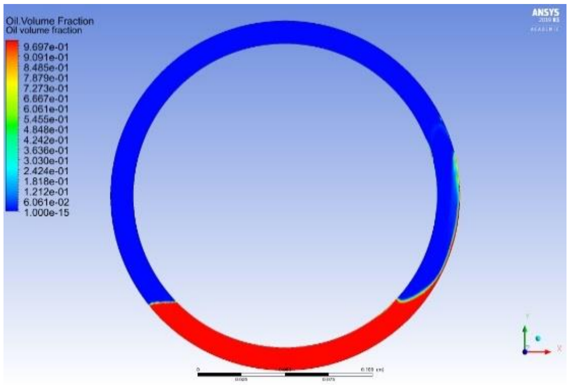

(a) Oil and Air distribution

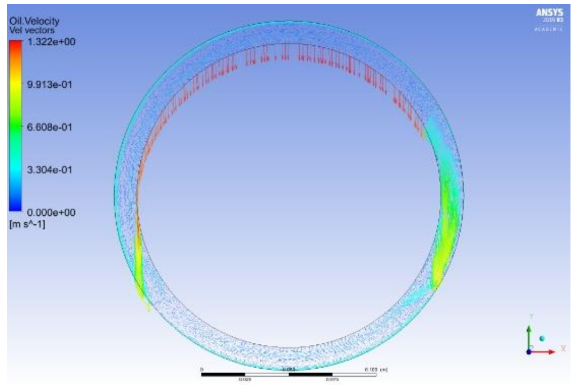

(b) Velocity vectors

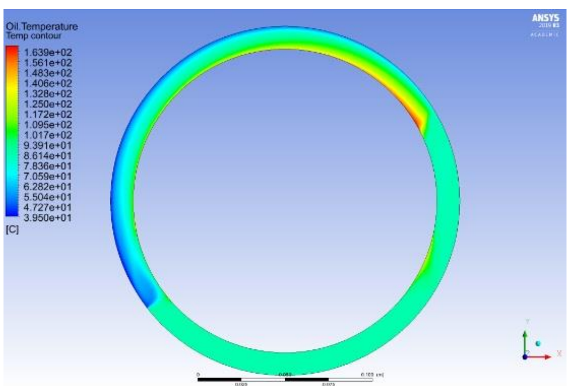

(c) Temperature contour

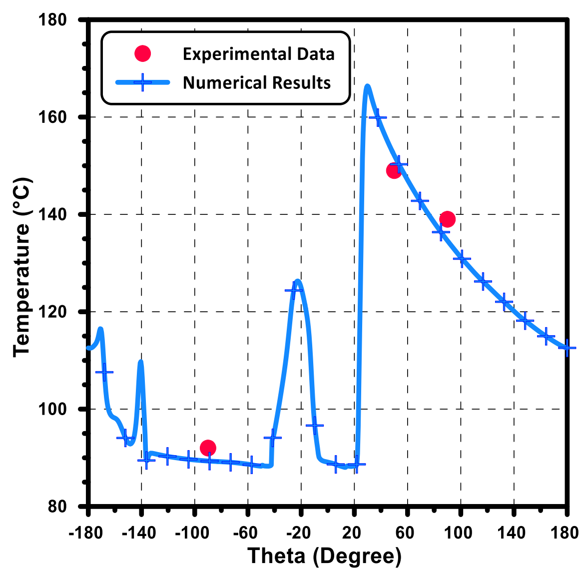

(d) Circumferential motor temperature distribution

Figure 2.8 Numerical and experimental results of the multiphase case for OV=32% and N=45rpm

2.5 Results and Discussion

As indicated before, the main objective of this study is to understand the effect of oil level and rotational speed on heat transfer within the SCDM drive system. A parametric study has been carried out considering the following parameters: r_i = 12.5 mm, r_o = 59.5 mm, i.e., radius ratio = 0.21, $T_{amb.}$ = 25 °C, and q'' = 1900 W/m^2. The chosen radius ratio of 0.21 represents the case of a large SCDM drive system in which overheating is a significant concern. The outer cylinder rotational speed, *N*, has been changed from 0 up to 150 rpm, with a step of 50 rpm. The oil volume ratio, OV, has been varied, considering five oil levels of 0%, 42 %, 64%, 86%, and 100%. It is worth noting here that at OV < 42%, the oil level is very low and will not provide enough cooling for the motor or proper lubrication for the gearbox. Therefore, OV values between 0 and 42% have not been considered here and the range between 42% and 100% has been divided into 4 levels, by considering the 64% and 86% cases.

2.5.1. Case of air only, OV = 0%

The effect of rotational speed, N, on fluid flow and heat transfer inside the system for the case of OV = 0% (i.e., annular space is entirely filled with air) has been investigated. Figure 2.9 shows the effect of N on the streamlines in the horizontal annular space. At N = 0, pure natural convection is dominated in the annular gap. Therefore, it is noticed that a symmetrical shape for the streamlines about the vertical line passes through the annulus center. Two symmetrical eddies developed at each half. The right and left eddies are moving in the clockwise and counterclockwise directions, respectively. From buoyancy effect, flow moves upward from the top of the inner cylinder until it reaches the inner surface of the outer cylinder. After that it falls down after being cooled from the cold outer cylinder.

When N is increased, and since N in this case is in the counterclockwise direction, the left-side eddy became bigger than the right-side one. As mentioned from the buoyancy, flow will move upwardly. But this time when it reaches the outer rotating drum. The left-side eddy will increase in size as the forced motion from the rotating drum and the flow from natural convection is assisting each other. While on the other hand, the right eddy will become smaller as the forced motion from the rotating drum is opposing the flow falling down which came from natural convection.

From Figure 2.9d, it is very clear from the streamlines near to the rotating drum in case of N=150 rpm that a larger boundary layer is formed over the inner surface of the outer cylinder. You can notice Figure 2.9c, that at N=100 rpm, it has less streamlines for flow rotating circularly with the drum compared to N=150 rpm. So that increasing the drum rotational speed will reduce size of the space available for natural convection eddies. Which in return will affect the heat transfer as discussed later.

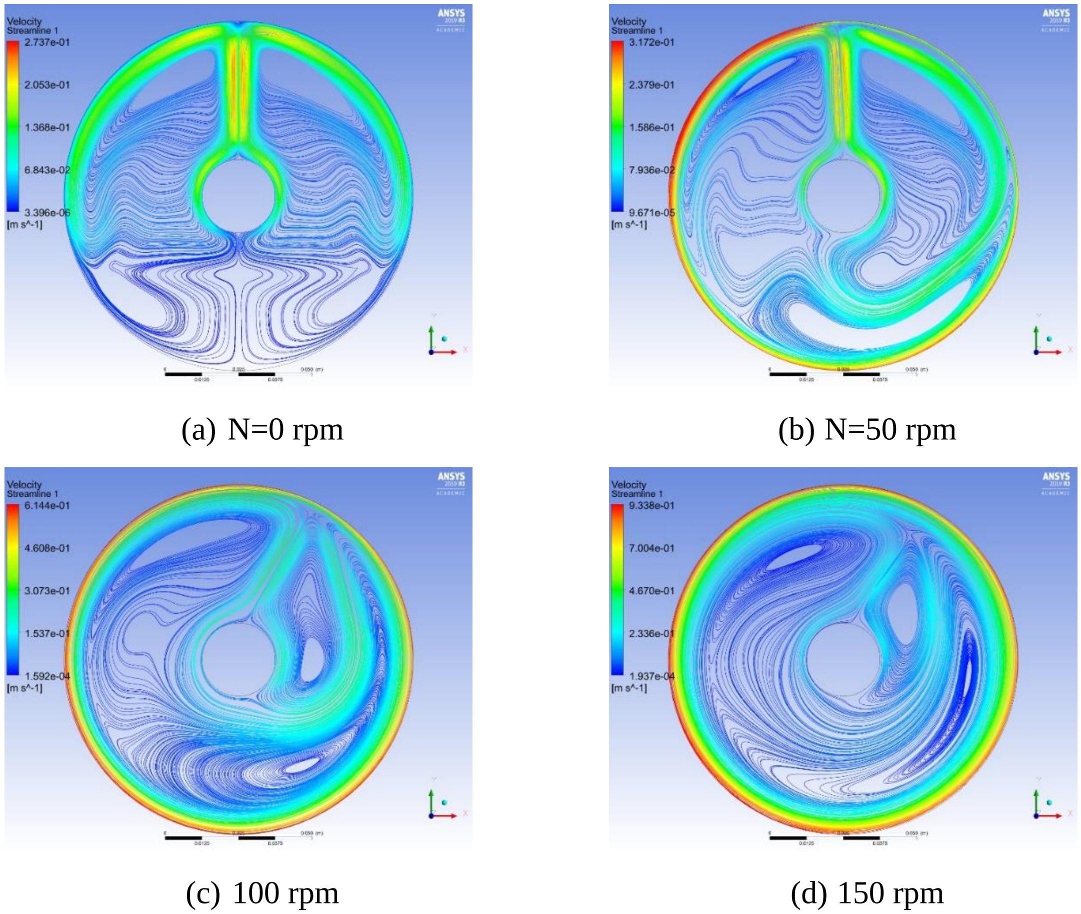

Figure 2.9 Effect of rotational speed on streamlines within the annular space for OV= 0% case

The effect of N on the rate of heat transfer within the system is indicated by results shown in Table 2-2. Increasing N resulted in a decrease in the average temperature of the outer cylinder (the drum). This decrease was expected due to the resulted enhancement in the rate of heat transfer from the outer cylinder to ambient air as N is increased. This trend is consistent with results reported in the literature. However, all other parameters listed in Table 2-2 encountered a different trend.

The annular space average and maximum temperatures and the average temperature of the inner cylinder decreased as N was increased from 0 to 50 rpm. However, all the three temperatures increased as N was increased from 50 to 150. A similar trend was observed for the average Nusselt number from the inner cylinder. This trend is due to the change in the heat transfer inside the annular space caused by drum rotation. Although the heat transfer coefficient from the drum to ambient increased with N. But changes in flow and thermal fields within the annular space resulted in reduction in the Nusselt number around the inner cylinder. Nu increased from 8.3 at N = 0 to 9.3 at N = 50 rpm (by ~12%). However, as N was further increased from 50 to 100, and then to 150, Nu decreased to 8.9 (~4%) and to 7.2 (~22%), respectively.

Increasing drum rotational speed caused an increase in the boundary layer thickness developed around the drum inner surface, as shown in Figure 2.10. The thickening of the thermal boundary layer as N was increased is also evident from temperature distributions shown in Figure 2.11. The contradicting change in the Nusselt number around the inner cylinder with N is due to two conflicting effects. The first is the enhancement in the heat transfer coefficient from the drum to ambient air resulted as N was increased. The second is since increasing N resulted in a thicker boundary layer forming along the inner surface of the drum. So that, it resulted in a decrease in the natural convection from the motor surface. The first effect appeared to be dominant when N was increased from 0 to 50, which resulted in the observed increase in Nu. The second effect became more dominant as N was further increased from 50 to 150, resulting in a significant decrease in Nu. It is worth noting here that results presented in Table 2-2 are for the case of OV= 0%. Therefore, the nonlinear behavior discussed above is expected to change as the oil level is changed from 0 to 100%, which demonstrates the level of complexity of the problem at hand.

Table 2-2 Effect of rotational speed on the heat transfer within the annular space for the case of OV= 0 %.

OV (%)	0%			
N (rpm)	0	50	100	150
$T_{av,i,oc}$ (°C)	118.5	96	73.5	66.5
$T_{av,as}$ (°C)	170.9	139.2	150.2	187.1
T_{max} (°C)	591.4	514.8	540.6	565.7
$T_{av,o,ic}$ (°C)	389.6	336.9	355.9	442.5
$Nu_{av,o,ic}$	8.3	9.3	8.9	7.2
$h_{o,oc}$ (W/m^2°C)	4.5	5.9	8.1	9.9

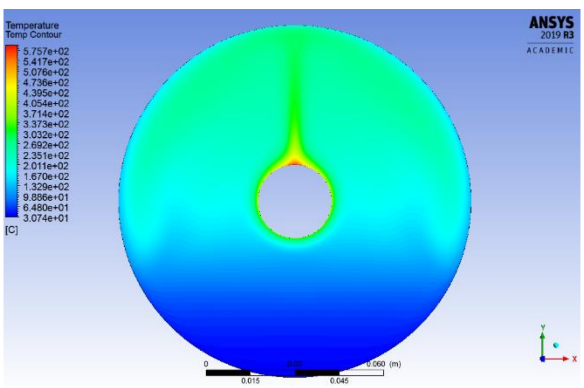

(a) N=0 rpm

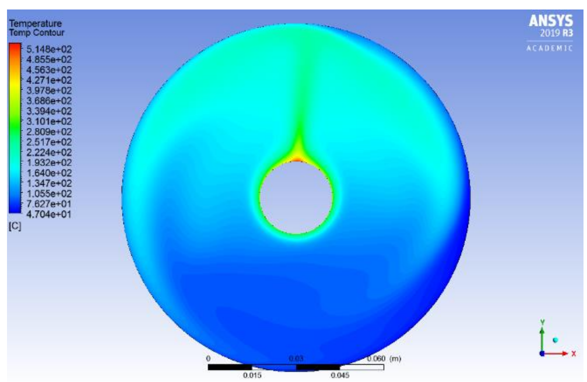

(b) N=50 rpm

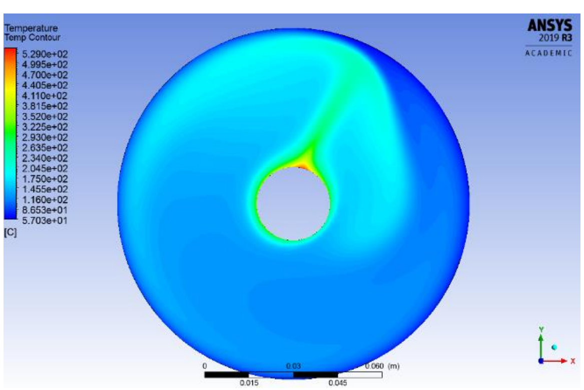

(c) 100 rpm

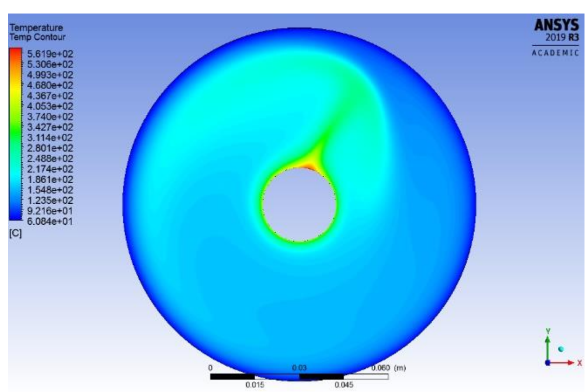

(c) 150 rpm

Figure 2.10 Effect of rotational speed on temperature distribution within the annular space for OV= 0 %.

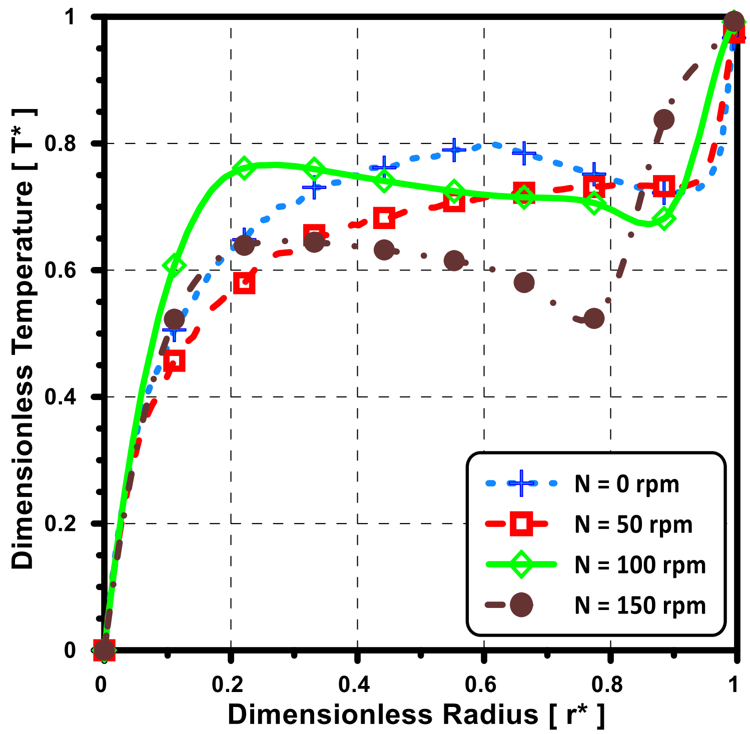

Dimensionless temperature distribution as function of N along a line at θ = 90° placed inside the annular space.

Figure 2.11 Effect of rotational speed on thermal boundary layer for OV = 0%.

Increasing the rotational speed also affected the location of the maximum temperature along the inner cylinder surface, as shown in Figure 2.12. At N = 0, due to symmetry, maximum temperature occurred at θ = 90°. When the rotational speed was increased, the location of maximum temperature shifted in the direction opposite to the direction of rotation. So that it occurred at θ = 75°. Which is consistent with the observed change in size of the right-side eddy, discussed before and shown in Figure 2.9.

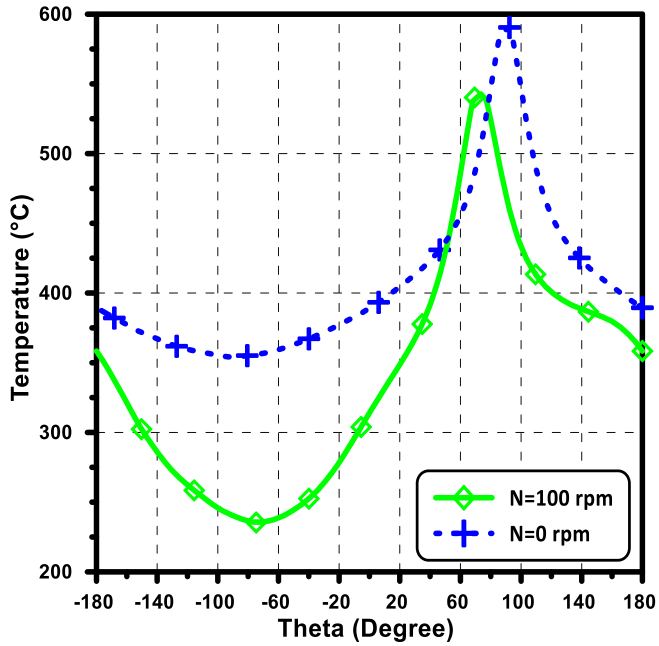

Figure 2.12 Effect of rotational speed on temperature distribution along inner cylinder (motor) surface for case of OV = 0 %.

2.5.2. Case of oil only, OV = 100%

Results indicating the effect of rotational speed, N, on the heat transfer inside the system for the case of OV = 100% are presented in Table 2-3 and Figure 2.13.

Table 2-3 Effect of rotational speed on the heat transfer within the annular space for the case of OV=100 %

OV (%)	100%	
N (rpm)	50	150
$T_{av,i,oc}$ (°C)	97.1	67.3
$T_{av,as}$ (°C)	113.9	101.5
T_{max} (°C)	138.2	145.6
$T_{av,o,ic}$ (°C)	131.8	142.4
$Nu_{av,o,ic}$	13.9	8.3

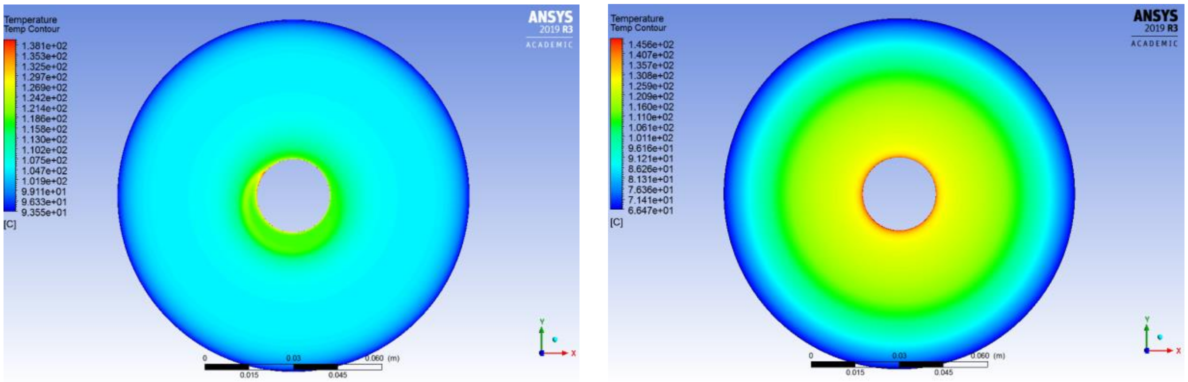

(a) N=50 rpm (b) 150 rpm

Figure 2.13 Effect of rotational speed on temperature distribution within the annular space for OV=100 case

The heat transfer within the system is significantly enhanced in the case of OV = 100% compared to the case of OV = 0%. At N = 50, the average Nusselt number around the inner cylinder has increased by about 50%; from 9.3 for OV =0 % to 13.9 for OV = 100%. This significant enhancement in the Nusselt number is attributed to higher thermal conductivity and thermal diffusivity of oil than that of air. Consequently, the maximum and average temperatures of the inner cylinder have been greatly reduced from 514.8 °C to 138.2 °C and from 336.9 °C to 131.8 °C, respectively. The observed decrease in the outer cylinder average temperature and in the Nusselt number within the system as N was increased from 50 to 150 is due to the two effects discussed before in section 2.5.1.

2.5.3. Cases of 0% < OV < 100%

Oil flow and heat transfer within the annular space are expected to be significantly affected by the outer cylinder rotational speed and by the oil level within the system. A significant enhancement in the heat transfer from the inner cylinder can be achieved. This will happen if enough oil can be dragged by the drum and splashed on the surface of the inner cylinder. However, the amount of dragged oil would depend on the magnitude of the drum rotational speed and on oil level.

Figure 2.14 shows distribution of oil fraction within the system for the case of OV = 64% and N = 50 rpm. These results indicated that, at such relatively low rotational speed, viscous drag and centrifugal force are not able to overcome the effect of gravity. So that, no oil was dragged along drum surface. Therefore, at such low rotational speeds, maximum temperatures remained high. No cooling due to oil splashing over the inner cylinder was attainable.

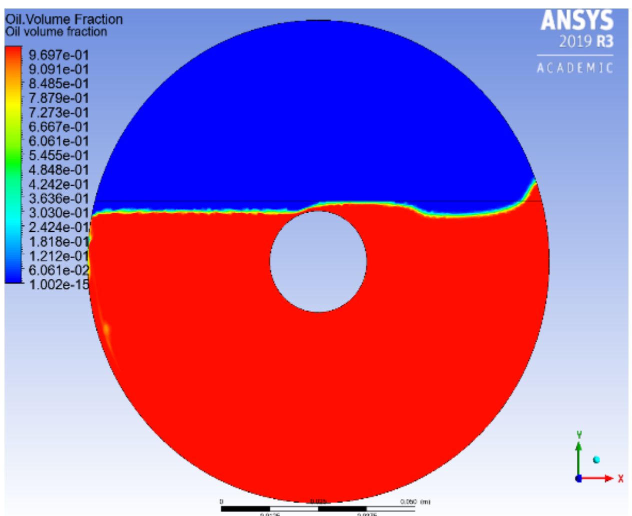

Figure 2.14 Oil volume fraction distribution for N = 50 rpm and OV=64% at steady state

Even at high rotational speeds, i.e., N = 150 rpm, oil splashing might not be possible. If oil level is too low or too high, as shown in Figure 2.15a and c, for the cases of OV = 42% and 86%, respectively.

For case of OV = 42%, the oil present is not sufficient to entirely cover the inner cylinder. While in case of OV = 86%, the amount of oil is too much as it completely covers the inner cylinder. So, all the splashing happening in this case is far away from cooling the inner cylinder properly by forced oil flow. Therefore, the optimum oil level is reached when oil free surface is almost covering the inner cylinder. This level corresponds to OV = 64% for the SCDM drive system considered in this study.

Figure 2.15b shows oil distribution for the case of OV = 64% and N = 150 rpm, illustrating the best combination of oil level and rotational speed for the present SCDM drive system. A significant amount of oil has been dragged along the drum surface. Oil splashing over the inner cylinder has taken place. Consequently, the heat transfer within the system has been significantly enhanced, as indicated by temperatures and Nu values shown in Table 2-4.

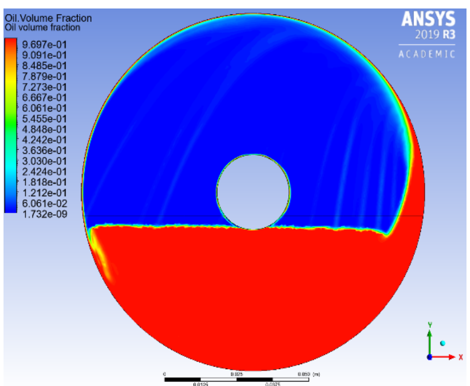

(a) OV= 42%

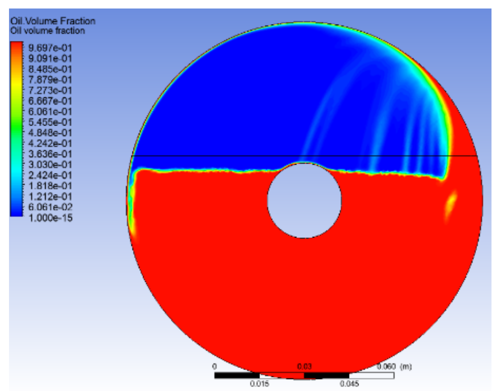

(b) OV= 64%

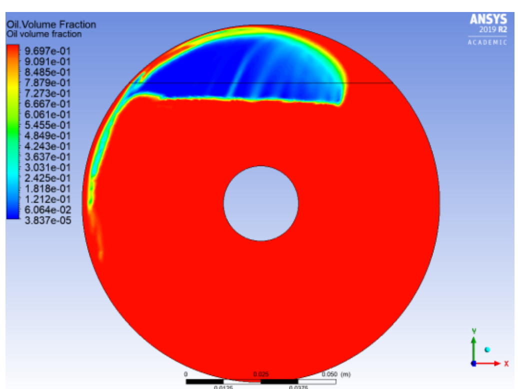

(c) OV= 86%

Figure 2.15 Oil volume fraction distribution at N=150 rpm for different oil levels.

Table 2-4 Effect of OV on the heat transfer within the gap for the case of N = 150 rpm.

OV (%)	0 %	42 %	**64 %**	86 %	100 %
$T_{av,as}$ (°C)	187.1	70.4	**69.9**	70.5	101.5
T_{max} (°C)	565.7	95.1	**87.8**	88.2	145.6
$T_{av,o,ic}$ (°C)	442.5	76.8	**74.9**	79.2	142.4
Br	1.6e-6	0.0256	**0.0197**	0.0124	7.6e-4
$Nu_{av,o,ic}$	7.2	54.1	**66.9**	39.8	8.3
$h_{o,ic}$ (W/m^2. °C)	10.7	282.9	**374.5**	222.9	46.7

The case of OV = 64 % and N = 150 rpm resulted in the best thermal performance within the system. It gave the highest heat transfer coefficient over the inner cylinder surface, the lowest maximum oil temperature, and the lowest average inner cylinder temperature. In this case, the amount of oil was not large enough to entirely submerge the inner cylinder. Where submerging the inner cylinder will prevent forced convective cooling from oil splashing. As in the case of OV = 86% and 100%, the thermal performance deteriorates due to the lack of motion surrounding the inner cylinder as in Figure 2.15c.

At the same time, the amount of oil in case of OV=64% was not too low so that the inner cylinder was mainly cooled by conduction and natural convection through air. As in the case of OV = 42% where the inner cylinder is not cooled sufficiently by oil as shown in Figure 2.15a. Therefore, at OV =64% cooling of the inner cylinder was due to a combination of forced and natural convection through oil. Figure 2.16 shows oil velocity vectors at steady state for the case of OV = 64% and N = 150 rpm. Figure 2.16 clearly shows oil splashing on the inner cylinder top surface. So that, the inner cylinder is now being cooled by forced convection from oil splashing over the top surface.

In case of OV=86%, the amount of oil is very large to completely submerge the inner cylinder as shown in Figure 2.15c. Consequently, the oil splashing is not reaching the inner cylinder and no fluid motion is reaching it. In that case the inner cylinder is being cooled by natural convection only. The same happened in case of OV=100% in addition to the increase of the viscous dissipation coming from viscous oil.

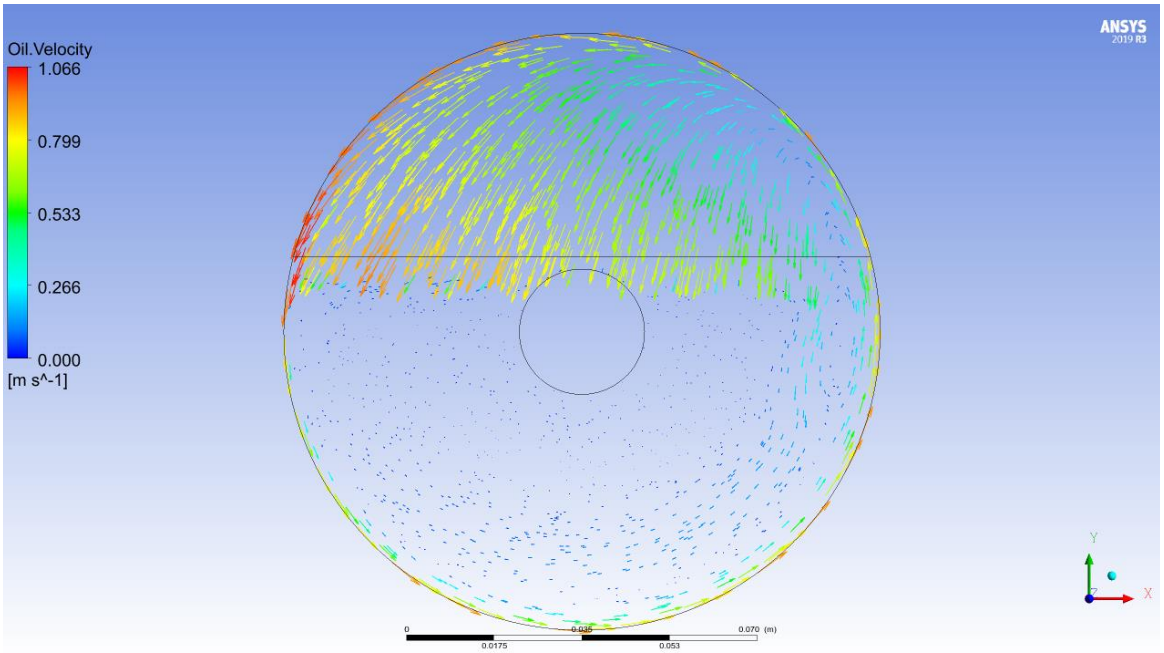

Figure 2.16 Velocity vectors at N=150 and OV=64% at steady state

As discussed above, because oil splashing depends on both oil level and rotational speed. The combined effect of these parameters on the heat transfer coefficient around the inner cylinder surface was investigated. Results are presented in Figure 2.17. At N = 150 rpm, the optimum oil level corresponded to OV equal to about 60%. At lower rotational speeds, the heat transfer coefficient has significantly decreased. Especially for OV < 50%, in which case a large portion of the inner cylinder was subjected to air and no oil splashing was attainable.

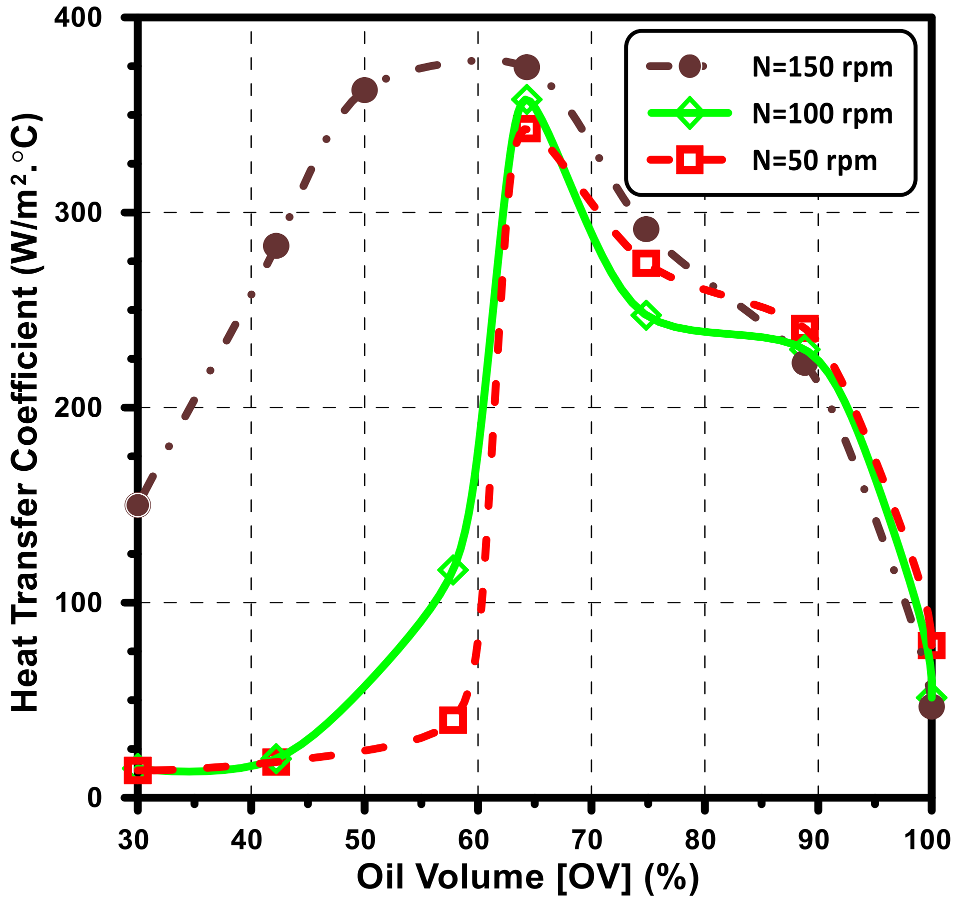

Figure 2.17 Effect of OV % and rotational speed on the heat transfer coefficient around the inner cylinder

At N=100 and 50 rpm, the optimum oil level was about 64% and as mentioned before no oil splashing was attainable. In these cases, a sufficient amount of oil was needed in order to have the inner cylinder completely covered with oil. So that heat transfer from the inner cylinder is through natural convection and conduction through oil, rather than air.

Figure 2.18 shows oil volume fraction distribution at N = 50 rpm and OV = 64, 75, and 86%. When the amount of oil corresponded to OV > 64%, almost no oil movement was observed near the inner cylinder surface. Convection was completely suppressed, which resulted in a significant deterioration in the heat transfer coefficient around the inner cylinder.

In case of OV=64% and 50 rpm as in Figure 2.18a, the inner cylinder is covered by oil. But this case is much better than OV= 86% as the free surface between oil and air is very near to the inner cylinder in case of OV= 64%. The benefit of having this free surface near to the inner cylinder is that it has wavy motion. Which in return will enhance the heat transfer due to cooling by forced convection rather than by natural convection in cases of OV>64%.

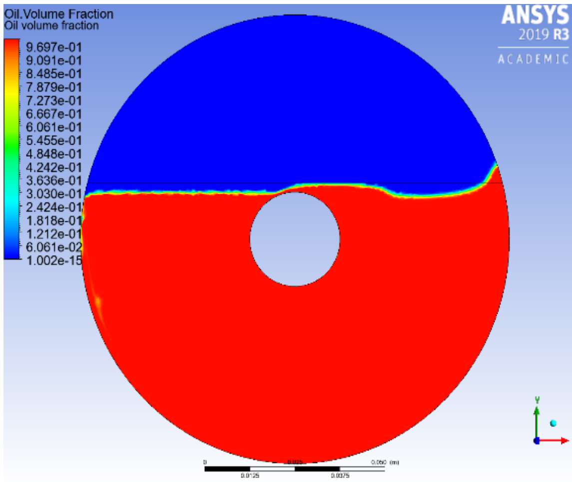

a) OV= 64%

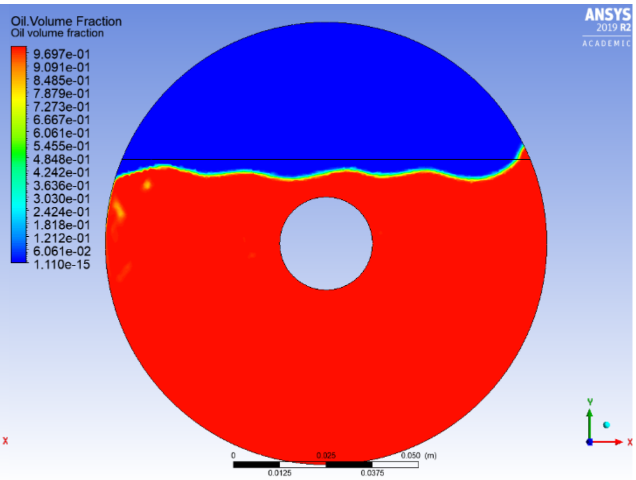

b) OV= 75%

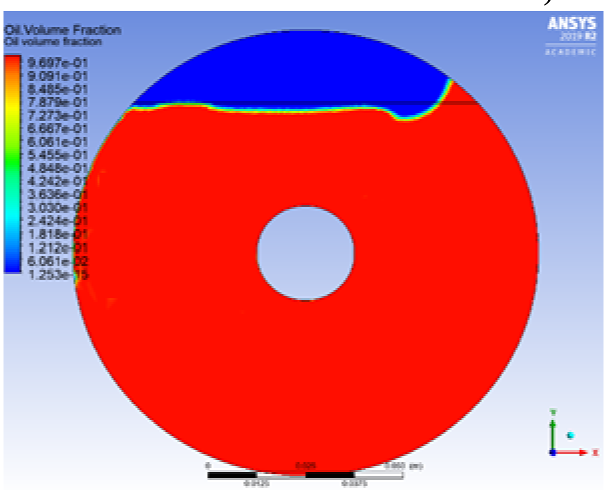

c) OV= 86%

Figure 2.18 Distribution of oil volume fraction at N=50 rpm for different OV cases.

2.6 Heat Transfer Correlation

A correlation of the inner cylinder average Nusselt number as function of rotational Reynolds number and OV has been developed and is presented in equation (24).

$$Nu = 9.3 + 3.2 * 10^{-7}\, OV \times Re^2\, (1 - 0.0103 \times OV) + (OV - 87.7)\sin\left((3.3342 * 10^{-9})\, OV^2 \times\, Re^3\right) \qquad (24)$$

The rotational Reynolds number is defined in equation (25). Oil properties used in equation (25) have been determined at oil average temperature.

$$Re = \frac{\pi N {r_o}^2}{30\nu} \qquad (25)$$

It is worth noting here that the harmonic function in equation (24) had to be used to capture the observed nonlinear dependency of the rate of heat transfer on drum rotational speed and oil level. This correlation has been developed for rotational Reynolds number in the range from 1600 to 10,000 and $30 < OV \leq 100$ % and it gives a mean absolute error of 5 %. This correlation provides a useful tool that can be used to determine the optimum oil level at a given rotational speed.

The correlation of equation (24) is shown in 3-D map as in Figure 2.19. Where the optimum conditions are at OV=57% and Re=10000.

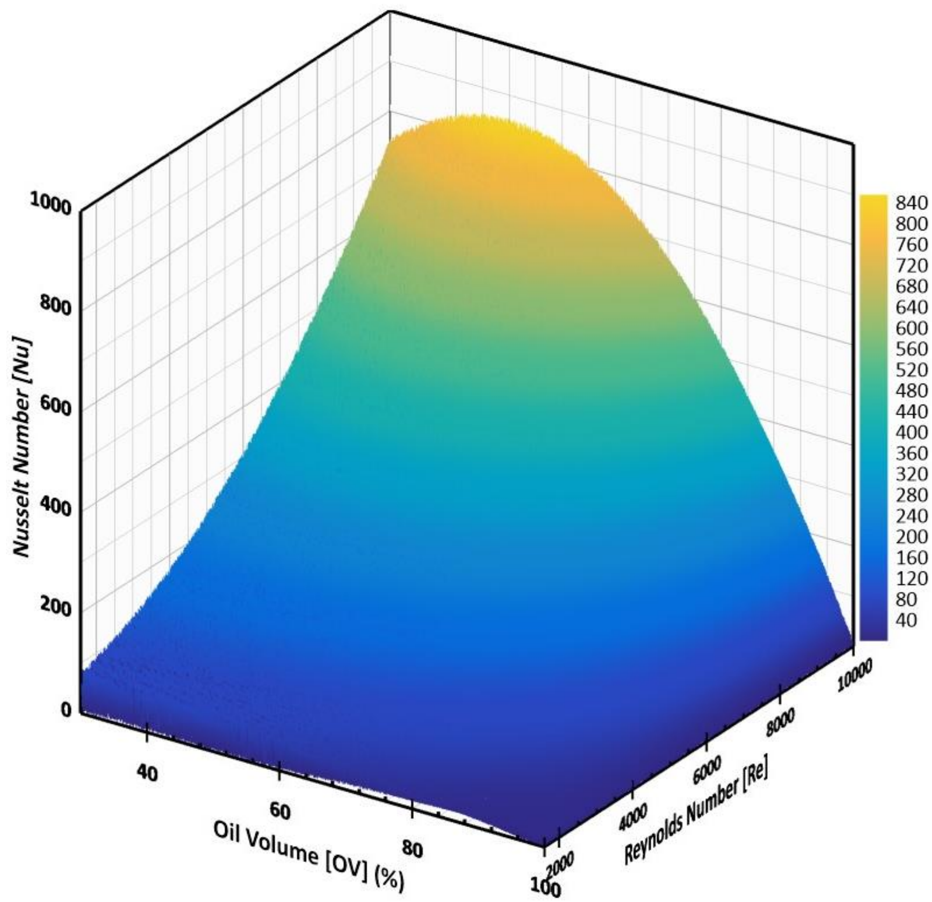

Figure 2.19 A 3D Map of the developed correlation presented in equation (24).

2.7 Conclusion

Flow and heat transfer of a multiphase Taylor-Couette flow that occurs within self-contained drum motor (SCDM) drive systems has been investigated numerically. Results of the single-phase cases considering 100% air and 100% oil have been presented and discussed. Our single-phase cases results indicated that increasing drum rotational speed would have a significantly negative effect on the thermal performance of SCDM drive systems having a small radius ratio (0.21). Since in this case, the cooling of the inner cylinder is primarily due to natural convection, increasing drum rotational speed causes a thicker boundary layer to develop over the inner surface of the rotating cylinder. So, increasing the rotational speed in the single-phase cases causes a deterioration of heat transfer around the inner cylinder. The case of 100% oil is significantly better than 100% air, due to the higher thermal conductivity of oil.

Results of the multiphase cases indicated that, the thermal performance of the SCDM drive system would significantly deteriorate if the annular space was completely filled with oil compared to the multiphase case. Also, increasing drum rotational speed enhances heat transfer inside the annular space. The best thermal performance of the SCDM drive system can be achieved by maintaining oil at an optimum oil level, which depends on drum rotational speed. The Nusselt number within the system has been correlated as a function of drum rotational speed and oil level. The proposed correlation can be used as a design tool to optimize the system thermal performance by determining the optimum oil level at a given rotational speed.

2.8 Acknowledgment

The authors would like to acknowledge financial and technical provided by Van der Graaf Inc. and financial support received from Mathematics of Information Technology and Complex Systems (MITACS).

2.9 References

[1] *Van der Graaf Drum Motors*. Available: https://www.vandergraaf.com/

[2] B. Özerdem, "Measurement of convective heat transfer coefficient for a horizontal cylinder rotating in quiescent air," *International Communications in Heat and Mass Transfer*, vol. 27, no. 3, pp. 389-395, 2000/04/01/ 2000.

[3] H. Ma *et al.*, "Experimental investigation on the steady, external laminar mixed convection heat transfer characteristics around a large diameter horizontal rotating cylinder," *International Communications in Heat and Mass Transfer*, vol. 57, pp. 239-246, 2014/10/01/ 2014.

[4] J. T. Anderson, O. A. Saunders, and G. I. Taylor, "Convection from an isolated heated horizontal cylinder rotating about its axis," *Proceedings of the Royal Society of London. Series A. Mathematical and Physical Sciences*, vol. 217, no. 1131, pp. 555-562, 1953/05/21 1953.

[5] C. C. Chiou and S. L. Lee, "Forced convection on a rotating cylinder with an incident air jet," *International Journal of Heat and Mass Transfer,* vol. 36, no. 15, pp. 3841-3850, 1993/10/01/ 1993.

[6] R. E. M. Morales, A. Balparda, and A. Silveira-Neto, "Large-eddy simulation of the combined convection around a heated rotating cylinder," *International Journal of Heat and Mass Transfer,* vol. 42, no. 5, pp. 941-949, 1999/03/01/ 1999.

[7] B. Farouk and K. S. Ball, "Convective flows around a rotating isothermal cylinder," *International Journal of Heat and Mass Transfer,* vol. 28, no. 10, pp. 1921-1935, 1985/10/01/ 1985.

[8] Y. Y. Yan and Y. Q. Zu, "Numerical simulation of heat transfer and fluid flow past a rotating isothermal cylinder – A LBM approach," *International Journal of Heat and Mass Transfer*, vol. 51, no. 9, pp. 2519-2536, 2008/05/01/ 2008.

[9] V. T. Morgan, "Heat Transfer by Natural Convection from a Horizontal Isothermal Circular Cylinder in Air," *Heat Transfer Engineering,* vol. 18, no. 1, pp. 25-33, 1997/01/01 1997.

[10] B. G. Van Der Hegge Zijnen, "Heat transfer from horizontal cylinders to a turbulent air flow," *Applied Scientific Research, Section A*, vol. 7, no. 2, pp. 205-223, 1958/03/01 1958.

[11] C. D. Andereck, S. S. Liu, and H. L. Swinney, "Flow regimes in a circular Couette system with independently rotating cylinders," *Journal of Fluid Mechanics*, vol. 164, pp. 155-183, 1986.

[12] P. S. Marcus, "Simulation of Taylor-Couette flow. Part 1. Numerical methods and comparison with experiment," *Journal of Fluid Mechanics*, vol. 146, pp. 45-64, 1984.

[13] P.-T. Hsu, "The inverse estimation of the thermal behavior and the viscosity of fluid between two horizontal concentric cylinders with rotating inner cylinder," *Applied Thermal Engineering*, vol. 28, no. 5, pp. 380-387, 2008/04/01/ 2008.

[14] N. Hasan and S. Sanghi, "The Dynamics of Two-Dimensional Buoyancy Driven Convection in a Horizontal Rotating Cylinder," *Journal of Heat Transfer*, vol. 126, no. 6, pp. 963-984, 2005.

[15] J.-S. Yoo, "Mixed convection of air between two horizontal concentric cylinders with a cooled rotating outer cylinder," *International Journal of Heat and Mass Transfer*, vol. 41, no. 2, pp. 293-302, 1998/01/01/ 1998.

[16] D. Paghdar, S. Jogee, and K. Anupindi, "Large-eddy simulation of counter-rotating Taylor–Couette flow: The effects of angular velocity and eccentricity," *International Journal of Heat and Fluid Flow*, vol. 81, p. 108514, 2020/02/01/ 2020.

[17] D. Alshahrani and O. Zeitoun, "Natural convection in air-filled horizontal cylindrical annuli," *Alex Eng J*, vol. 44, 11/01 2005.

[18] T. Fusegi, B. Farouk, and K. S. Ball, "MIXED-CONVECTION FLOWS WITHIN A HORIZONTAL CONCENTRIC ANNULUS WITH A HEATED ROTATING INNER CYLINDER," *Numerical Heat Transfer,* vol. 9, no. 5, pp. 591-604, 1986/05/01 1986.

[19] F. Tachibana, S. Fukui, and H. Mitsumura, "Heat Transfer in an Annulus with an Inner Rotating Cylinder," *Bulletin of JSME,* vol. 3, no. 9, pp. 119-123, 1960.

[20] F. Moukalled and S. Acharya, "Natural convection in the annulus between concentric horizontal circular and square cylinders," vol. 10, no. 3, pp. 524-531, 1996.

[21] S. Jangili, N. Gajjela, and O. Anwar Bég, "Mathematical modeling of entropy generation in magnetized micropolar flow between co-rotating cylinders with internal heat generation," *Alexandria Engineering Journal,* vol. 55, no. 3, pp. 1969-1982, 2016/09/01/ 2016.

[22] M. Sheikholeslami, P. Jalili, and D. D. Ganji, "Magnetic field effect on nanofluid flow between two circular cylinders using AGM," *Alexandria Engineering Journal,* vol. 57, no. 2, pp. 587-594, 2018/06/01/ 2018.

[23] M. Sheikholeslami, M. Nimafar, and D. D. Ganji, "Nanofluid heat transfer between two pipes considering Brownian motion using AGM," *Alexandria Engineering Journal,* vol. 56, no. 2, pp. 277-283, 2017/06/01/ 2017.

[24] S. Chatterjee, G. Sugilal, and S. V. Prabhu, "Heat transfer in a partially filled rotating pipe with single phase flow," *International Journal of Thermal Sciences,* vol. 125, pp. 132-141, 2018/03/01/ 2018.

[25] A. Nouri-Borujerdi and M. E. Nakhchi, "Heat transfer enhancement in annular flow with outer grooved cylinder and rotating inner cylinder: Review and experiments," *Applied Thermal Engineering,* vol. 120, pp. 257-268, 2017/06/25/ 2017.

[26] G. A. Etemad, *Free convection heat transfer from a rotating horizontal cylinder to ambient air: with interferometric study of flow*. University of California, Berkeley, 1954.

[27] *Oil Enduratex EP 150*. Available: https://lubricants.petro-canada.com/en-ae/brand/enduratex-ep#4c438c61-0a61-4851-b43d-b1bfffe8539d

[28] C. J. S. t. g. ANSYS, ANSYS, "Release 12.0 User's guide," 2009.

[29] P. K. Kundu and I. M. Cohen, *Fluid Mechanics: Fourth Edition* (Fluid Mechanics: Fourth Edition. Edited by Pijush K. Kundu and Ira M. Cohen with contributions by P. S. Ayyaswamy and H. H. Hu. ISBN 978-0-12-373735-9. Published by Academic Press). 2008.

[30] F. M. White and I. Corfield, *Viscous fluid flow*. McGraw-Hill New York, 2006.

Chapter 3

Numerical and Experimental Study of a Multiphase Flow Inside a Self-Contained Drum Motor Drive System

Chapter 3

Numerical and Experimental Study of a Multiphase Flow Inside a Self-Contained Drum Motor Drive System

Relative Contributions:

Ahmed M. Teamah: Wrote the first draft of the manuscript.

Mohamed S. Hamed: Revised and edited the manuscript.

Numerical and Experimental Study of a Multiphase Flow Inside a Self-Contained Drum Motor Drive System

Ahmed M. Teamah* and Mohamed S. Hamed

Thermal Processing Laboratory, Department of Mechanical Engineering,

McMaster University, Hamilton, Ontario, Canada

*Corresponding Author: teamaha@mcmaster.ca, Tel: +1 905-920-6960

Abstract

The multiphase Taylor-Couette flow of air and oil enclosed within the annular space between two concentric cylinders has been studied experimentally and numerically. The outer cylinder rotates at a constant speed and exchanges heat by convection and radiation with ambient air. The inner cylinder is stationary and subjected to a constant uniform heat flux. Such flow can be found in a self-contained drum motor drive system (SCDMDS). The heat flux imposed on the inner cylinder mimics the amount of heat generated due to several thermal losses within the SCDMDS. A layer of lagging material is sometimes added to the outer cylinder to enhance belt traction.

The effect of the inner-to-outer cylinder radius ratio (RR), Reynolds number (Re), oil volume (OV), outer cylinder surface emissivity (ε), and lagging material thickness (δ) on the flow and heat transfer between the two cylinders and the ambient has been investigated considering a quasi-steady state analysis. The current investigation considered the following ranges found in a typical SCDMDS: RR = 0.35 - 0.85, Re = 200 - 3000, OV = 50 - 100%, ε = 0 - 0.95, and δ

= 0 - 100 mm. The numerical part of the present study has been carried out using ANSYS-CFX software package. The numerical results have been validated using experimental data.

Results indicated that increasing RR, Re and ε enhanced the heat transfer within the SCDMDS. The rate of heat transfer within the annular space reached its highest value at OV = 65% above which the rate of heat transfer is deteriorated. Because the lagging material is acting as an insulation over the outer cylinder, a critical thickness of δ = 35 mm resulted in the minimum overall resistance above which the rate of heat transfer is deteriorated.

The parametric study revealed that the best overall thermal performance was attained at RR = 0.85, Reynolds number = 3000, OV = 65%, ε = 0.95 and δ = 35 mm. In this case, the heat transfer coefficient between the inner cylinder and the oil reached its highest value of 410 W/m^2. °C, giving the lowest possible inner cylinder temperature. A correlation of Nusselt number in terms of the geometrical and operating parameters of a SCDMDS considered in the current study has been developed and validated. The developed correlation gave a maximum deviation of ± 8 %.

Keywords: Multiphase Taylor-Couette flow, Self-contained Drum Motor Drive System, Thermal Performance, Rotating Cylinders.

Nomenclature

Br	Brinkman number, $\mu(\omega^* R_{is,oc})^2 / k\ (T_{os,ic}-T_{is,oc})$.
D	Diameter, m.
Gr	Grashof number, $\frac{g\beta(T_{os,oc}-T_{amb})D_{os,oc}{}^3}{\nu^2}$
g	Gravitational acceleration, 9.81 m/sec^2.
h	Heat transfer coefficient, W/m^2. °C
h_{tot}	Specific total enthalpy, J/kg
k	Thermal conductivity, W/m.°C.
N	Rotational speed, rpm.
Nu	Nusselt number, $h\ D_{is,oc} / k$
OV	Oil volume percentage inside the annular area, %.
p	Static pressure, Pa.
Pr	Prandtl number, ν/α.
q”	Amount of heat per unit surface area, W/m^2
Q	Amount of heat, W.
R	Radius, m.

Re	Reynolds number, $\frac{\omega R_{is,oc}(R_{is,oc}-R_{os,ic})}{\nu}$
Re_o	Outside Reynolds number, $\frac{\omega {D_{Lag}}^2}{2\nu}$
RR	Radius ratio, $R_{os,ic}/R_{is,oc}$
t	Time, Second.
Ta	Taylor number, $\omega^2 R_o (D_h/2)^3/\upsilon^2$
T	Temperature, °C.
u	Velocity components (u_Θ, u_R, u_Z), m/sec.
U	Velocity vector, m/sec.

Greek symbols

α	Thermal diffusivity, m^2/sec.
β	Thermal expansion coefficient, 1/K.
δ	Lagging thickness, mm.
ε	Surface emissivity.
θ	Angle, °.
μ	Dynamic viscosity, kg/m. s.
ν	Kinematic viscosity, m^2/s.

ρ	Density, kg/m^3
τ	Shear stress tensor, N/m^2
ω	Angular speed, rad/sec.

Subscript

amb	Ambient.
av	Average.
as	Annular space.
Lag	Lagging.
oc	Outer cylinder.
is	Inner surface.
max	Maximum value.
ic	Inner cylinder.
os	Outer surface.
w	Wall.

3.1 Introduction

The main components of a self-contained drum motor drive system (SCDMDS) are shown in Figure 3.1. The optional lagging material, which is a layer of rubber material sometimes added over the outer surface of the drive drum to increase traction with the belt and avoid slippage, is not shown in Figure 3.1. Compared to the conventional open drive systems, a SCDMDS eliminates any cross contamination, hence, it is the preferred drive system type in the food and the pharmaceutical industries. In addition, the direct power transmission from the electric motor to the driving drum in a SCDMDS is more efficient than using a belt drive in a conventional open drive system. Despite its clean environment, the SCDMDS sometimes experiences a serious overheating problem that leads to its premature failure. The overheating problem is caused by several heat sources contained within the SCDMDS, such as thermal losses within the electric motor and the gear train and due to viscous dissipation within the lubricating oil. The lagging material, when used, inhibits the rate of heat transfer to ambient, which aggravates the overheating problem even further. In addition, the amount of heat rejected to the ambient through the rotating drum depends on the drum's rotational speed which is set according to the required rate of materials handling. So, the interplay of the various geometrical and operating parameters of a typical SCDMDS and their contribution to its overall thermal performance (overheating) must be investigated and fully understood in order to determine the optimum conditions that would result in the best possible thermal performance.

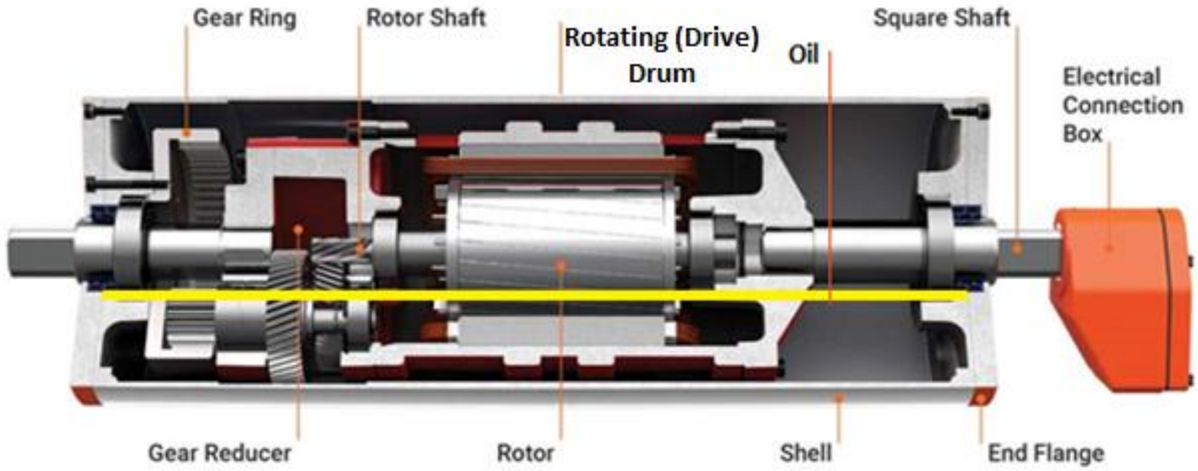

Figure 3.1 Main components of a typical SCDMDS [1]

3.2 Literature Review

Various studies of flow and heat transfer in configurations relevant to a typical SCDMDS can be found in the literature.

Özerdem [2] and Ma, et al. [3] investigated the rate of heat transfer from a rotating heated cylinder to ambient air; by natural convection [2] and by mixed convection [3]. They found that the rate of heat transfer dramatically increased by increasing the cylinder's rotational speed. Özerdem [2] developed a correlation of the Nusselt number in terms of the rotational Reynolds number, in the range of 2000 – 40,000.

Becker [4] carried out a similar study to that of [2] and [3], however, he investigated the effect of the heated cylinder's rotational speed on the rate of heat transfer to ambient water. His study covered a range of rotational Reynolds number of 1000 - 46,000 and Prandtl number of 2.2 - 6.4. Becker developed a correlation of his results and concluded that natural convection was negligible within the range of parameters considered in his study. Anderson, et al. [5] studied the same problem considering ambient air , however, they considered a smaller value of the rotational Reynolds number of 90, in which case the dominant mode of heat transfer was natural convection. They considered the effect of air pressure surrounding the rotating cylinder, up to 4 atm and found that for Reynolds numbers above $1.09 \times Gr^{1/2}$, the effect of natural convection became negligible, and the rate of heat transfer was mainly due to forced convection. The value of Grashof (Gr) number considered in [5] ranged between 4.9×10^4 and 5.4×10^6.

Elghnam [6] carried out an experimental and numerical study using ANSYS-Fluent to investigate the rate of heat transfer of a small rotating cylinder placed in still air. The rotational Reynolds number (Re) and Grashof number (Gr) varied from 0 to 10^5 and 100 to 10^6, respectively. Elghnam investigated the local Nusselt number around the cylinder. The maximum and minimum local Nusselt number values in the case of a stationary cylinder were located at the bottom and top stagnation points. As the rotational speed was increased, these values shifted in the direction of rotation and the difference between them decreased until it became approximately zero at Re = 2500. The average Nusselt number was found to be independent of Gr number for Re greater than 8000.

Badr and Dennis [7] numerically studied forced convection from a rotating horizontal cylinder subjected to a perpendicular forced airflow. The value of the forced air velocity corresponded to Reynolds number up to 10^2. They observed that the rate of heat transfer was adversely affected by the cylinder rotation due to flow separation.

Many researchers, e.g., Van Der Hegge Zijnen [8], Yan and Zu [9], Morgan [10], Morales, et al. [11], Farouk and Ball [12] and Chiou and Lee [13], investigated the rate of heat transfer from a rotating cylinder placed in a still air or subjected to an axial external airflow. They concluded that increasing the rotational speed enhanced the rate of natural convection to the surrounding air and that increasing the axial external air flow increased the rate of heat transfer from the rotating cylinder as well.

A number of researchers investigated the flow within an annular space (gap) between two concentric cylinders, which is sometimes referred to as the Taylor-Couette flow. Yoo [14] carried out a numerical study of the Taylor-Couette flow of air between two concentric isothermal horizontal cylinders. The inner cylinder was stationary while the outer one was rotating. The radius ratio (inner-to-outer) of the two cylinders was 0.5. The inner cylinder was kept at a temperature greater than that of the outer cylinder. Yoo [14] confirmed that the Taylor-Couette flow pattern depended on the value of the rotational Reynolds number. They did not observe any eddies forming at Reynolds numbers greater than 500. However, one eddy was observed at Reynolds number between 300 and 500 and two eddies were observed at Reynolds number below 300.

The Taylor-Couette flow can develop some flow instabilities when the inner cylinder or both cylinders are rotating. Many studies have investigated the effect of the inner cylinder rotational speed, the gap thickness, and the eccentricity between the two cylinders on these instabilities, e.g., Paghdar, et al. [15], Marcus [16], Lopez, et al. [17], Andereck, et al. [18], Naseem, et al. [19], Dong [20] and Rüdiger, et al. [21]. These researchers concluded that increasing the inner cylinder rotational speed, the higher flow instabilities can be triggered by decreasing the gap width, and increasing the eccentricity resulted in higher flow instabilities.

An axial flow inside the annular gap can been superimposed on the classical Taylor-Couette flow discussed above. In this case, the flow within the gap is named the Taylor-Couette-Poiseuille flow. Fénot, et al. [22] presented a comprehensive review of heat transfer of the

Taylor-Couette-Poiseuille flows. They discussed the effect of gab thickness, inner and outer cylinder rotational speeds, and axial flow rate on the fluid flow and heat transfer. They showed that decreasing the gap thickness, adding slots on the inner or outer cylinder surface or on both, increasing the rotational speed of the inner or the outer cylinder, and increasing the axial flow rate all resulted in an increase in the rate of heat transfer within the gap.

The previously published articles on single-phase Taylor-Couette flows have shown that increasing the rotational speed of the inner or the outer cylinder enhanced the rate of heat transfer within the annular space (gap). It is worth noting here that these studies considered the cases of Taylor-Couette flows within relatively small gaps, i.e., gaps with high radius ratios (RR) ≥ 0.5. However, the heat transfer of single-phase Taylor-Couette flow at small radius ratios < 0.5 have not been studied yet although it is relevant to some SCDMDS models, hence, it requires further investigation.

Moukalled and Acharya [23], Alshahrani and Zeitoun [24], Tachibana, et al. [25] and Fusegi, et al. [26] investigated the Taylor-Couette flow, with and without the presence of an axial airflow. They found that the presence of the axial airflow resulted in an enhancement in the rate of heat transfer within the gap.

Chatterjee, et al. [27] carried out an experimental study of a two-phase flow of air and water inside a single, horizontal, rotating, heated cylinder. The cylinder was subjected to an axial water flow that did not fill its entire cross-section area. So, a two-phase flow of air and water existed inside the cylinder. The cylinder was subjected to a constant heat flux. The axial water flow rate, rotational speed and heat flux varied from 6 to 80 L/hr, 5 to 300 rpm and 799 to 12522 W/m^2, respectively. They concluded that increasing the rotational speed, the axial water flow rate or the heat flux enhanced the rate of heat transfer. They correlated their results of the average Nusselt number as function of the rotational and the axial Reynolds number and a dimensionless number representing the imposed constant heat flux.

Chatterjee, et al. [28] extended their previous experimental study [27] considering the effect of the cylinder's inclination angle (θ) on the rate of heat transfer. They varied θ between 3 and 6 degrees. They measured the local Nusselt number along the entire cylinder length. They found that increasing θ resulted in a reduced heat transfer rate. They revised their previous correlation of Nusselt number as function of the rotational and the axial Reynolds numbers (Re_r and Re_a), the dimensionless heat flux and Froude number.

In order to enhance the rate of heat transfer within a Taylor-Couette flow, Jeng, et al. [29] investigated experimentally the effect of adding a set of longitudinal ribs on the outer surface of the rotating inner cylinder. The outer cylinder was kept stationary. An air axial flow was superimposed within the gap. The axial Reynolds number and the rotational Reynolds number were varied in the ranges of 30 – 1200 and 0 – 2922, respectively. The use of the longitudinal ribs enhanced the rate of heat transfer by about 140% compared to the case of no ribs at Re_r = 2000 and Re_a = 600.

Other researchers, e.g., Nouri-Borujerdi and Nakhchi [30], studied the effect of adding grooves over the inner surface of the stationary outer cylinder, while keeping the surface of the inner rotating cylinder unchanged. The number of grooves, their aspect ratio, the Taylor number and the outer cylinder surface temperature were varied in the range of 0 - 20, 0 – 1.5, 0 - 8.36×10^6, and 50 - 90 °C, respectively. They found that increasing the number of grooves, the rotational speed and the groove aspect ratio enhanced the rate of heat transfer.

Other methods to enhance the rate of heat transfer within the Taylor-Couette flow have also been investigated by a number of researchers, e.g., Sheikholeslami, et al. [31], Jangili, et al. [32] and Sheikholeslami, et al. [33]. They considered the use of magnetic fields or adding nanoparticles to the main flow.

The above literature review indicates that many investigations have been carried out considering some aspects of the integrated, multi-physics flow and heat transfer problem in a typical SCDMDS. However, to the best of the authors' knowledge, there has not been any studies that considered a multi-phase flow and heat transfer inside an annular space between a stationary heated inner cylinder and a rotating outer cylinder, except the authors' previous study, Teamah and Hamed [34], in which the radius ratio (RR) was kept constant at 0.21.

Since the RR is an important geometrical feature that is typically varied in various SCDMDS models, the effect of RR has been investigated in the present study considering both single-phase and multi-phase flows. The effect of the lagging material and the emissivity of the outer cylinder surface on the overall thermal performance of a typical SCDMDS has also been studied.

3.3 Problem Definition

The problem of interest considers a multiphase (air and oil) flow and heat transfer within an annular space (gap) between two concentric cylinders. The inner cylinder (motor stator) is stationary and subjected to a constant heat flux that represents the rate of heat generated within a typical SCDMDS. The outer cylinder (drive drum) is rotating at a constant speed, as dictated by the required rate of materials handling, and exposed to ambient air or covered with a layer of a lagging material to enhance belt traction. Figure 3.2 shows a cross-sectional view of the configuration of the present problem.

The value of the heat flux applied to the inner cylinder representing the motor and the gear train is estimated according to the heat losses generated within the electric motor and the gear train. The heat transfer coefficient between the outer rotating cylinder and ambient air has been calculated as a function of the rotational Reynolds number using the correlation reported in Elghnam [6], equation (1).

$$\overline{Nu} = 0.022 * {Re_o}^{0.821} \tag{1}$$

The gap between the inner cylinder (the motor) and the outer cylinder (the rotating drive drum) is filled with Enduratex-EP 150 oil and air. The oil properties have been have been correlated as function of oil temperature by the authors based on the manufacturer's data [35]. These correlations are reported in Table 3-1.

Table 3-1 Properties of Enduratex-EP 150 Oil [35]

Property	Manufacturer's data [35]	Correlations developed by authors
Density (ρ) [kg/m^3]	855 kg/m^3 @40°C 820 kg/m^3 @100°C	$\rho(T) = 880 - 0.441 * T - 0.006 * T^2 + 6.398 * 10^{-5} * T^3 - 2.08816 * 10^{-7} * T^4$
Dynamic viscosity (μ) [mPa.s]	128.4 mPa.s @40°C 12.17 mPa.s @100°C	$\mu(T) = 14.6 + 2625.4 * e^{(-0.102338T)} + 9.7258 * 10^{-1} * T^2 * e^{(-0.077355T)} - 7.0317 * 10^{-2} * T$
Thermal conductivity (λ) [mW/m.K]	140 mW/m.K	-

The effect of oil level has been investigated in terms of the percentage of oil volume (OV) to the total gap volume. The OV has been varied in this study between 50% and 100%. Teamah and Hamed [34] concluded that the OV must be greater than 50% in order for the outer cylinder motion to establish a sufficient oil flow that would provide proper cooling for the motor. The radius ratio (RR) has been varied between 0.35 and 0.85 by keeping the outer cylinder radius constant at 59.5 mm and varying the inner cylinder radius, which is a typical practice in the manufacturing of SCDMDSs. The range of RR considered in the current study covers the practical range found in the SCDMSs used in the industry. The effect of the emissivity of the drum surface has been investigated in the range of 0 to 0.95. The lower value of 0 represents a reflective polished steel shell while the upper value of 0.95 corresponds to a typical black-dull lagging rubber material. The effect of the lagging material thickness, δ, was investigated in the range of 0 to 100 mm which covers the typical cases of no lagging and with lagging considered in the industry.

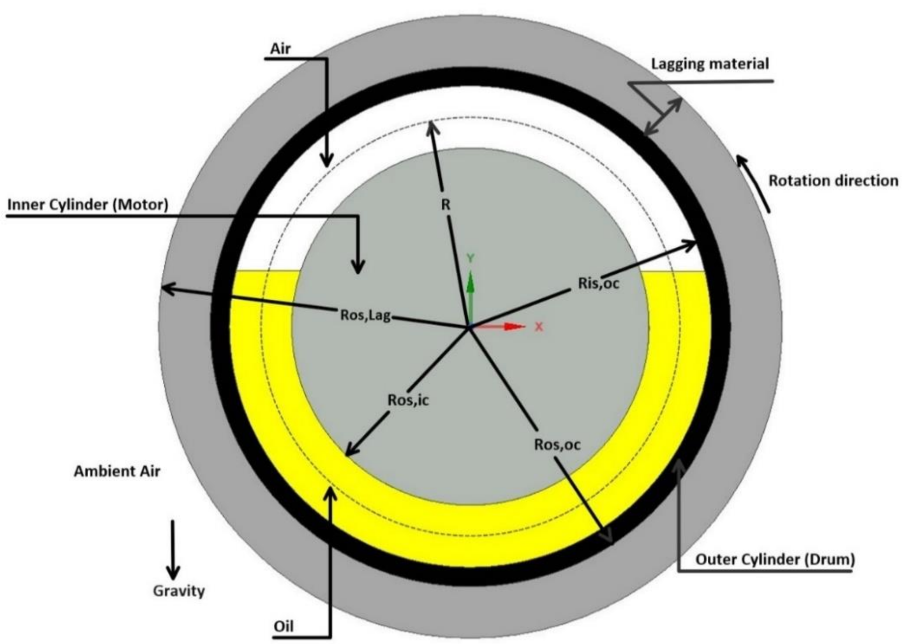

Figure 3.2 Schematic diagram of the present Problem

3.4 Mathematical Model

This problem was numerically simulated using ANSYS-CFX.

3.4.1. Governing Equations for the Problem

The problem of interest is governed by the following conservation of mass, momentum and energy equations, ANSYS [36]:

$$\frac{\partial \rho}{\partial t} + \nabla \cdot (\rho U) = 0.0 \tag{2}$$

$$\frac{\partial (\rho U)}{\partial t} + \nabla \cdot (\rho U \otimes U) = -\nabla p + \nabla \cdot \tau \tag{3}$$

$$\frac{\partial (\rho h_{tot})}{\partial t} - \frac{\partial p}{\partial t} + \nabla \cdot (\rho U h_{tot}) = \nabla \cdot (k \nabla T) + \nabla \cdot (U \cdot \tau) \tag{4}$$

$$\tau = \mu \left(\nabla U + (\nabla U)^T - \frac{2}{3} \delta \nabla \cdot U \right) \tag{5}$$

$$h_{tot} = enthalpy + \frac{1}{2} U^2 \tag{6}$$

The Shear Stress Transport (SST) turbulence model was used to precisely resolve the near wall region especially considering the flow separation that happens along the inner surface of the rotating cylinder. The SST turbulence model resolves the viscous sublayer region.

3.4.2. Boundary Conditions

Considering the configuration shown in Figure 3.2, the boundary conditions of the problem of interest are defined for each domain as follows:

i. The Annular Space (Multiphase Air/Oil Fluid Domain):

a. At $R=R_{os,ic}$, i.e., at the outer surface of the inner cylinder (motor casing):

$$U = 0 \tag{7}$$

$$q'' = constant. \tag{8}$$

b. At $R=R_{is,oc}$, i.e., at the inner surface of the rotating cylinder (the drum):

$$u_{\Theta} = \omega R_{is,oc} \tag{9}$$

$$u_R = u_z = 0 \tag{10}$$

$$q''_{conv]_{as\to oc}} = q''_{cond]_{drum}} \tag{11}$$

so that

$$h_{as\to oc}\left(T_{av,as} - T_{is,oc}\right) = -k_{oc} \frac{\partial T}{\partial R}\Big|_{R=R_{is,oc}} \tag{12}$$

ii. The Rotating Cylinder (The Drive Drum):

a. At $R=R_{is,oc}$, i.e., at the inner surface of the rotating drum:

$$u_{\Theta} = \omega R_{is,oc} \tag{13}$$

$$u_R = u_z = 0 \tag{14}$$

as it is an interface with the annular space, so it will have the same boundary condition as of the annular space as in equation (12).

b. At R= $R_{os,oc}$, i.e., at the outer surface of the rotating drum:

$$u_\Theta = \omega R_{os,oc} \tag{15}$$

$$u_R = u_z = 0 \tag{16}$$

$$q''_{cond]_{drum}} = q''_{cond]_{Lag}} \tag{17}$$

so that

$$-k_{oc}\left.\frac{\partial T}{\partial R}\right]_{R=R_{os,oc}} = -k_{Lag}\left.\frac{\partial T}{\partial R}\right]_{R=R_{os,oc}} \tag{18}$$

iii. The Lagging Material:

a. At R=$R_{is,Lag}$, i.e., at the inner surface of the lagging:

$$u_\Theta = \omega R_{is,Lag} \tag{19}$$

$$u_R = u_z = 0 \tag{20}$$

as it is an interface with the rotating drum so it will have the same temperature calculated in the rotating drum boundary condition (b) with the same amount of heat as in equation (18). The contact resistance is neglected.

b. At R=$R_{os,Lag}$ at the outer surface of the lagging:

$$u_\Theta = \omega R_{os,Lag} \tag{21}$$

$$u_R = u_z = 0 \tag{22}$$

$$q''_{cond]_{Lag}} = q''_{conv]_{amb}} \tag{23}$$

so that

$$-k_{Lag} \frac{\partial T}{\partial R}\bigg]_{R=R_{os,Lag}} = h_{oc\to amb}\left(T_{os,Lag} - T_{amb}\right) \tag{24}$$

For the axial direction there is no change in any flux so the boundary condition of it is symmetry

$$\frac{\partial \Phi}{\partial z} = 0 \tag{25}$$

Where, Φ is defined as any parameter like temperature, velocity components, etc.

3.4.3. Solution Procedure

The governing equations are solved using ANSYS-CFX. The solver uses an implicit iterative transient scheme until a quasi-steady state solution is reached.

i. Grid Independence Test

The grid independence test for this problem was carried out by changing the total number of elements used up to 10^7 elements. The effect of the total number of elements on the average fluid temperature within the annular space was examined. Figure 3.3 shows the variation of the average fluid temperature with the total number of elements. The reasonable total number of elements was found to be 5.19 x10^5 , which gave a maximum change in the average fluid temperature within the gap of less than 1.4 %, hence, this number of elements was deemed acceptable. The chosen mesh has an average skewness of 0.2 and a maximum aspect ratio of 9, which represents a reasonable mesh quality.

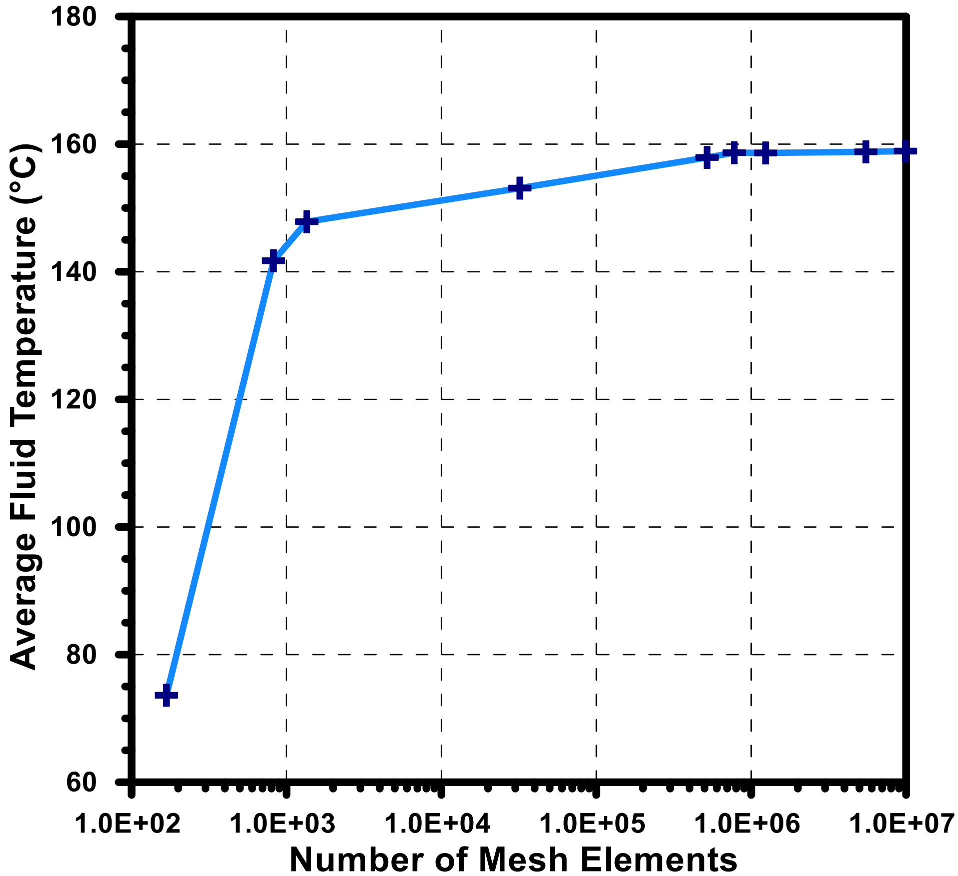

Figure 3.3 Grid independence test at Re = 3000.

3.4.4. Model Validation

The validation of the numerical model was carried out by comparing the numerical results with experimental data. The experimental setup represents one of the most popular SCDMDS models (TM215B40). Figure 3.4 shows external dimensions of this model according to the manufacturer's data [37].

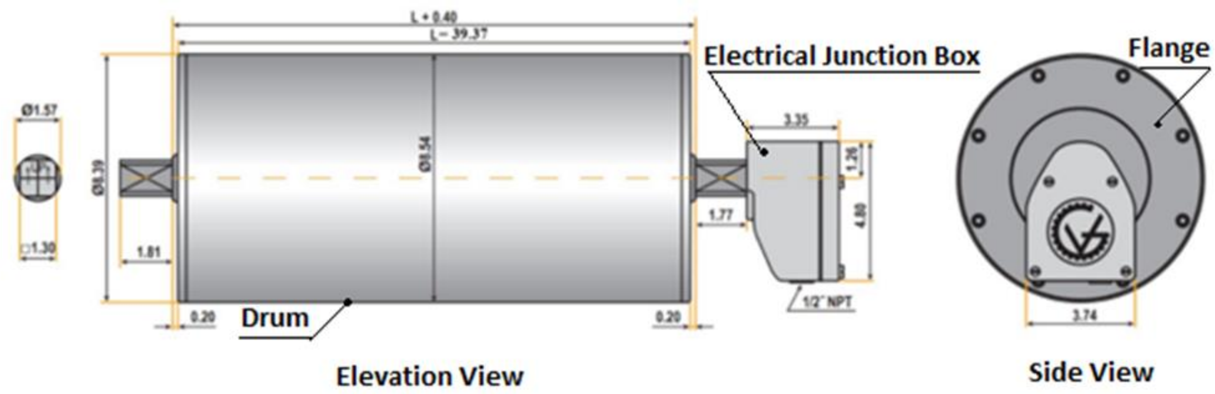

Figure 3.4 External dimensions of model TM215B40. All dimensions are in inches [37]

Images of the experimental setup are shown in Figure 3.5. Figure 3.5-a shows a typical SCDMDS with a steel shell, which was replaced with a transparent shell in some tests as shown Figure 3.5-b. The transparent shell allowed the use of a high-speed camera to visualize and observe the oil flow and distribution inside the SCDMDS. A tachometer has been used to measure the drum rotational speed. A calibrated infrared thermometer has been used to measure the drum surface temperature. A wattage meter connected to the electrical motor inside the drum was used to determine the amount of heat losses generated within the motor.

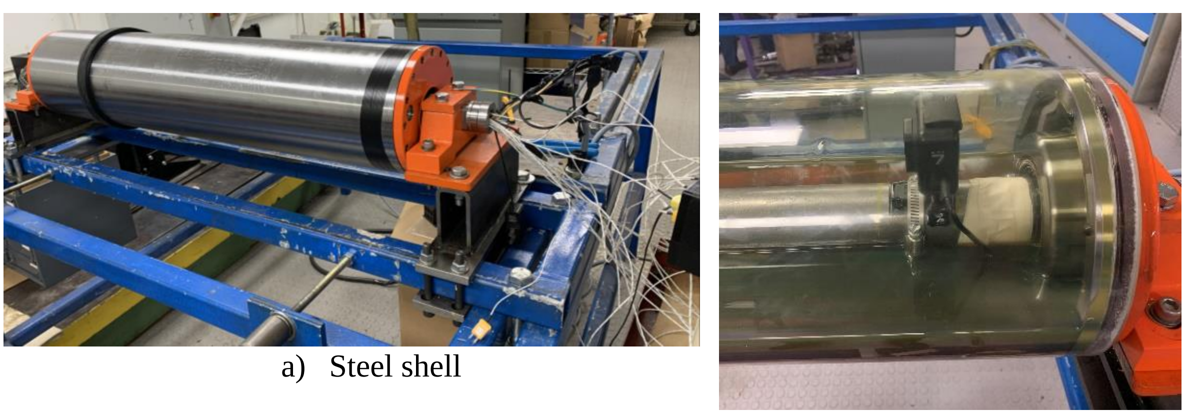

a) Steel shell

b) Transparent shell with a high-speed camera

Figure 3.5 Images of the experimental test setup.

Nine type-K thermocouples were located circumferentially in the midplane of the inner cylinder, i.e., the stator of the motor. Locations of these thermocouples are shown in Figure 3.6.

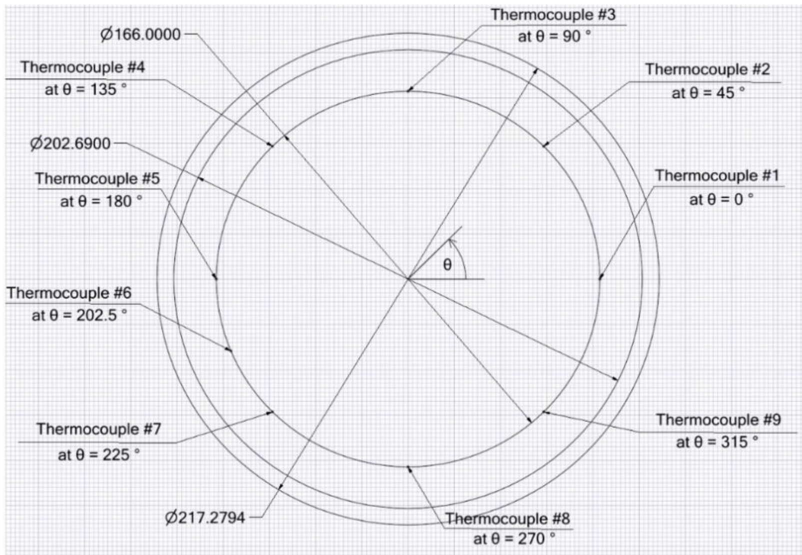

Figure 3.6 Locations of the nine type-K thermocouples placed along the motor stator surface.

The numerical model was validated by comparing the experimental data and the numerical results carried out under conditions listed in Table 3-2. Such comparison is shown in Figure 3.7.

Table 3-2 Operating conditions used for the validation case

Variable	Value	Unit
Oil Volume Percentage (OV)	20	%
Drum Rotational Speed (N)	500	rpm
Lagging Thickness (δ)	0	mm
Radius Ratio (RR)	0.82	dimensionless
Surface Emissivity (ε)	0.42	dimensionless
Amount of Heat (Q)	190	W

Figure 3.7 shows the temperature distribution along the inner cylinder (motor) and the outer rotating cylinder (drive drum) obtained experimentally and numerically. Figure 3.7 shows a reasonable agreement. The maximum deviation of all points is about 6%.

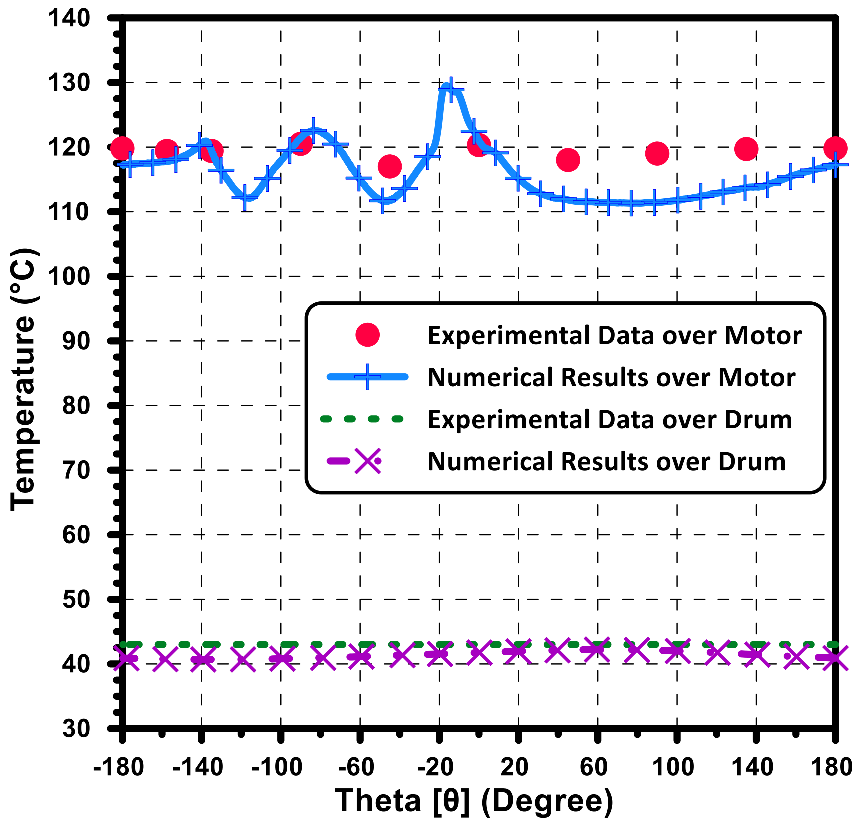

Figure 3.7 Comparison of the temperature distribution over the motor and the drum surfaces with experimental data obtained for SCDMDS model TM215B40 at OV=20%, N=500 rpm and Q =190 W.

It is worth noting that the multiphase flow and heat transfer has been validated with multiple actual case studies from the industrial partner Vander Graaf (VDG) for various SCDMDSs.

As mentioned before, in order to visualize the oil flow inside the SCDMDS, a set of experiments have been conducted using a transparent drum made from Plexiglass. Because the Plexiglass drum cannot withstand high temperatures, this set of experiments was carried out without heating, i.e., at room temperature.

A set of numerical simulations have been carried out at the same geometrical and operating conditions used in these flow visualization experiments. It was worth mentioning that at higher rotational speeds (N) > 130 rpm, the oil foaming blocked the high speed camera sight. Figure 3.8 shows a comparison of the experimentally and numerically determined oil distribution inside the SCDMDS at OV 50%, RR = 0.82, and a rotational speed 130 rpm. One can note that the oil flow in this case was associated with some oil splashing. Figure 3.8 shows a reasonable agreement of the oil distribution observed experimentally and that predicted numerically.

a) Oil distribution observed experimentally

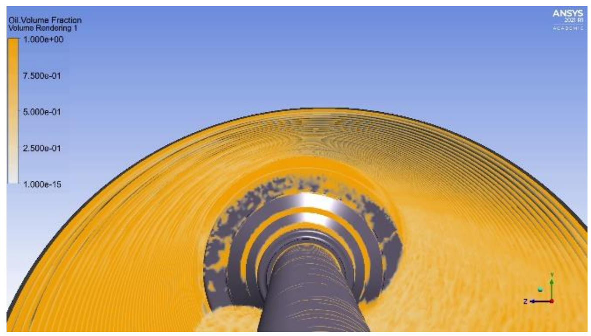

b) Numerical results showing oil distribution at the same instant of time as in (a)

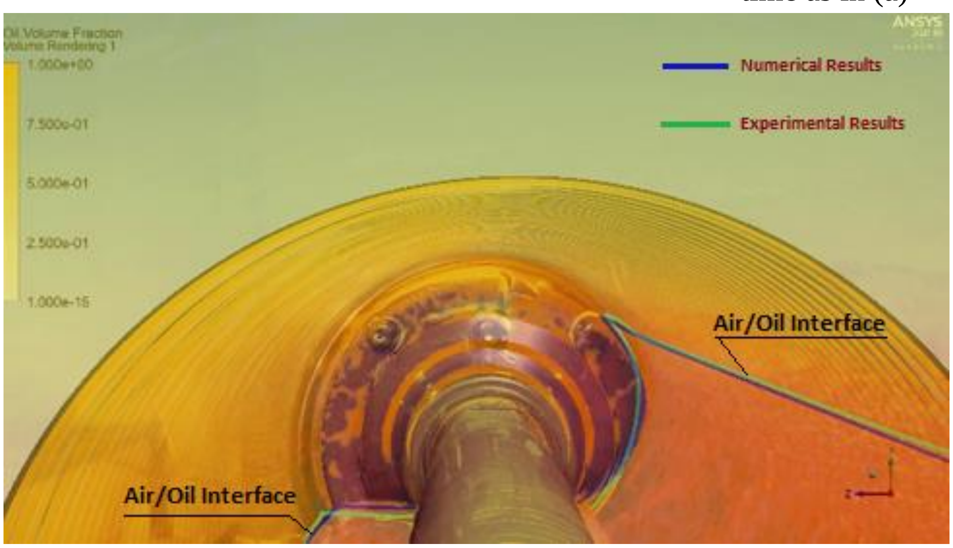

c) Experimental and numerical results imposed on top of each other using a 50% image transparency.

Figure 3.8 Comparison of oil distribution observed experimentally and obtained numerically at OV=50% and N=130 rpm.

3.5 SCDMDS Thermal Resistance Network

A thermal resistance network approach has been used for the current problem. Figure 3.9 shows the whole thermal resistance network from the temperature node of the inner cylinder, motor, ($T_{av,ic}$) to the ambient temperature (T_{amb}).

The multiphase oil/air flow in the gap between the two cylinders is distributed among two series resistances, $R_{ic\rightarrow as}$ and $R_{as\rightarrow oc}$. The first resistance ($R_{ic\rightarrow as}$) is the resistance between the inner cylinder (motor) average temperature and the annular space average temperature. The second resistance ($R_{as\rightarrow oc}$) is the resistance from the annular space average temperature and the outer cylinder (Drum) average temperature.

The conduction resistance inside the drum material is neglected compared to the other resistance as discussed later. In the cases where the lagging material is present, a conduction resistance is added for the lagging (R_{Lag}). There are two parallel resistances, $R_{radiation|oc\rightarrow amb}$ and $R_{convection|oc\rightarrow amb}$, of radiation and convection from the outer surface to the ambient air respectively.

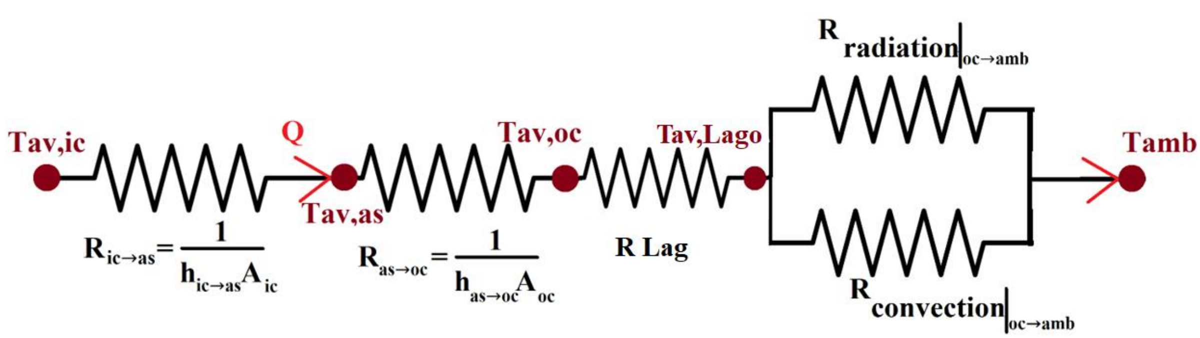

Figure 3.9 Thermal resistance network of a typical SCDMDS with lagging.

3.6 Results and Discussion

The focus of the present study is to investigate the effects of RR, N, OV, ε and δ on the overall thermal performance of the SCDMDS. The ranges of these parameters considered in the present study cover the typical practical ranges used in the manufacturing of typical SCDMDS models. The ranges considered are: RR = 0.35-0.85, N= 50-150 rpm, OV = 50-100 %, ε = 0 - 0.95, and δ = 0-100 mm. The authors investigated the effect of OV between 0 and 50%, Teamah and Hamed [34], considering a constant RR of 0.21. Our previous results showed that when OV is kept between 0 and 50%, a significant overheating problem took place.

It is worth noting that overheating is defined when the average oil temperature within the SCDMDS exceeds 90°C or the maximum temperature of the motor stator exceeds 140°C. This overheating criterion is defined based on two considerations: (1) the type of oil used (Enduratex EP 150) losses its lubrication effectiveness when its temperature exceeds 90°C and (2) the motor is designed to operate at a maximum operating temperature of 140°C.

3.6.1. Effect of the Radius Ratio (RR) on the Rate of Heat Transfer within the Gap

i. Case of Single-phase Flow (OV = 0%, air only)

As mentioned in the literature review section, the heat transfer in the single-phase Taylor-Couette flow has been studied considering cases of RR ≥ 0.5. Results indicated that increasing the rotational speed, N, resulted always in an enhancement of the rate of heat transfer within the gap. However, the effect of N for RR < 0.5 has not been investigated. Therefore, the case of a single-phase flow of air (i.e., OV = 0%) with RR < 0.5 has been investigated.

The effect of changing the N at RR = 0.35 and 0.85 on the flow and temperature fields within the annular gap is shown in Figure 3.10. At RR = 0.35, increasing N resulted in a weaker natural convection current within the gap, as indicated in Figure 3.10a. The weaker natural convection current led to deterioration in the rate of heat transfer within the gap, which resulted in high average temperatures, as indicated in Figure 3.10b and Table 3-3. The same trend was observed in Teamah and Hamed [34] at RR = 0.21.

At RR = 0.85, increasing N resulted in a stronger natural convection within the smaller gap resulting in an enhancement in the rate of heat transfer which led to lower average temperatures of the inner cylinder, as shown in Figure 3.10c and d and Table 3-3. Figure 3.11 shows the effect of N and RR on the average Nusselt number within the gap. The average Nusselt number ($Nu_{ic\rightarrow oc}$) is defined in equation (26).

$$Nu_{ic\rightarrow oc} = \frac{h_{ic\rightarrow oc} D_{is,oc}}{k} \tag{26}$$

At RR > 0.5 (e.g., RR = 0.85),the average $Nu_{ic\rightarrow oc}$ increased by about 10% from 11.8 at N = 50 rpm to 13 at N =150 rpm, which is consistent with the trend observed in previous studies. However, at RR < 0.5 (e.g., RR = 0.35), the average $Nu_{ic\rightarrow oc}$ decreased by about 23% from 9.2 at N = 50 rpm to 7.1 at N =150 rpm, which contradicts the trend observed before. . These results indicate that the value of the RR has a significant effect on the rate of heat transfer within the gap that must be taken into consideration. As the trend of the effect of N on the average Nusselt number observed in previous investigation seems to be none monotonic, it completely reverses based on the value of RR.

Table 3-3 Effect of N and RR on average temperatures within the gap at OV= 0%

Radius Ratio, RR	**RR=0.35**		**RR=0.85**	
Drum rotational speed, [N] (rpm)	50	150	50	150
Average outer cylinder temperature [$T_{av,oc}$] (°C)	98	69	99	69
Average air temperature [$T_{av,air}$] (°C)	155	173	167	140
Average inner cylinder temperature [$T_{av,ic}$] (°C)	321	369	244	218

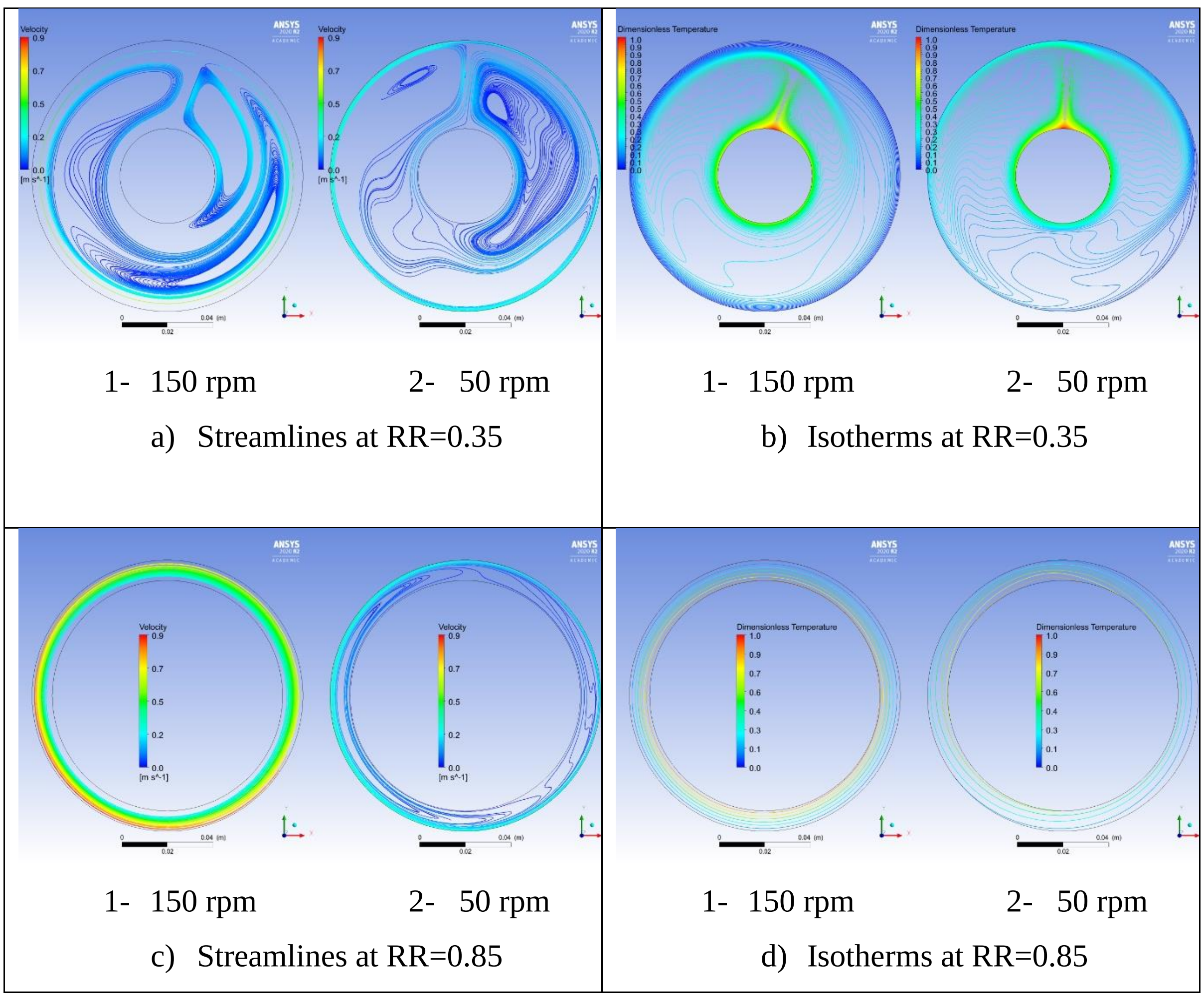

1- 150 rpm 2- 50 rpm

a) Streamlines at RR=0.35

1- 150 rpm 2- 50 rpm

b) Isotherms at RR=0.35

1- 150 rpm 2- 50 rpm

c) Streamlines at RR=0.85

1- 150 rpm 2- 50 rpm

d) Isotherms at RR=0.85

Figure 3.10 Effect of RR and N on the flow and thermal fields within the gap at OV = 0 %.

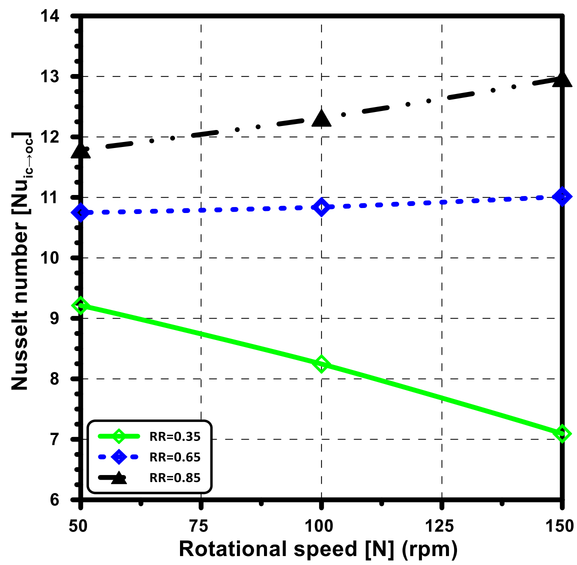

Figure 3.11 Effect of N and RR on the average Nusselt number within the gap at OV = 0%.

ii. Case of Multi-phase Flow (50% < OV < 100%)

The presence of oil within the gap could enhance the rate of heat transfer because of its better thermal conductivity compared to that of air. Results discussed here are for a SCDMDS operating at a constant rotational speed of 150 rpm with no lagging put on the drive drum. The drum outer surface emissivity was kept constant at 0.2. The effects of OV and RR have been investigated for OV = 50%-100% and RR = 0.35-0.85.

Table 3-4 shows the effect of RR and OV on the average temperatures within the gap. As the oil volume increased from 65% to 100%, the average temperature within the gap increased. When RR is increased, the rate of heat transfer within the gap increases as indicated by the decrease in the average temperatures.

Figure 3.12 shows the velocity and temperature distributions for the case of OV = 100% at RR = 0.35 and 0.85. Both cases have the same maximum velocity at the outer rotating cylinder as N is the same for both cases. The case of RR = 0.85 has a smaller gap thickness which in turn reduced the thermal resistance within the gap. The reduction in the thermal resistance is evident by the temperature contours shown in Figure 3.12 c and d.

The value of OV that results in the best possible SCDMDS thermal performance was previously investigated by the authors [34] and found to be about 65%. When dealing with multiphase cases, the problem is complex due to the need to determine oil distribution which depends on the drum rotational speed, oil viscosity, surface tension and the value of OV. The main objective is to maintain sufficient oil distribution over the entire surface of the inner cylinder to avoid overheating. It is worth noting that the overheating problem occurs when the amount of oil is insufficient, or the rotational speed is very low [34].

Figure 3.13 shows the effect of RR at OV = 65%, N =150 rpm and ε= 0.2 on oil and temperature distributions within the gap. Results show that the oil covered the entire inner cylinder in both cases of RR =0.35 and 0.85. Therefore, the value of OV = 65% seemed to be sufficient for the entire range of RR considered here.

The oil distribution shown in Figure 3.13a for the case of RR = 0.35 show a large portion of the inner cylinder submerged within a still oil, which results in a lower rate of heat transfer in this case compared with the case of RR = 0.85 shown in Figure 3.13b, which shows a better oil distribution over the inner cylinder surface.

The velocity contours shown in Figure 3.13c and d show a higher oil motion and hence a higher rate of heat transfer at RR = 0.85 compared with the case of RR =0.35 as evident by the lower average temperatures within the gap for the case of R = 0.85

Table 3-4 Effect of RR and OV on the temperatures at N=150rpm and ε=0.2 without lagging

Radius Ratio, RR	**RR=0.35**		**RR=0.85**	
Oil Volume, [OV] (%)	65	100	65	100
Average outer cylinder temperature [$T_{av,oc}$] (°C)	66	67	65	65
Average oil temperature [$T_{av,oil}$] (°C)	69	96	67	77
Maximum inner cylinder temperature [$T_{max,ic}$] (°C)	82	150	71	91
Average inner cylinder temperature [$T_{av,ic}$] (°C)	74	148	69	90
Brinkmann number [Br]	0.026	0.020	0.062	0.011

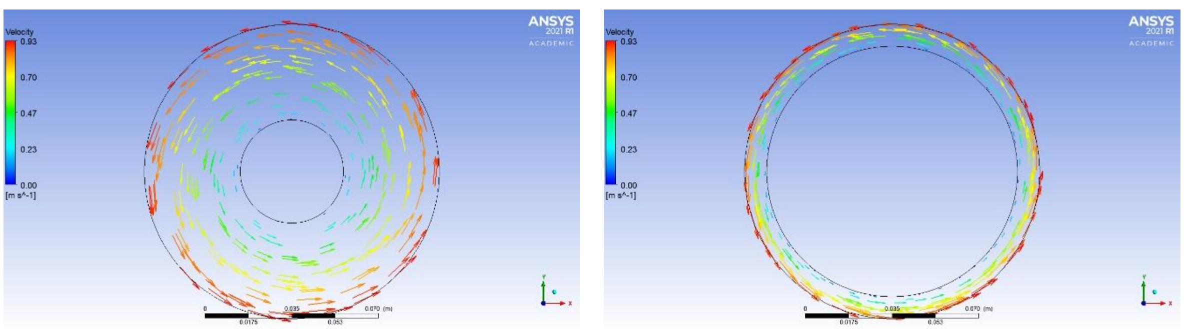

a) Velocity vectors at RR=0.35 b) Velocity vectors at RR=0.85

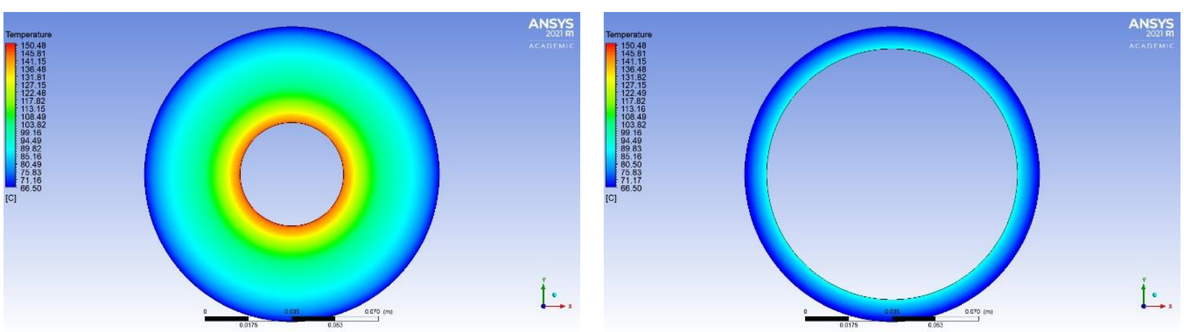

c) Temperature contours at RR=0.35 d) Temperature contours at RR=0.85

Figure 3.12 Effect of radius ratio on the velocity vectors and the temperatures contours at OV=100% ,ε=0.2 and N=150rpm without lagging

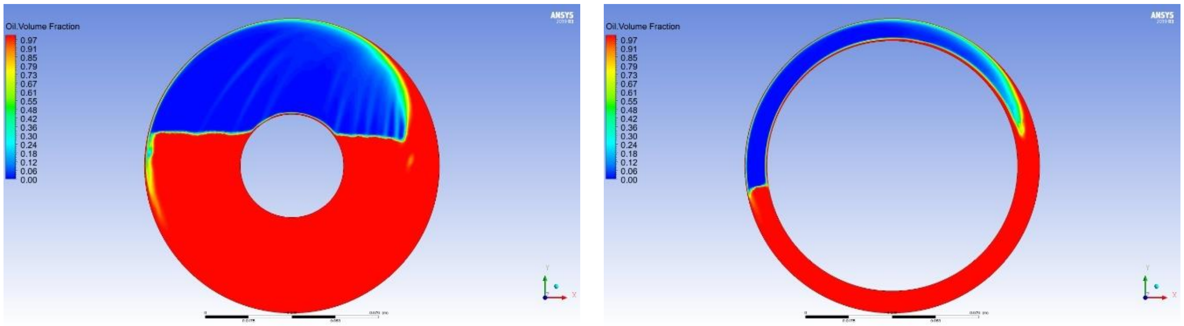

a) Oil volume fraction at RR=0.35 b) Oil volume fraction at RR=0.85

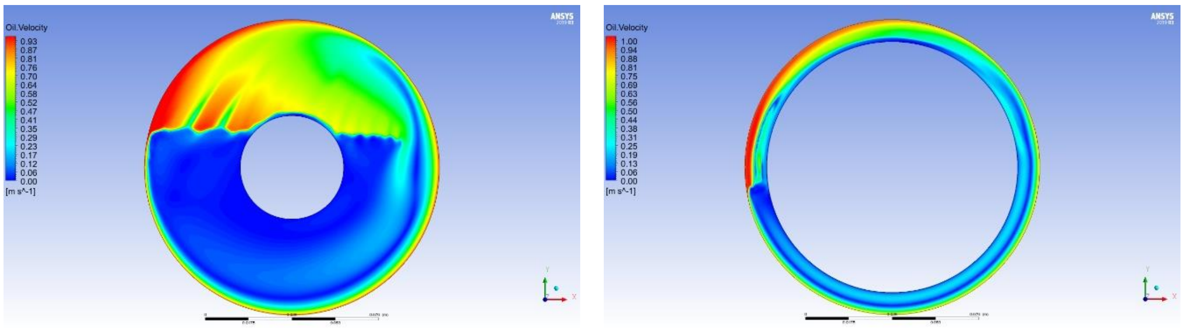

c) Velocity contours at RR=0.35 d) Velocity contours at RR=0.85

Figure 3.13 Effect of radius ratio on the oil volume fraction and the velocity contours at OV=65%, ε=0.2 and N=150rpm without lagging

The cases above and below 65 % are not recommended. When OV < 65% , the amount of oil is insufficient to cover the entire surface of the inner cylinder, as shown in Figure 3.14 c which indicates that At OV > 65 % ,Figure 3.14 a, the amount of oil is more than enough in order to cover the entire surface of the inner cylinder.

Figure 3.15 and Figure 3.16 show the effect of OV on the rate of heat transfer between the inner cylinder and the multi-phase flow (Figure 3.15) and between the multi-phase flow and the outer cylinder (Figure 3.16). Results shown in Figure 3.15 and Figure 3.16 confirm that the optimum value of OV that gave the maximum rate of heat transfer is 65%.

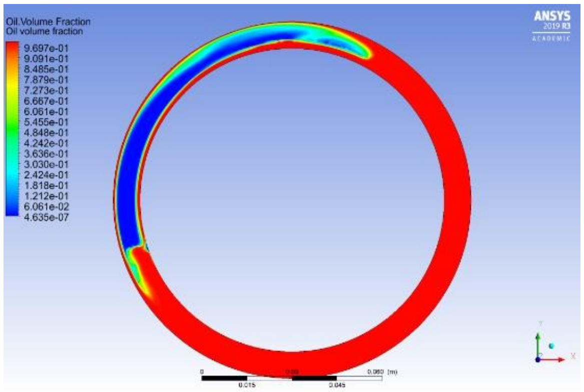

a) OV=75%

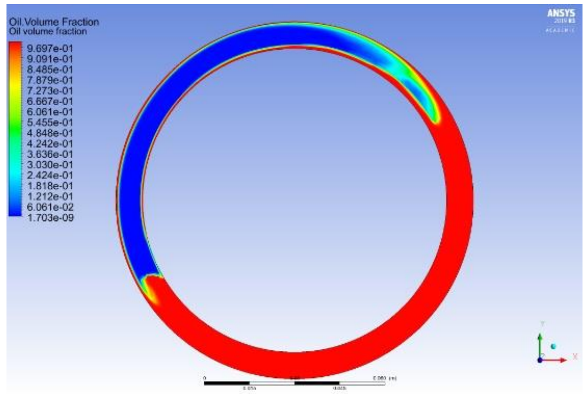

b) OV=65%

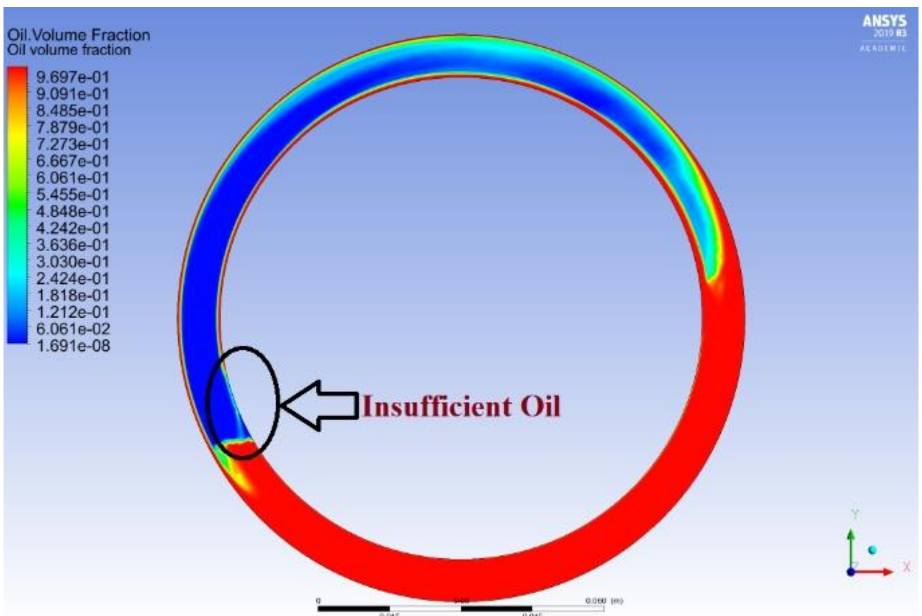

c) OV=60%

Figure 3.14 Effect of changing OV on the distribution of oil at RR=0.85, ε=0.2 and N=150rpm without lagging

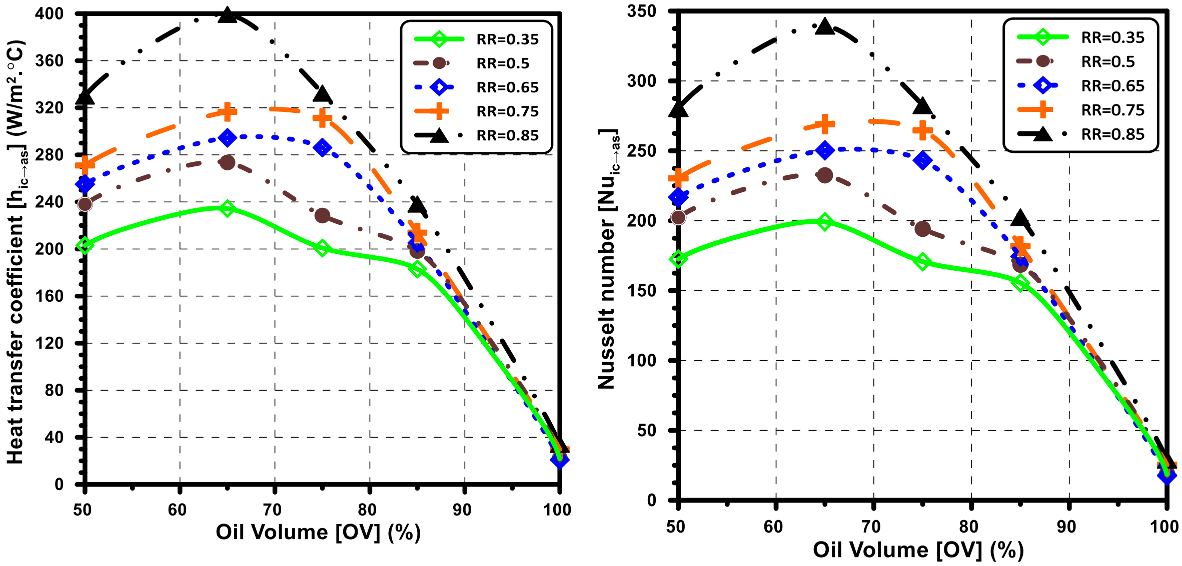

a) Heat transfer coefficient

b) Nusselt number

Figure 3.15 Effect of OV and RR on the heat transfer coefficient and the Nusselt number from the inner cylinder to the annular space at N=150rpm and ε=0.2 without lagging

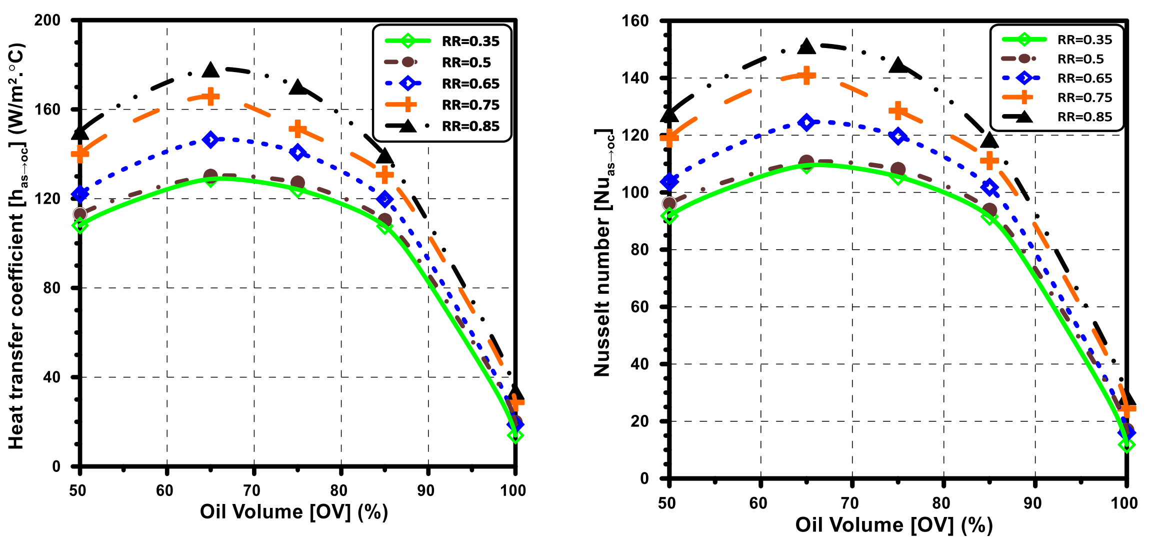

a) Heat transfer coefficient

b) Nusselt number

Figure 3.16 Effect of OV and RR on the heat transfer coefficient and the Nusselt number from the annular space to the outer cylinder at N=150rpm and ε=0.2 without lagging

3.6.2. Effect of Lagging Material at constant RR, N and ε

The effect of the lagging material thickness, δ, from 0 to 100 mm is shown in Figure 3.17 for RR = 0.85 and N = 150 rpm. The type of lagging material considered here is Styrene butadiene rubber (SBR) which has a thermal conductivity of 1.48 W/m.K and emissivity of 0.75, as per the manufacturer's data [38].

Increasing the lagging thickness from 0 up to 35 mm enhanced the rate of heat transfer due to the increase in the rate of heat transfer by radiation because of the higher emissivity value and the increase of the rate of heat transfer by convection due to the increase in the surface area. At δ > 35 mm, the lagging material thickness had a negative effect on the rate of heat transfer because of the significant increase in the conduction resistance which became more dominant than the decreased convective and radiative resistances. Therefore, the optimum lagging material thickness should be determined for each case separately according to the geometrical and operational parameters of the SCDMDS of interest.

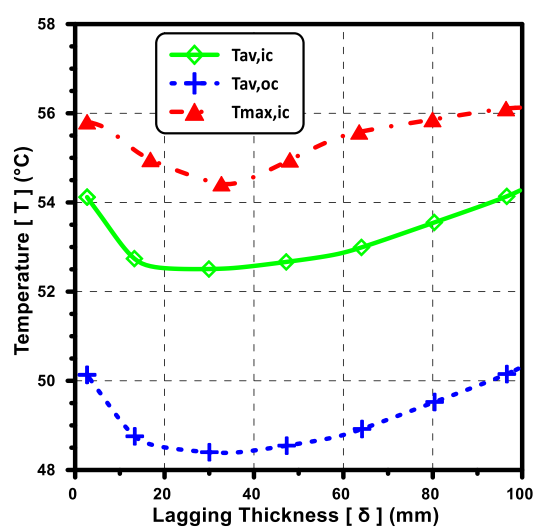

a) Lagging thickness effect at ε=0.75

Figure 3.17 Effect of lagging thickness on the temperatures inside the annular gap at RR = 0.85, N = 150 rpm and ε = 0.75.

3.6.3. Effect of The Outer Surface Emissivity

The effect of the outer drive drum surface emissivity on the average temperatures within the SCDMDS has been investigated at RR = 0.85, N = 150 rpm and the optimum lagging material thickness of 35 mm. Such variation of ε can be achieved by using special coating materials applied on the lagging material.

Results shown in Figure 3.18 indicate that the average temperature within the annular gap is decreased with increasing the outer surface emissivity due to the enhanced rate of heat radiative transfer between the drum and the ambient air. The maximum temperature over the inner cylinder (the motor) decreased to about 51°C at ε =0.95 from 63°C at ε = 0.

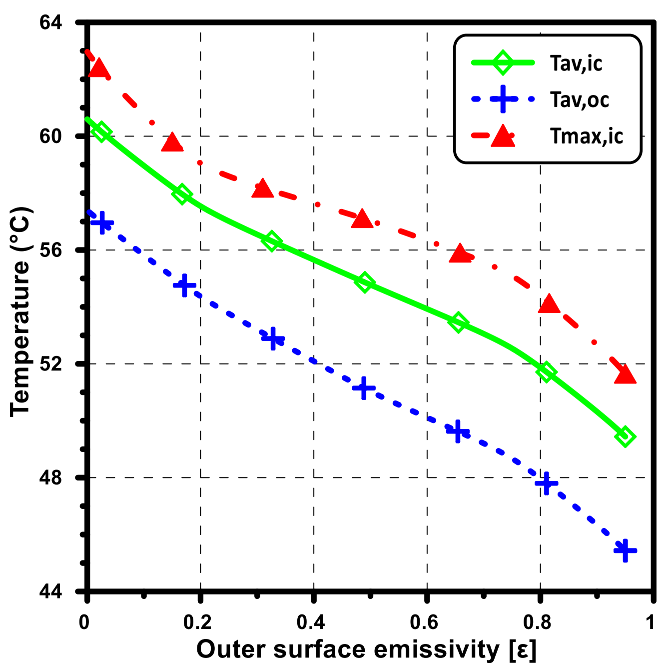

Figure 3.18 Effect of surface emissivity on average temperatures within the gap at RR = 0.85, N = 150 rpm and δ = 35 mm.

3.7 Heat Transfer Correlations

Predicting the interplay of the various geometrical and operating conditions on the thermal performance of a SCDMDS is very important in order to achieve the best possible thermal performance. The results of the parametric study presented here have been used to develop a number of essential heat transfer correlations. Two correlations have been developed to estimate the average Nusselt numbers within the gap. The first correlation is developed for the average Nusselt number between the inner cylinder and the multi-phase flow within the gap:

$$Nu_{ic\rightarrow as} = [40.35 + 94.33 * \sin(658.5OV) + 6.035 * 10^{-5} * RR^3 * OV^3 - 0.00797 * Re_{RR} - 90.83 * RR^2 - 0.01018 * OV^2 * \sin(658.5OV)] * [\frac{2}{1-RR}] \quad (27)$$

The second correlation is for the Nusselt number between the multi-phase flow within the gap and the outer cylinder:

$$Nu_{as\rightarrow oc} = [2.153 * OV + 0.0263 * Re_{RR} - 33.012 - 42.47 * RR - 0.0003598 * OV * Re - 0.01422 * OV^2] * [\frac{2}{1-RR}] \quad (28)$$

The above correlations of (27) and (28) are applicable for $0.35 \leq RR \leq 0.85$, $200 \leq Re \leq 3000$ and $50 < OV < 100\%$ with a maximum absolute error of 8 %.

The Reynolds number used in these correlations is calculated using equation (29)

$$Re_{RR} = \frac{\omega R_{is,oc}(R_{is,oc} - R_{os,ic})}{\nu} \quad (29)$$

All fluid properties have been calculated at the average fluid temperature.

In order to demonstrate the applicability of the developed correlations, a case study has been considered for the same SCDMDS model investigated experimentally. The operating conditions of the case study is provided in Table 3-5.

Table 3-5 Operating conditions of the multiphase case study

Variable	Value	Unit
Oil Volume Percentage (OV)	60	%
Drum Rotational Speed (N)	350	rpm
Lagging Thickness (δ)	0	mm
Radius Ratio (RR)	0.82	dimensionless
Surface Emissivity (ε)	0.42	dimensionless
Amount of Heat (Q)	420	W
Ambient Temperature (T_{amb})	25	℃

The thermal resistance network of a typical SCDMDS is shown in Figure 3.19. The convective resistance is calculated using equation (1) proposed by Elghnam [6]. Solving from right node of Tamb to the left node, the Tav,oc is estimated to be about 55.8 ℃. The value of Tav,oc measure experimentally using an infrared thermometer was about 56.5 ℃, as shown in Table 3-6. The average $Nu_{ic \to as}$ = 259.1 and $Nu_{as \to oc} = 165$ were calculated using equations (27) and (28). The corresponding values of $h_{ic \to as}$ and $h_{as \to oc}$ are 169 and 107, respectively. Calculating Ras-oc and Ric-as, the value of $T_{av,ic}$ was estimated to be about 66.08 ℃. The average value of the nine-thermocouples surrounding the motor casing was 68.2 ℃. The maximum error in the estimated value of $T_{av,ic}$ using the developed correlations is about 3 %. The conduction resistance through the mild steel drum was neglected because its value is less than 1% of the other thermal resistances in the system.

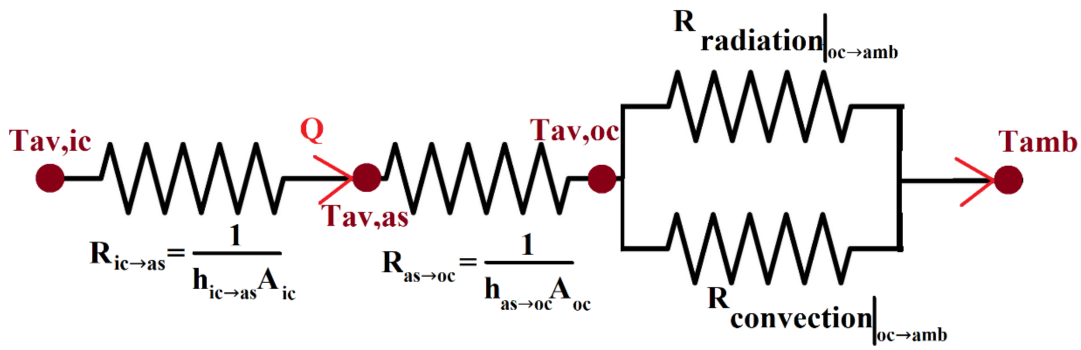

Figure 3.19 Thermal resistance network of a typical SCDMDS with no lagging.

Table 3-6 Comparison of experimental data of a case study and the estimated values using the developed correlations

Variable	Experimental data	Estimated using developed correlations	Percentage of error (%)
$T_{av,oc}$ (°C)	56.5	55.8	1.2
$T_{av,ic}$ (°C)	68.2	66.08	3.1

3.8 Conclusions

The effect of the rotational speed on the rate of heat transfer of single-phase flow within the gap depends on the value of the radius ratio of the gap. Increasing the rotational speed at RR > 0.5 enhanced the rate of heat transfer, however, it had an adverse effect at RR < 0.5.

The effect of the rotational speed on the rate of heat transfer of multi-phase flow within the gap does not depend on the value of the radius ratio of the gap. Increasing the rotational speed always resulted in an enhancement in the rate of heat transfer regardless of the value of RR.

Having a large amount of oil inside the gap might have a negative effect on the rate of heat transfer. There is an optimum oil level within the gap that would ensure sufficient amount of oil is present to cover the entire inner cylinder (motor) surface. The optimum oil volume ratio for the geometrical and operating conditions considered in this study was found to be 65%.

There is an optimum thickness of lagging material that can result in the minimum total thermal resistance. Increasing the outer surface emissivity enhanced the rate of heat transfer to the ambient and hence reduced the maximum temperatures within the gap and the inner cylinder.

The results for the multiphase flow cases were used to develop correlations of the average Nusselt number within the gap. A case study was analyzed using the developed correlations and compared with experimental data. Reasonable agreement was found.

3.9 Acknowledgements

The authors would like to acknowledge the financial support provided by MITACS and the technical and financial support provided by VDG Inc.

3.10 References

[1] *Van der Graaf Drum Motors*. Available: https://www.vandergraaf.com/

[2] B. Özerdem, "Measurement of convective heat transfer coefficient for a horizontal cylinder rotating in quiescent air," *International Communications in Heat and Mass Transfer,* vol. 27, no. 3, pp. 389-395, 2000/04/01/ 2000.

[3] H. Ma *et al.*, "Experimental investigation on the steady, external laminar mixed convection heat transfer characteristics around a large diameter horizontal rotating cylinder," *International Communications in Heat and Mass Transfer,* vol. 57, pp. 239-246, 2014/10/01/ 2014.

[4] K. M. Becker, "Measurements of convective heat transfer from a horizontal cylinder rotating in a tank of water," *International Journal of Heat and Mass Transfer,* vol. 6, no. 12, pp. 1053-1062, 1963/12/01/ 1963.

[5] J. T. Anderson, O. A. Saunders, and G. I. Taylor, "Convection from an isolated heated horizontal cylinder rotating about its axis," *Proceedings of the Royal Society of London. Series A. Mathematical and Physical Sciences,* vol. 217, no. 1131, pp. 555-562, 1953/05/21 1953.

[6] R. I. Elghnam, "Experimental and numerical investigation of heat transfer from a heated horizontal cylinder rotating in still air around its axis," *Ain Shams Engineering Journal,* vol. 5, no. 1, pp. 177-185, 2014/03/01/ 2014.

[7] H. M. Badr and S. C. R. Dennis, "Laminar forced convection from a rotating cylinder," *International Journal of Heat and Mass Transfer,* vol. 28, no. 1, pp. 253-264, 1985/01/01/ 1985.

[8] B. G. Van Der Hegge Zijnen, "Heat transfer from horizontal cylinders to a turbulent air flow," *Applied Scientific Research, Section A,* vol. 7, no. 2, pp. 205-223, 1958/03/01 1958.

[9] Y. Y. Yan and Y. Q. Zu, "Numerical simulation of heat transfer and fluid flow past a rotating isothermal cylinder – A LBM approach," *International Journal of Heat and Mass Transfer*, vol. 51, no. 9, pp. 2519-2536, 2008/05/01/ 2008.

[10] V. T. Morgan, "Heat Transfer by Natural Convection from a Horizontal Isothermal Circular Cylinder in Air," *Heat Transfer Engineering,* vol. 18, no. 1, pp. 25-33, 1997/01/01 1997.

[11] R. E. M. Morales, A. Balparda, and A. Silveira-Neto, "Large-eddy simulation of the combined convection around a heated rotating cylinder," *International Journal of Heat and Mass Transfer,* vol. 42, no. 5, pp. 941-949, 1999/03/01/ 1999.

[12] B. Farouk and K. S. Ball, "Convective flows around a rotating isothermal cylinder," *International Journal of Heat and Mass Transfer,* vol. 28, no. 10, pp. 1921-1935, 1985/10/01/ 1985.

[13] C. C. Chiou and S. L. Lee, "Forced convection on a rotating cylinder with an incident air jet," *International Journal of Heat and Mass Transfer,* vol. 36, no. 15, pp. 3841-3850, 1993/10/01/ 1993.

[14] J.-S. Yoo, "Mixed convection of air between two horizontal concentric cylinders with a cooled rotating outer cylinder," *International Journal of Heat and Mass Transfer,* vol. 41, no. 2, pp. 293-302, 1998/01/01/ 1998.

[15] D. Paghdar, S. Jogee, and K. Anupindi, "Large-eddy simulation of counter-rotating Taylor–Couette flow: The effects of angular velocity and eccentricity," *International Journal of Heat and Fluid Flow,* vol. 81, p. 108514, 2020/02/01/ 2020.

[16] P. S. Marcus, "Simulation of Taylor-Couette flow. Part 1. Numerical methods and comparison with experiment," *Journal of Fluid Mechanics,* vol. 146, pp. 45-64, 1984.

[17] J. M. Lopez, F. Marques, and M. Avila, "Conductive and convective heat transfer in fluid flows between differentially heated and rotating cylinders," *International Journal of Heat and Mass Transfer,* vol. 90, pp. 959-967, 2015/11/01/ 2015.

[18] C. D. Andereck, S. S. Liu, and H. L. Swinney, "Flow regimes in a circular Couette system with independently rotating cylinders," *Journal of Fluid Mechanics,* vol. 164, pp. 155-183, 1986.

[19] U. Naseem, M. B. Awan, B. Saeed, N. Abbas, S. Nawaz, and M. Hussain, "Experimental investigation of flow instabilities in a wide gap turbulent rotating Taylor-Couette flow," *Case Studies in Thermal Engineering,* vol. 14, p. 100449, 2019/09/01/ 2019.

[20] S. Dong, "Direct numerical simulation of turbulent Taylor–Couette flow," *Journal of Fluid Mechanics,* vol. 587, pp. 373-393, 2007.

[21] G. Rüdiger, M. Gellert, R. Hollerbach, M. Schultz, and F. Stefani, "Stability and instability of hydromagnetic Taylor–Couette flows," *Physics Reports,* vol. 741, pp. 1-89, 2018/04/26/ 2018.

[22] M. Fénot, Y. Bertin, E. Dorignac, and G. Lalizel, "A review of heat transfer between concentric rotating cylinders with or without axial flow," *International Journal of Thermal Sciences,* vol. 50, no. 7, pp. 1138-1155, 2011/07/01/ 2011.

[23] F. Moukalled and S. Acharya, "Natural convection in the annulus between concentric horizontal circular and square cylinders," vol. 10, no. 3, pp. 524-531, 1996.

[24] D. Alshahrani and O. Zeitoun, "Natural convection in air-filled horizontal cylindrical annuli," *Alex Eng J,* vol. 44, 11/01 2005.

[25] F. Tachibana, S. Fukui, and H. Mitsumura, "Heat Transfer in an Annulus with an Inner Rotating Cylinder," *Bulletin of JSME,* vol. 3, no. 9, pp. 119-123, 1960.

[26] T. Fusegi, B. Farouk, and K. S. Ball, "MIXED-CONVECTION FLOWS WITHIN A HORIZONTAL CONCENTRIC ANNULUS WITH A HEATED ROTATING INNER CYLINDER," *Numerical Heat Transfer,* vol. 9, no. 5, pp. 591-604, 1986/05/01 1986.

[27] S. Chatterjee, G. Sugilal, and S. V. Prabhu, "Heat transfer in a partially filled rotating pipe with single phase flow," *International Journal of Thermal Sciences,* vol. 125, pp. 132-141, 2018/03/01/ 2018.

[28] S. Chatterjee, G. Sugilal, and S. V. Prabhu, "Impact of inclination on single phase heat transfer in a partially filled rotating pipe," *International Journal of Heat and Mass Transfer,* vol. 123, pp. 867-878, 2018/08/01/ 2018.

[29] T.-M. Jeng, S.-C. Tzeng, and C.-H. Lin, "Heat transfer enhancement of Taylor–Couette–Poiseuille flow in an annulus by mounting longitudinal ribs on the rotating inner cylinder," *International Journal of Heat and Mass Transfer,* vol. 50, no. 1, pp. 381-390, 2007/01/01/ 2007.

[30] A. Nouri-Borujerdi and M. E. Nakhchi, "Heat transfer enhancement in annular flow with outer grooved cylinder and rotating inner cylinder: Review and experiments," *Applied Thermal Engineering,* vol. 120, pp. 257-268, 2017/06/25/ 2017.

[31] M. Sheikholeslami, M. Nimafar, and D. D. Ganji, "Nanofluid heat transfer between two pipes considering Brownian motion using AGM," *Alexandria Engineering Journal,* vol. 56, no. 2, pp. 277-283, 2017/06/01/ 2017.

[32] S. Jangili, N. Gajjela, and O. Anwar Bég, "Mathematical modeling of entropy generation in magnetized micropolar flow between co-rotating cylinders with internal heat generation," *Alexandria Engineering Journal,* vol. 55, no. 3, pp. 1969-1982, 2016/09/01/ 2016.

[33] M. Sheikholeslami, P. Jalili, and D. D. Ganji, "Magnetic field effect on nanofluid flow between two circular cylinders using AGM," *Alexandria Engineering Journal,* vol. 57, no. 2, pp. 587-594, 2018/06/01/ 2018.

[34] A. M. Teamah and M. S. Hamed, "Investigation of transient multiphase Taylor-Couette flow," *Alexandria Engineering Journal*, vol. 61, no. 4, pp. 2723-2738, 2022/04/01/ 2022.

[35] *Oil Enduratex EP 150*. Available: https://lubricants.petro-canada.com/en-ae/brand/enduratex-ep#4c438c61-0a61-4851-b43d-b1bfffe8539d

[36] C. J. S. t. g. ANSYS, ANSYS, "Release 12.0 User's guide," 2009.

[37] *Vander Graaf Model Manual*. Available: http://www.vandergraaf.com/media/VanderGraaf/site-images/PDFS/TM100_TM215-STANDAR-DUTY-CATALOG_600-01-v5b.pdf

[38] *Styrene butadiene rubber properties*. Available: https://shinadt.com/polymer/styrene-butadiene-rubber.html

Chapter 4

Numerical Investigation of Thermal Losses within an Internal Gear Train Submerged in a Multiphase Flow and Enclosed in a Rotating Casing

Chapter 4

Numerical Investigation of Thermal Losses within an Internal Gear Train Submerged in a Multiphase Flow and Enclosed in a Rotating Casing

Complete Citation:

A. M. Teamah and M. S. Hamed, "Numerical investigation of thermal losses within an internal gear train submerged in a multiphase flow and enclosed in a rotating casing," International Journal of Thermofluids, vol. 15, p. 100188, 2022/08/01/ 2022.

Copyright:

Relative Contributions:

Ahmed M. Teamah: Wrote the first draft of the manuscript.

Mohamed S. Hamed: Revised and edited the manuscript.

Numerical Investigation of Thermal Losses within an Internal Gear Train Submerged in a Multiphase Flow and Enclosed in a Rotating Casing

Ahmed M. Teamah* and Mohamed S. Hamed

Thermal Processing Laboratory, Department of Mechanical Engineering,

McMaster University, Hamilton, Ontario, Canada

*Corresponding Author: teamaha@mcmaster.ca, Tel: +1 905-920-6960

Abstract

This paper presents results of a numerical study of thermal losses generated within an internal gear train consisting of a pinion and an annular gear. The gear train is submerged in a multiphase flow of Air and Oil and enclosed within a horizontal rotating cylinder (casing) attached to the annular gear. The casing rotates at a constant speed and exchanges heat through thermal radiation and natural convection to the ambient air. The study has been carried out using KISSsys and KISSsoft computer software. Numerical results have been validated using published experimental data. The maximum deviation is about 9.3%. The effects of several operating parameters; including the casing rotational speed (N), the torque (ζ) and the oil level (OV) on the various thermal losses generated within the gear train have been investigated. The effects of N, ζ and OV have been investigated in the following ranges: 20-160 rpm, 13-100 N.m, and 0-100%, respectively. The types of thermal losses considered in the present study are the churning, the meshing and the bearing losses. The gear ratio used in the present study is

4.45, therefore, the pinion gear rotational speed varied from 90 to 712 rpm. The present results indicated that increasing the rotational speed or the torque increases the thermal losses within the gear train. Increasing the oil level leads to an increase in the churning losses, up to a specific value of OV of about 31%, above which churning losses remained constant. The oil level at the 31% OV value is the oil level required to just submerge the pinion gear. Increasing the casing rotational speed enhanced the rate of heat transfer to the ambient air which improved the overall thermal performance of the gear train by about 12% at N = 460 rpm, compared to the stationary casing case.

Keywords: Gear train thermal losses, churning losses, meshing losses, multiphase flow, Thermal Performance, Rotating Casing.

Nomenclature

A	Lateral surface area, πDL, m^2.
b	Face width, m.
$C_{1,2}$	Factors in calculating gear churning losses.
C_{Sp}	Splash oil factor.
D	Diameter, m.
d_m	Mean bearing diameter, m.
$f_{0,1}$	Coefficients for bearing losses.
F_{bt}	Tooth normal force, N.

h	Heat transfer coefficient, W/m^2. °C
$\bar{h}$	Normalized oil height, defined to be:
	Oil vertical height from lowest point of gears [m] / Gear radius [m]
h_{ov}	Height of oil inside the gear train from the bottom, m.
H_V	Gear loss factor.
k	Thermal conductivity, W/m.°C
L	Drum axial length, m.
N	Rotational speed, rpm.
Nu	Nusselt number, $\alpha D/\lambda$.
OV	Oil volume percentage inside the annular area, %.
p_1	Bearing load, N.
P_B	Bearing load dependent losses, W.
P_L	Load dependent losses, W.
P_M	Gear meshing losses, W.
P_N	Load independent losses, W.
P_Q	Heat dissipation, W.
Ps	Normalized power loss, (Total power losses)/300[W].
P_V	Heat generated, W.

P_W	Gear churning losses, W.
P_{WB}	Bearing load independent losses, W.
r	Radius, m.
Re	Reynolds number, $\frac{\rho UD}{\mu}$
T	Temperature, °C.
T_H	Hydraulic loss torque, N.m
U	Linear velocity over drum surface, m/sec.
$u_{\Theta,r,z}$	Velocity components in circumferential, radial and axial, m/sec.
V_t	Pitch line velocity, m/sec.
z	Number of teeth.
Z	Axial axis, m.

Greek symbols

ε	Surface emissivity.
ζ	Torque, N.m
μ	Dynamic viscosity, kg/m.s
μ_m	Mean coefficient of friction in gear mesh.
ν	Kinematic viscosity, m^2/s

ρ	Density, kg/m^3
σ	Stefan Boltzmann constant, 5.67*10^{-8} W/ (m^2.K^4)
ω	Angular velocity, rad/sec.

Subscript

amb	Ambient
av	Average
oc	Outer cylinder
m	Mean

4.1 Introduction

Gear trains are essential components in many mechanical machines. They are used to transmit motion at the desired speed and torque. Heat is usually generated within these mechanical machines and hence they require proper means of cooling to avoid overheating of their internal components. The gear train, itself, is a heat source within these machines. Any operating gear train generates heat due to several thermal losses. Depending on the application, these losses could significantly contribute to the overall thermal performance of the entire mechanical machine leading, possibly, to a serious overheating problem. One of those mechanical machines is the self-contained drum motor drive system (SCDMDS). The SCDMDS provides a clean and an efficient way of materials handling compared to the conventional open-belt conveyor system. All components of a SCDMDS are submerged in oil and enclosed inside a rotating drum (casing). Hence, contamination is eliminated, which makes the SCDMDS well suited for the food and the pharmaceutical industries. The main components of a SCDMDS are shown in Figure 3.1. The SCDMDS consists of a rotating drum (1), an electric motor (2), an internal gear train (3), and a fixed shaft (4).

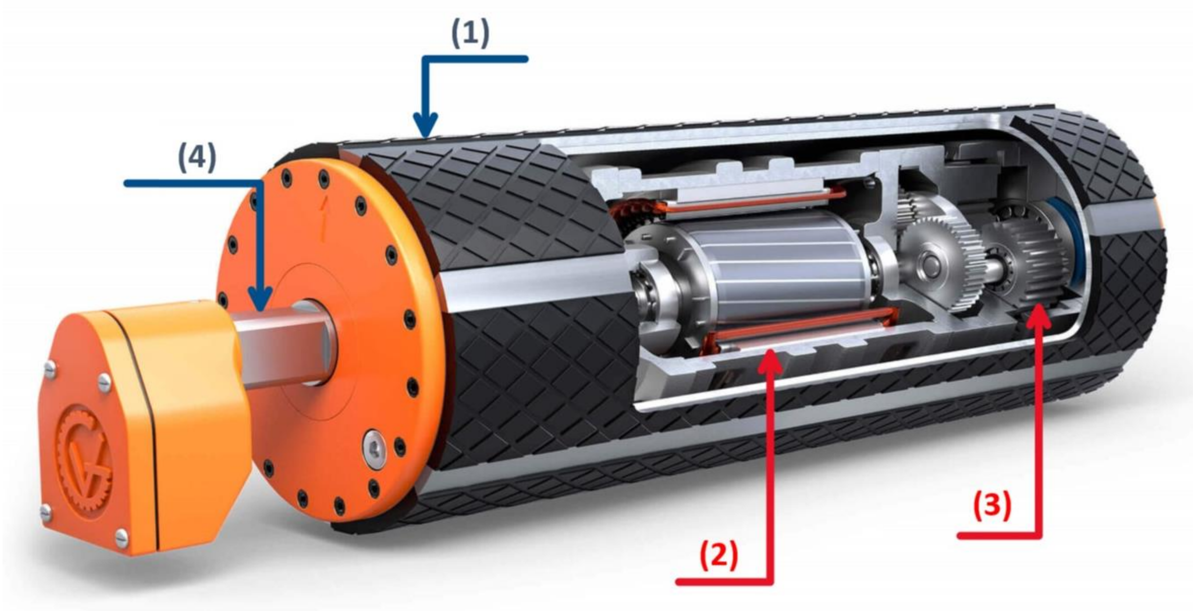

Figure 4.1 A section of a SCDMDS showing its components [1].

Power losses from gear trains can be classified by dependency on load losses and interaction type. For the dependency on load losses, there are some losses affected by load (torque) and others independent on the load. The dependent on load losses originates from the friction interaction between metal parts as in meshing losses (gear contact) and bearings losses. The independent power losses are oil squeezing (pocketing) and windage (churning) losses. The squeezing losses, as the name implies, arise from lubricant being squeezed between the mating gears or having pockets of oil of volume changing with rotation as in Figure 4.2.

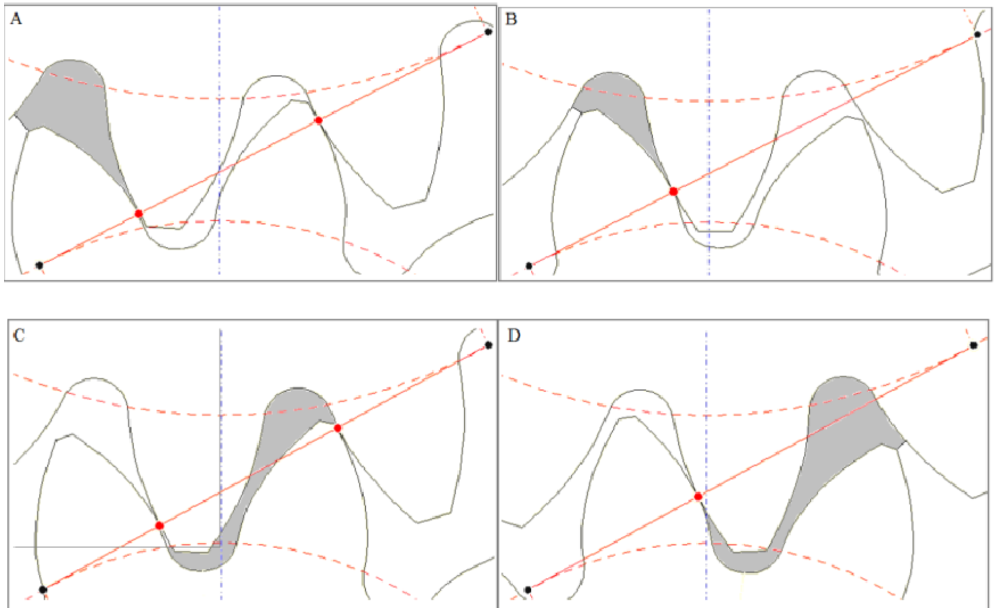

Figure 4.2 Oil squeezing or pocketing phenomena by Concli and Gorla [2]

The windage losses result from the interaction of the mechanical components and just one fluid, like air or oil which is present surrounding the gears. If there is multiphase flow like oil and air surrounding the gears, the windage losses become churning losses.

4.2 Literature Review

A numerical study of heat transfer and fluid flow of two spur gears was carried out by Concli and Gorla [2]. The gears were fully submerged in oil. They investigated the effect of speed on thermal losses caused by oil squeezing. They concluded that increasing the rotational speed and decreasing the oil temperature resulted in higher thermal loss.

Patil and Kumar [3] studied numerically the effect of convective heat transfer, rotational speed and load on the stresses and the thermal performance of a four-stage gearbox. The gears were totally submerged in oil. Convective heat transfer coefficient was altered according to the radius of each gear. The rate of heat transfer, rotational speed and torque were varied in the ranges of 100-500 W/m^2 K, 1000-10,000 rpm, and 80-650 N.m, respectively. The higher rotational speed at the lower gear ratio resulted in the highest deformation and stresses.

Liu, et al. [4] investigated numerically the churning thermal losses and oil distribution within two externally mating gears, partially immersed in oil. The gear train in their study was placed in a stationary casing. The study was focused on the churning losses resulted from oil circulation inside the gearbox at high circumferential speeds, up to 20 m/s. The K-ε turbulence model was used. They found that churning losses increased with increasing oil level and rotational speed. However, the rotational speed was found to be the most dominant parameter on the churning losses.

An experimental study of a two-stage external gear train was carried out by Marques, et al. [5]. They focused on the churning losses at low rotational speeds and higher torques, in the range of 100-1900 rpm and up to 1300 N.m. The gearbox housing temperature and oil level were kept constant. They considered both laminar and turbulent flow regimes, based on the value of the Reynolds number. The casing surrounding the gear train was static all over their study. Four different oil types were used. They showed that increasing the rotational speed or the torque will increase the churning losses. They also identified a way to determine the transition between different flow regimes by calculating a critical Reynolds number. This critical Reynolds number is function of the pitch radius, tooth face width, rotational speed, and kinematic viscosity.

Concli, et al. [6] presented a novel numerical approach to estimate the churning power losses from a spur gear train. The study focused on the effect of several operating conditions and geometrical parameters on the churning losses using OpenFOAM numerical code. They varied the oil level considering a partially filled case (half-filled and below gears axis by 20 mm) and a fully filled case. Their results indicated that the tip (outside) diameter influence is the most effective parameter on the churning losses with direct relation. A slight increase in the tip diameter led to a significant increase in the losses, especially at high speeds. Increasing oil level led to higher churning losses.

Seetharaman and Kahraman [7] conducted a numerical study of churning and windage losses on pairs of spur gears. The gear ratio was kept at unity to determine the share of each type of power losses. The effects of lubricant properties, gear geometry and operating conditions were considered on the churning losses. They found that increasing the rotational speed, oil viscosity, module or face width leads to higher churning losses.

A computational fluid dynamics study was carried out by Hill, et al. [8] investigating the effect of using shrouding with spur gears on windage losses. Their results showed that an axial or a radial shrouding decreased the windage and the viscous losses.

Changenet, et al. [9] studied numerically the power loss from a six-speed spur gearbox. The power losses studied by Changenet, et al. [9] are the bearing losses, churning losses and friction losses. This study showed a simple way to predict the losses and temperatures using thermal networks by dividing the system into multiple lumped systems. The pinion rotational speed varied from 1000 to 7000 rpm. The maximum oil level was maintained at the shaft centerline. The thermal network was constructed of thermal resistances. They developed an equation for estimating churning losses using dimensional analysis for the six-speed gearbox.

Terauchi, et al. [10] carried out an experimental study of friction power losses in internal gears immersed in oil. The effects of gear surface finish, rotational speed and torque were considered. The study showed that the effect of surface finish can be neglected, increasing the speed slightly decreased losses; however, losses increased significantly with torque. The friction losses decreased slightly with the increase in the rotational speed due to the mixed lubrication condition. In the mixed lubrication, the friction coefficient is reduced with increasing the sliding speed.

Cho, et al. [11] simulated flow and temperature distributions inside a planetary gear train partially filled with oil. Three different volume oil levels of 30%, 50% and 70% were investigated. Results indicated that oil level has a significant effect on the rate of heat transfer and on the churning losses. Increasing the oil level results in higher churning losses.

Stavytskyy, et al. [12] compiled a comprehensive review on the load independent power losses in helical, spur and bevel gear trains. Their review included a various correlations developed for different configurations of gear trains. These correlations were for estimating different types of load independent power losses like the oil squeezing, churning and windage losses.

Other researchers considered the effect of thermal losses due to fluid motion (i.e., churning losses) in other applications such as in power generation systems, Engineer, et al. [13], and in two-phase flow heat exchangers, Ahmadi, et al. [14].

The above literature review indicates that many investigations have been carried out considering some aspects of the integrated, multi-physics, problem related to thermal performance of great trains. All these studies considered the effect of the rotational speed and oil level on the heat losses from the gear train. However, all studies considered the case of a stationary gear train casing. To the best of the authors' knowledge, there has not been any work investigating thermal performance of gear trains placed inside rotating casings, as in the case of SCDMDSs. The casing rotation affects heat dissipation to ambient air and the nature of the two-phase flow developed within the gear train; therefore it is expected to have a significant effect on the overall thermal performance of the gear train, hence, it is investigated in the present study.

4.3 Problem Definition

The problem of interest considers the thermal performance of a gear train placed inside a rotating casing attached to an annular gear. Thus, the casing is rotating at the same speed as the annular gear.

The gear train consists of an annular gear and a pinion gear, as shown in Figure 4.3. The number of teeth, z, of the pinion gear and of the annular gear is 11 and 49, respectively. The pressure angle of the gear train is 20°. The face width, b, is 20 mm. The outer diameters of the pinion and annular gears are 18.85 and 84 mm, respectively.

The flow and heat transfer is solved using the KISSsys and KISSsoft software [[15], which solve the kinematics and the heat transfer within the gear train and its casing. The operating conditions considered in the present study are those frequently used in self-contained drum motor drive systems. The oil level was varied from 0% (air only) to 100% (oil only). The casing rotational speed and torque were varied from 20 to 160 rpm and from 13 to 100 N.m, respectively.

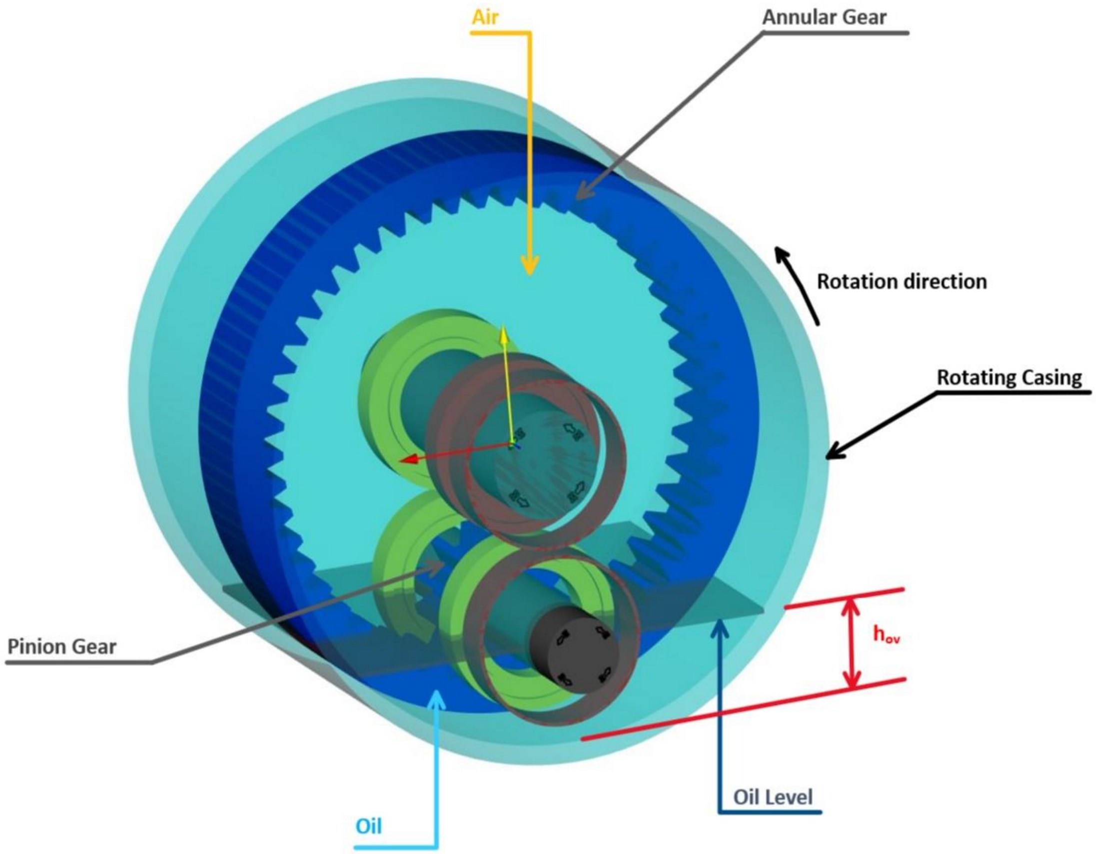

Figure 4.3 Details of gear train considered in the present study.

The gear train in the current study uses oil bath lubrication. The oil type used is the Enduratex-EP 150 oil. All oil properties have been obtained from the manufacturer's data [16]. Correlations of oil properties as function of temperature have been developed and presented in Table 4-1.

Table 4-1 Properties of Enduratex-EP 150 oil correlated as a function of temperature.

Fluid Property	Values from manufacturer's data [16]	Correlations developed by authors for the oil Enduratex-EP 150 properties
Density (ρ) [kg/m³]	856 kg/m³ @40°C 818 kg/m³ @100°C	$\rho(\mathrm{T}) = 880 - 0.44 * T - 0.0061 * T^2 + 6.398 * 10^{-5} * T^3 - 2.08817 * 10^{-7} * T^4$
Dynamic viscosity (μ) [Pa.s]	0.1284 Pa.s @40°C 0.01217 Pa.s @100°C	$\mu(\mathrm{T}) = 0.0146 + 2.6254 * e^{(-0.102338T)} + 9.7258 * 10^{-4} * T^2 * e^{(-0.077355T)} - 7 * 10^{-5} * T$
Thermal conductivity (λ) [W/m.°C]	0.14 W/m.°C	-

4.4 Mathematical Formulation

4.4.1. Governing Equations

The mathematical model solved by the KISSsys software [15] consists of the following governing equations.

The heat generated inside the gearbox (P_V) is the summation of all the load-dependent losses (P_L) and the load-independent losses (P_N) as in equation (1).

$$P_V = P_L + P_N \tag{1}$$

The load-dependent losses (P_L) are the load bearing (P_B) and the gear meshing losses (P_M), given in equation (2).

$$P_L = P_B + P_M \tag{2}$$

The load-independent losses (P_N) are the sum of the churning losses coming from the gears (P_W) and the gear train bearings (P_{WB}), as in equation (3).

$$P_N = P_W + P_{WB} \tag{3}$$

The bearing losses are calculated according to the SKF-Bearings [17] using equations (4) and (5).

$$P_B = 10^{-3} * f_1 * p_1 * d_m * \omega \tag{4}$$

$$P_{WB} = 1.6 * 10^{-8} * f_0 * {d_m}^3 * \omega \tag{5}$$

The coefficients f_0 and f_1 are determined based on the bearing type and lubrication type from the tables found in the SKF-Bearings [17]. p_1 is the bearing load in N.

P_W in equation (3) is calculated using equation (6).

$$P_W = \sum_{i=1}^{n} T_{H_i} * \frac{\pi * N_i}{30} \tag{6}$$

Where, T_H is the hydraulic loss torque of each gear (i = 1, for the pinion and i = 2, for the annular gear), which is determined using equation (7).

$$T_H = C_{Sp} * C_1 * e^{C_2 * (\frac{V_t}{10})} \tag{7}$$

Where C_1 and C_2 are constants calculated from equations (8) and (9). C_{Sp} is a factor that depends on the immersion of gears inside the oil and it is determined by KISSsys from the ISO [18].

$$C_1 = 0.063 * \left(\frac{2*h_{ov}}{0.01}\right) + 0.0128 * (\frac{b}{0.01})^3 \quad (8)$$

$$C_2 = \left(\frac{h_{ov}}{0.4}\right) + 0.2 \quad (9)$$

P_M in equation (2) is calculated using equation (10).

$$P_M = \zeta * \omega * \mu_m * H_V$$

(10)

Where, μ_m is the mean coefficient of friction for the gear mesh which is calculated from equation (11).

$$\mu_m = 0.048 * \left(\frac{F_{bt}/_b}{V_p*\rho_c}\right)^{0.2} * (\mu * 10^3)^{-0.05} * Ra^{0.25}$$

(11)

H_V in equation (10) is the gear loss factor. It is calculated by KISSsys from a set of factors and charts available in the ISO [18].

The heat dissipation by natural convection and radiation from the rotating drum, P_Q, is calculated from equation (12).

$$P_Q = \mathrm{hA}(T_{oc} - T_{amb}) + \sigma\varepsilon A\left({T_{oc}}^4 - {T_{amb}}^4\right) \quad (12)$$

4.4.2. Boundary Conditions

In reference to Figure 4.3, the above governing equations are subjected to the following boundary conditions.

At r = r_{oc}:

$$u_\Theta = \omega \frac{D_{oc}}{2} \tag{13}$$

$$u_r = u_z = 0 \tag{14}$$

The casing is exchanging heat with the ambient air by thermal radiation and natural convection as in equation (15).

$$q''_{conv} + q''_{rad} = q''_{cond} \tag{15}$$

So that,

$$\mathrm{h}(T_{oc} - T_{amb}) + \sigma\varepsilon\left({T_{oc}}^4 - {T_{amb}}^4\right) = -\mathrm{k}\frac{\partial T}{\partial r}\Big|_{r=r_{oc}} \tag{16}$$

The natural convection heat transfer coefficient, h, from the rotating drum has been calculated as function of the rotating Reynolds number using the correlation developed by Elghnam [19]. Provided here in equation (17). The value of the surface emissivity, ε, of the outer surface of the rotating steel drum is assumed 0.42 according to Carvill [20].

$$\mathrm{Nu} = \frac{\mathrm{h} * D_{oc}}{k} = 0.022 * \mathrm{Re}^{0.821} \tag{17}$$

All fluid properties used in equation (17) have been calculated at the bulk temperature which is the mean temperature (T_{mean}) of the average casing temperature (T_{oc}) and the ambient temperature (T_{amb}).

Since the present analysis considers a two-dimensional case, the symmetry boundary condition is used at Z=0 and Z=L

i.e., $\frac{\partial \eta}{\partial z} = 0$ (18)

Where, Z is the coordinate normal to the page and η is a place holder for any of the considered parameters, e.g., velocity component, temperature, pressure, etc.

4.4.3. Solution Technique

Since many of the parameters and coefficients used in the mathematical model depends on the oil temperature, which is not known, an iterative procedure is needed to determine the thermal field within the gear train.

The solver starts with an initial guess of the unknown oil temperature. Considering the assumed temperature, the solver determines all the coefficients and factors and then it calculates the amount of heat generated (P_V) and the amount of heat dissipated (P_Q). The solver compares the two values of P_V and P_Q, if the absolute difference between the two values is less than a certain pre-set convergence limit, e.g., 10^{-4}, the solver stops. If the difference is significantly higher than the present value, the solver continues the iterations. The solution procedure is illustrated by the flowchart provided in Figure 4.4.

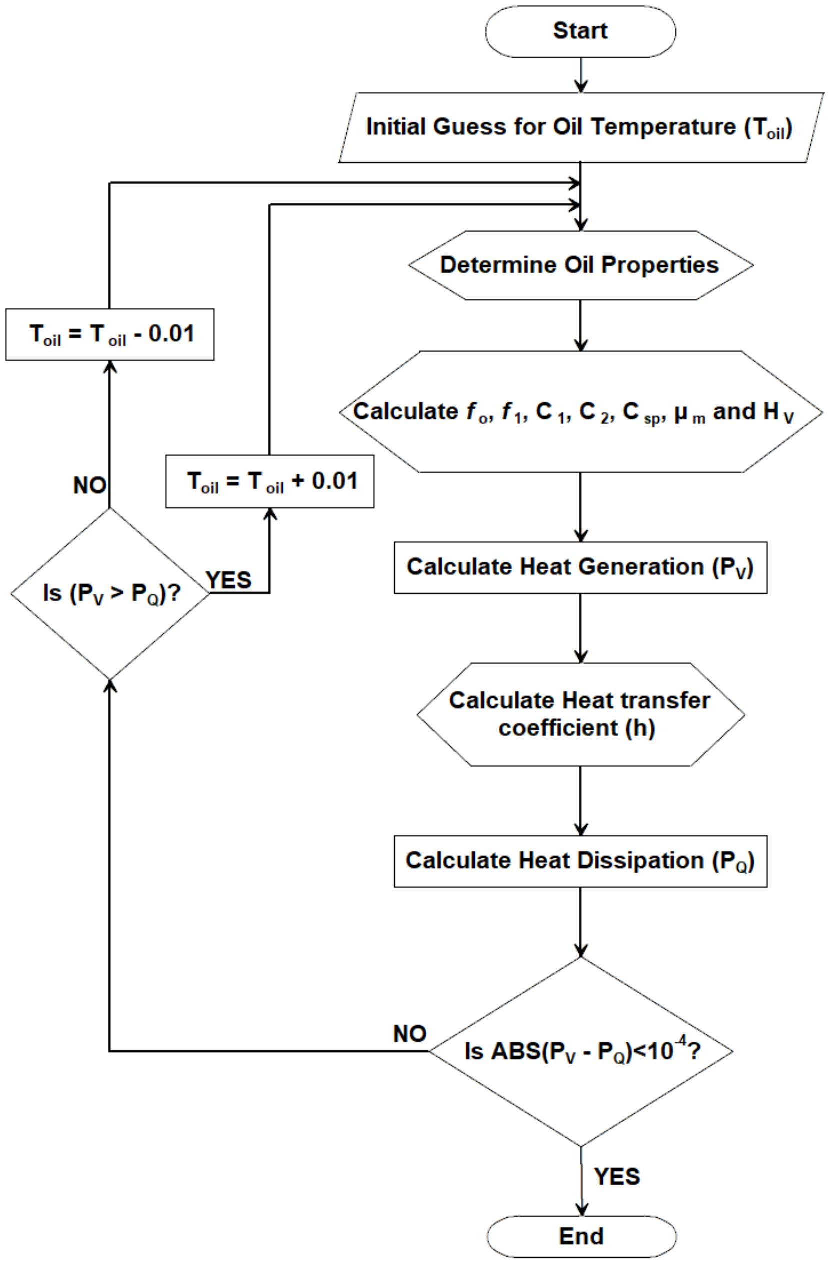

Figure 4.4 Flowchart of the solution technique.

4.4.4. Numerical Model Validation

The validation of the numerical model was carried out by comparing the numerical results with the experimental data reported by Polly [21]. The author studied the case of two helical gears rotating in an oil bath, as shown in Figure 4.5. Polly [21] investigated the total power losses at different rotational speeds, and normalized oil levels ($\bar{h}$). As shown in Figure 4.7, there is a reasonable agreement in the normalized power loss (Ps) between the current numerical model and the experimental data reported in Polly [21], with a maximum difference of 9.3%.

The difference between the current numerical results and the experimental data can be attributed to the uncertainties in each. The uncertainty in the experimental data used in the validation is about 3.4 %, as reported in Polly [21]. The expected uncertainty in the current numerical results is due to the fact that the numerical model uses the average oil temperature rather than the local oil temperatures in calculating the oil properties and the heat losses.

The validation case uses the normalized power loss (Ps) and the normalized oil level. The former is defined as the ratio of the total losses and the power input, as shown in equation (19). The total losses considered in the validation case are the meshing losses, the load-bearing losses and the churning losses. The normalized oil level ($\bar{h}$) is defined as the ratio of the oil level and the gear radius, as indicated in equation (20) and illustrated in Figure 4.6. Figure 4.6 shows the values of $\bar{h}$ considered in the validation case. The oil level is measured from the tangent to the gear bottom surface. Accordingly, the normalized oil level varies vertically from 0 to 2.

$$P_s = \frac{Total\ losses}{300\ W} \tag{19}$$

$$\bar{h} = \frac{\text{Oil vertical height from lowest point of gears}}{\text{Gear radius}} \tag{20}$$

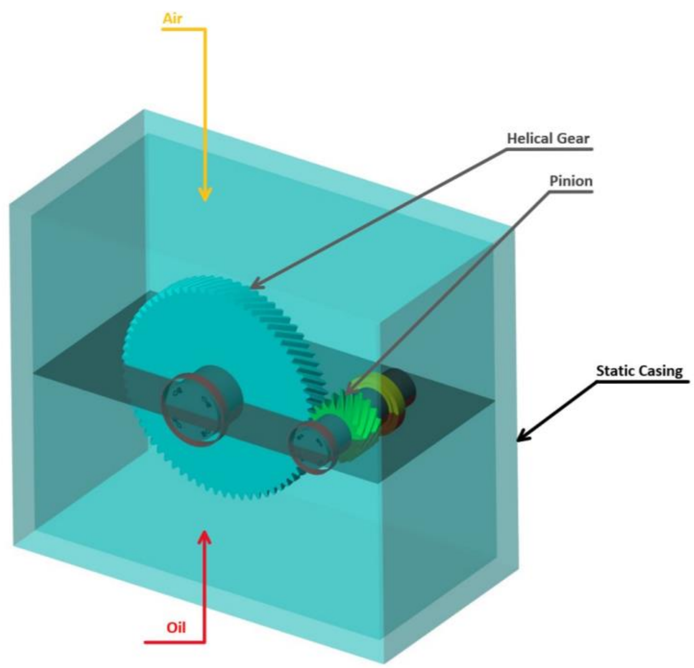

Figure 4.5 Details of the gear train considered by Polly [21] for the case of $\bar{h}$=1.

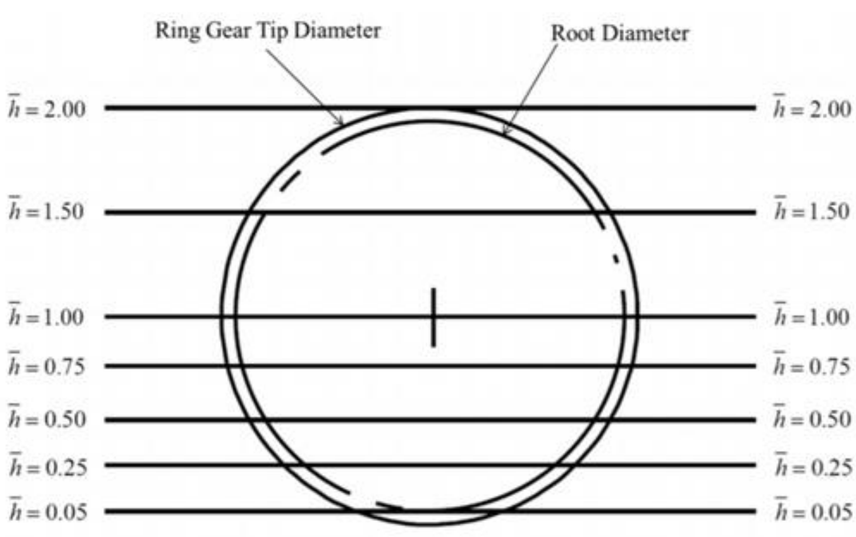

Figure 4.6 Levels of the normalized oil level ($\bar{h}$) considered by Polly [21].

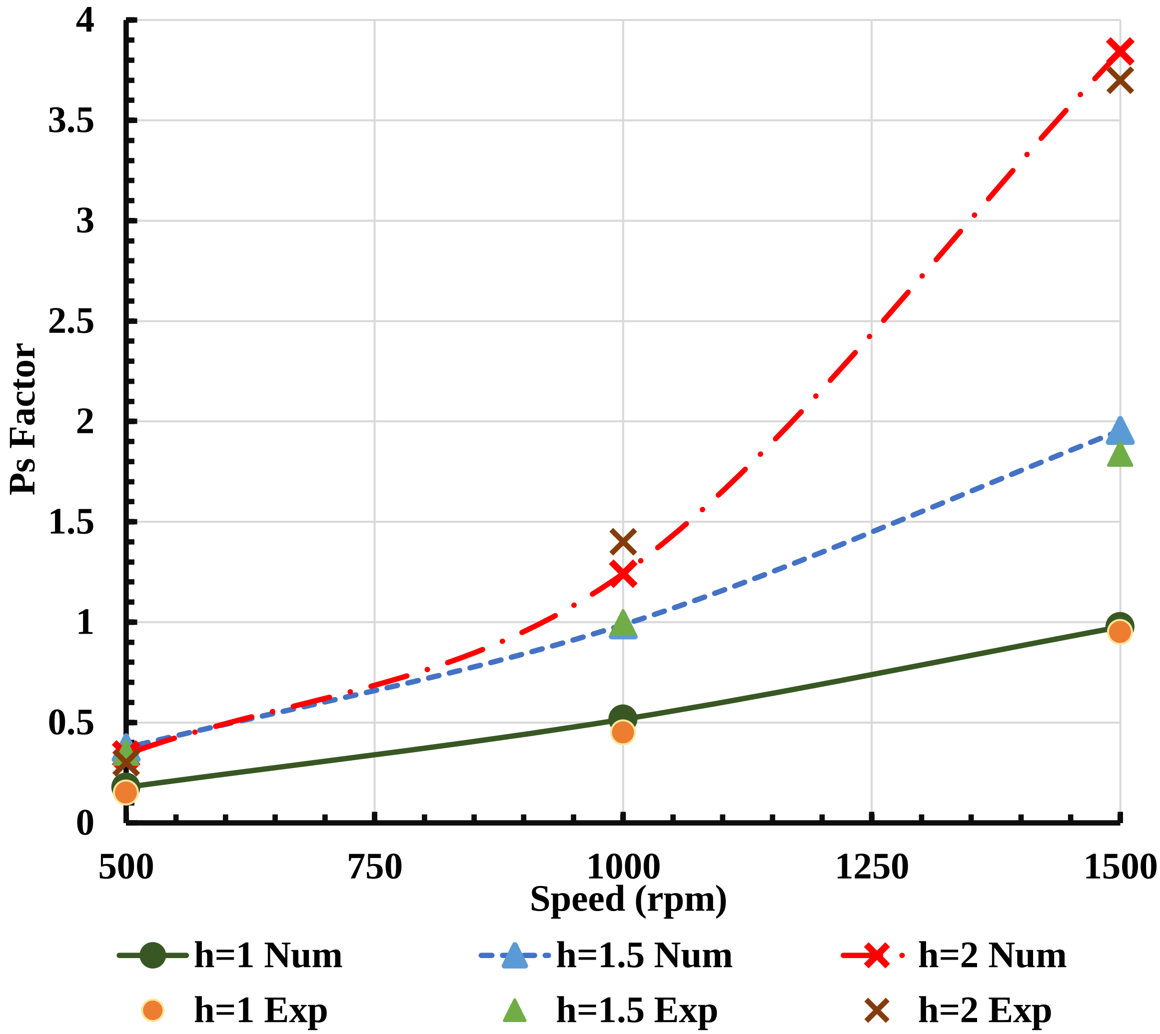

Figure 4.7 Comparison of present numerical results and experimental data reported in Polly [21].

4.5 Results and Discussion

The effect of oil volume percentage (OV), casing rotational speed (N) and torque (ζ) on the heat losses from the gear train has been investigated considering N of 20-160 rpm, OV of 0-100%, and ζ of 13-100 N.m. In addition, the effect of the casing rotational speed on the thermal performance of the gear train has been investigated. In the whole study, the heat losses from gear train considered are the meshing losses, bearing losses and churning losses. The squeezing losses are neglected as the operating rotational speeds of the gears are very low and the face width of the current gears is small. Hence, the difference in pressure built from the oil pocketing or oil squeezed between mating gears can be neglected. The bearings used are roller bearings opened to the oil surrounding. So, the bearing losses considered is not only a dependent on load losses. The bearing losses taken into consideration in the current paper includes a portion for an independent on load losses coming from the churning losses. This churning losses part in the bearing losses comes from the interaction of the rollers in the bearings with the multiphase flow (oil/air) surrounding it.

4.5.1. Effect of OV on gear train losses

Results obtained at N=100 rpm and ζ = 66 N.m at various OV values are shown in Figure 4.8. These results indicate that increasing the OV slightly decreased the meshing losses, due to the effect of oil lubrication. As the oil level increases, gear surface lubrication is increased and hence the friction factor between the mating gears is reduced. So, the friction losses (meshing losses) are reduced with increasing the amount of oil.

However, increasing the OV increased the churning losses up to OV = 31% at which case the pinion gear was completely submersed in oil. As the oil level is increased, the viscous dissipation coming from the oil is increased. The viscous dissipation represents the heat generated from the work done by the fluid to overcome the shear force with the adjacent layers. So, the load independent losses (churning losses) increase with increasing the oil level.

Increasing the oil level above 31% does not affect the churning losses and the total losses. Figure 4.9 shows the oil level corresponding to OV = 31 % beyond which the churning and total losses remained constant. All types of losses remained constant after that OV limit as the mating point between gears and the pinion gear are submerged inside oil. So that, no more enhancement in the gear surface lubrication, bearing lubrication and viscous dissipation is almost constant. Hence, the meshing losses, bearing losses and the churning losses are not affected by the OV if the OV is sufficient to submerge the pinion gear.

As the OV increases, the friction inside the bearing is reduced slightly due to the oil lubrication. However, as the roller bearing is subjected to oil and the type used in the gear train is not sealed bearing. So, the bearing losses increases as the oil enters through the bearing cavities and hence the churning losses part inside the bearing losses increases. But when the OV exceeds 31% it submerges the bearing and hence the bearing losses becomes constant.

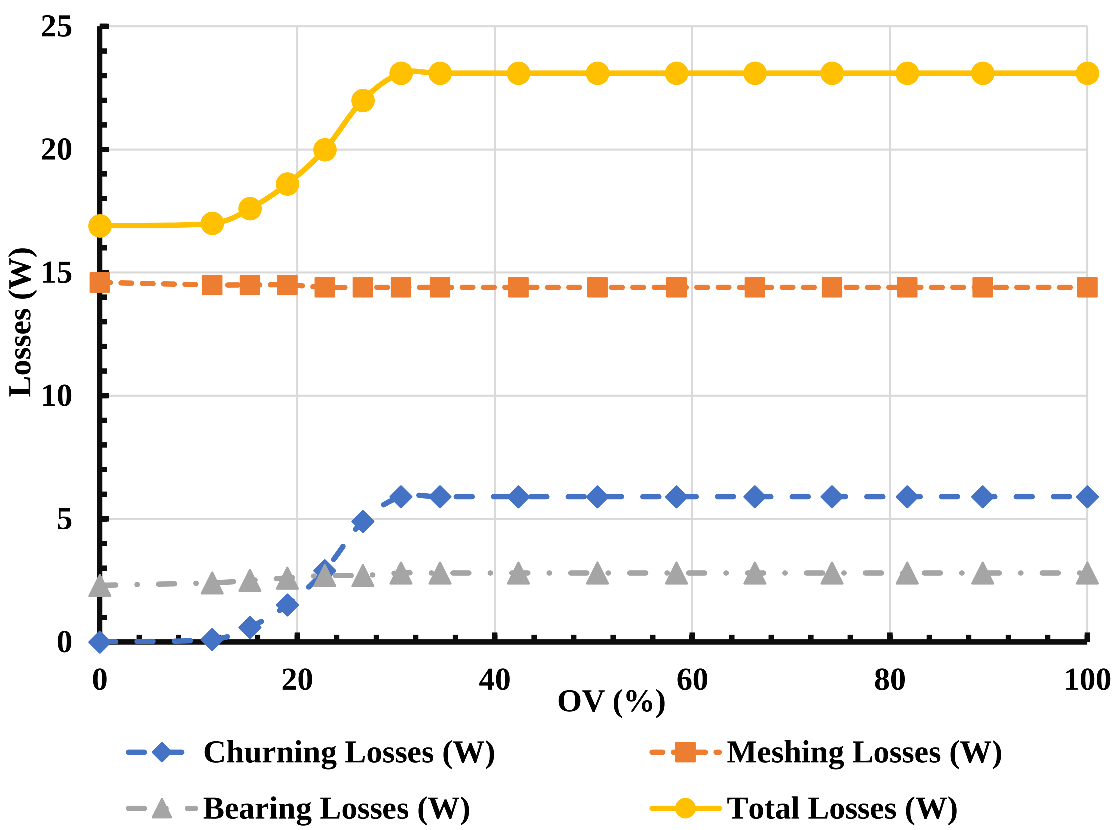

Figure 4.8 Effect of OV on gear train losses at N=100 rpm and ζ = 66 N.m.

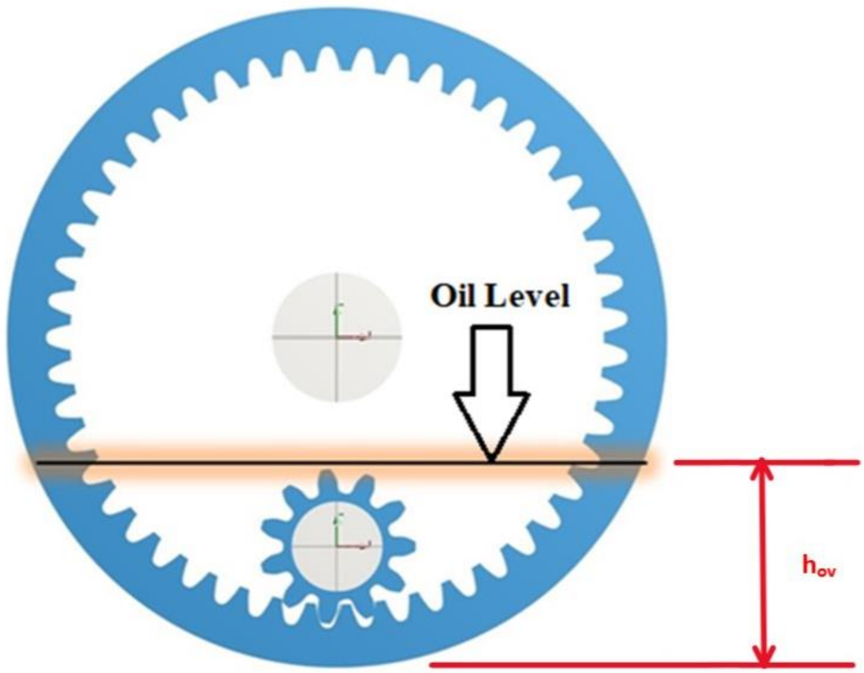

Figure 4.9 Oil level at OV = 31% corresponding to h_{ov} = 35 mm

4.5.2. Effect of rotational speed on gear train losses

The effect of casing rotational speed (N) at different oil levels is shown in Figure 4.10. The casing rotational speed has been varied from 20 to 160 rpm. The annular gear is attached to the rotating casing, so it has the same rotational speed as the rotating casing. The pinion gear rotational speed in the present gear train varies from 90 to 712 rpm. The torque in this section is kept constant at 66 N.m.

It is clear from Figure 4.10 that, increasing the rotational speed leads to a significant increase in the total losses. The major portion of increase in the total losses comes from the churning losses. As the rotational speed is increased, the viscous dissipation (internal friction between oil layers) increases dramatically. The viscous dissipation is related to the square of the strain rate, so the velocity increase has a great impact on it. Hence, the churning losses increases when increasing the rotational speed. At lower speeds, the OV effect on losses is almost neglected because the churning losses is changing slightly.

At high speeds, the effect of OV is very significant on the gear train losses as shown in Figure 4.10. The churning losses is changed dramatically at high rotational speeds hence varying the oil level at these high rotational speeds causes a considerable increase the gear train losses.

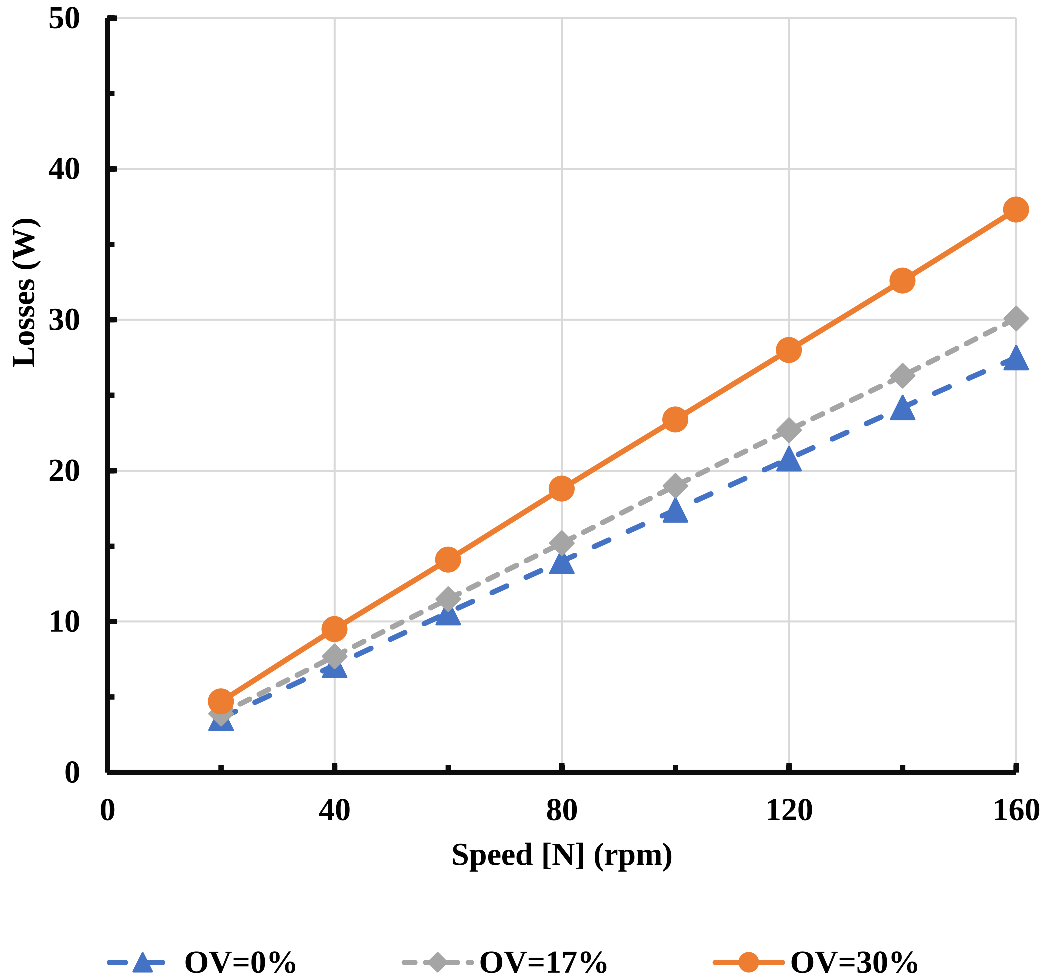

Figure 4.10 Effect of casing rotational speed (N) at torque (ζ) = 66 N.m on total losses from gear train

4.5.3. Effect of torque on gear train losses

The effect of casing torque (ζ) at different OV has been investigated as shown in Figure 4.11. The torque has been changed from 13 to 100 N.m. The rotational speed of the casing is fixed inside this section at 100 rpm.

When the torque increases, the total losses from the gear train increases as shown in Figure 4.11. This time the total losses increases as the meshing and bearing losses increases as the friction between the mating gears increases. The churning losses are not affected by changing the load as they are independent on load losses. The churning losses will only be affected by the rotational speed, oil level and lubricant properties.

From Figure 4.11, it is clear that having higher OV increases the total losses whatever the value of the torque. As the churning losses and viscous dissipation increases with increasing the amount of oil. The lines of constant OV are parallel to each other all over the entire range of torque. These lines are parallel as the churning losses are independent on load.

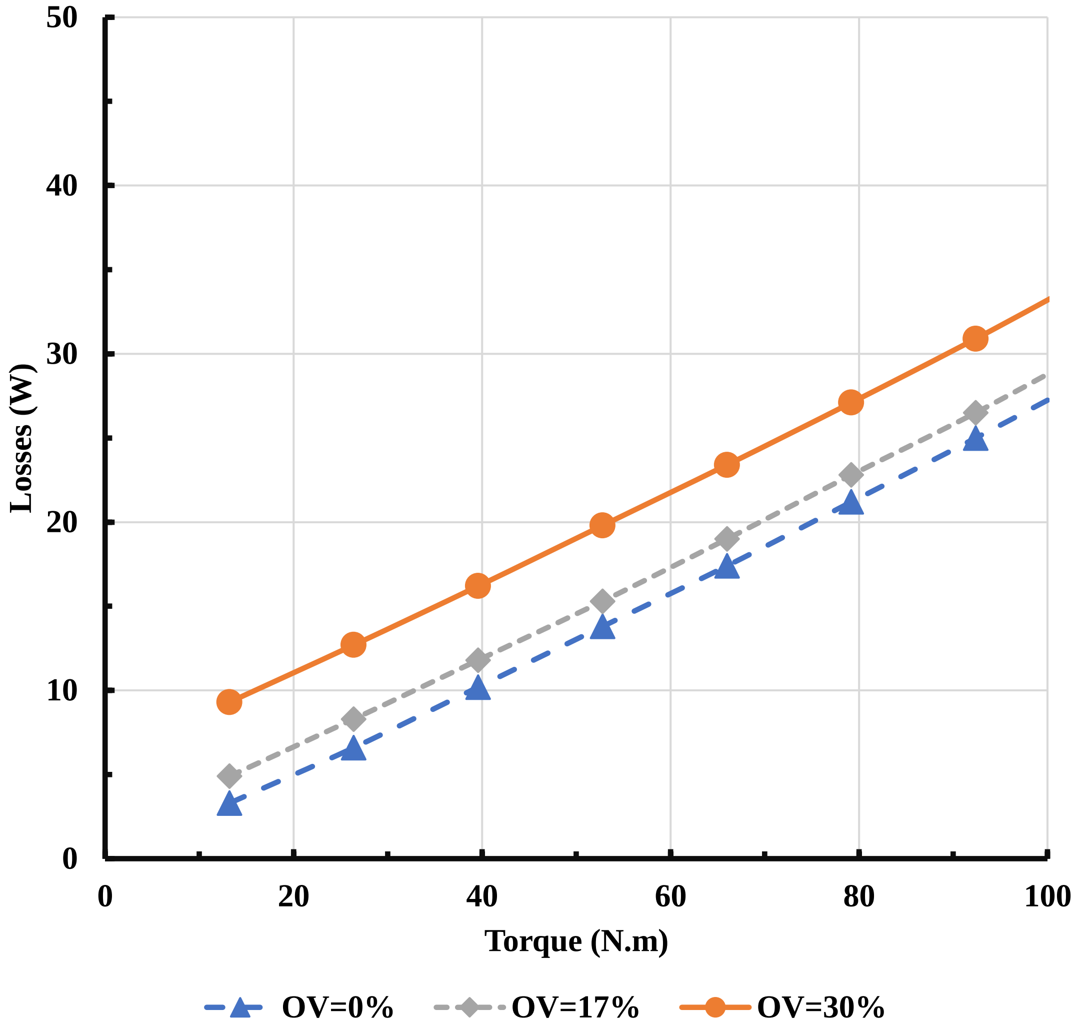

Figure 4.11 Effect of torque (ζ) at casing rotational speed (N) = 100 rpm on total losses from gear train

4.5.4. Effect of the casing speed on the overall thermal performance of the gear train

An investigation was performed to check the effect of having a rotating gear train casing compared to a stationary one. As shown in Figure 4.12, it is clear that having a rotating casing over the gear train dramatically affects the gear train losses. The rotating casing enhances the heat transfer from the rotating outer drum to the surrounding ambient air according to equation

(17). Hence, the oil temperature inside the gear train is higher in the stationary casing. As the temperature of oil rises its thermal properties changes, the oil viscosity (μ) drops in the stationary casing. As the oil loses its viscosity, its ability to make proper lubrication deteriorates because the film thickness formed over the gear surface is much thinner. In return the friction losses coming from the gear meshing losses and the bearing losses increases in the stationary casing compared to the rotating casing.

As clear from Figure 4.12, the loss from the gear train is reduced by about 12% compared to the stationary casing. This percentage increases at higher rotational speeds as the heat transfer coefficient to the surrounding ambient air is much better compared to the static casing.

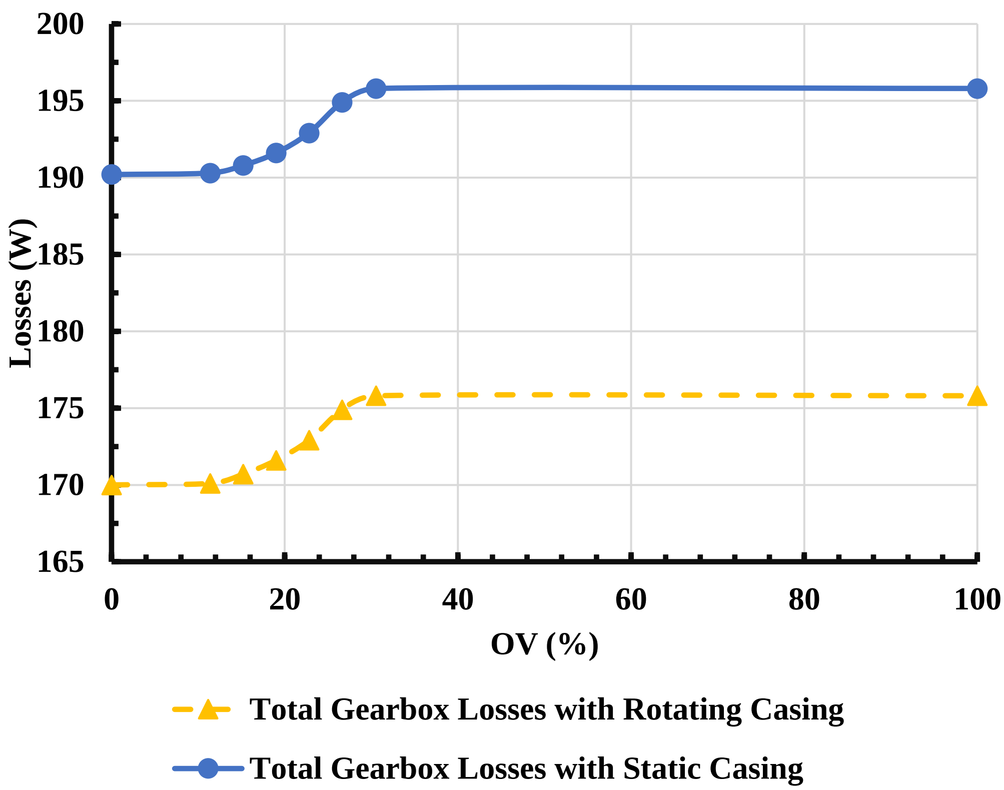

Figure 4.12 Effect of changing oil level and casing rotation on losses from gear train at ζ = 100 N.m and N = 460 rpm

4.6 Conclusions

The current paper investigated numerically the heat losses from an internal gear train. The effect of casing rotational speed, torque and oil volume percentage were considered. In addition, a comparison has been made between two cases including static or rotating casing.

Increasing the casing rotational speed increases the heat losses from the gear train. The effect of rotational speed becomes more significant when the oil level is high as the churning losses will rise it dramatically. The increase in the torque leads to an increase in the losses from the gear train whatever the value of the casing rotational speed or the oil volume percentage. The load just affects the meshing and bearing losses as they are the dependent on load losses.

The increase in the oil volume percentage increases the churning losses up to certain level then becomes constant. This specific oil level is determined by the height of oil required to submerge the pinion gear. After that level, increasing the oil level will not affect the heat losses from the gear train.

Having a rotating casing shows a positive impact on the performance of the gear train compared to a static casing. The rotational speed of the rotating casing improves the heat transfer to the surrounding air which in return improves the performance of the gear train by reducing the losses from the gear train.

4.7 Acknowledgement

The authors would like to acknowledge the financial and the technical support provided by Van der Graaf Inc. and financial support received from Mathematics of Information Technology and Complex Systems (MITACS).

4.8 References

[1] *Van der Graaf Drum Motors*. Available: https://www.vandergraaf.com/

[2] F. Concli and C. Gorla, "Analysis of the Oil Squeezing Power Losses of a Spur Gear Pair by Mean of CFD Simulations," in *ASME 2012 11th Biennial Conference on Engineering Systems Design and Analysis*, 2012, vol. Volume 2: Applied Fluid Mechanics; Electromechanical Systems and Mechatronics; Advanced Energy Systems; Thermal Engineering; Human Factors and Cognitive Engineering, pp. 177-184.

[3] P. P. Patil and A. Kumar, "Dynamic Structural and Thermal Characteristics Analysis of Oil-Lubricated Multi-speed Transmission Gearbox: Variation of Load, Rotational Speed and Convection Heat Transfer," *Iranian Journal of Science and Technology, Transactions of Mechanical Engineering,* vol. 41, no. 4, pp. 281-291, 2017/12/01 2017.

[4] H. Liu, T. Jurkschat, T. Lohner, and K. Stahl, "Determination of oil distribution and churning power loss of gearboxes by finite volume CFD method," *Tribology International,* vol. 109, pp. 346-354, 2017/05/01/ 2017.

[5] P. M. T. Marques, C. M. C. G. Fernandes, R. C. Martins, and J. H. O. Seabra, "Power losses at low speed in a gearbox lubricated with wind turbine gear oils with special focus on churning losses," *Tribology International,* vol. 62, pp. 186-197, 2013/06/01/ 2013.

[6] F. Concli, C. Gorla, A. Della Torre, and G. Montenegro, "Churning power losses of ordinary gears: A new approach based on the internal fluid dynamics simulations," *Lubrication Science,* vol. 27, pp. 313-326, 09/01 2014.

[7] S. Seetharaman and A. Kahraman, "Load-Independent Spin Power Losses of a Spur Gear Pair: Model Formulation," *Journal of Tribology,* vol. 131, no. 2, 2009.

[8] M. J. Hill *et al.*, "CFD Analysis of Gear Windage Losses: Validation and Parametric Aerodynamic Studies," *Journal of Fluids Engineering*, vol. 133, no. 3, 2011.

[9] C. Changenet, X. Oviedo-Marlot, and P. Velex, "Power Loss Predictions in Geared Transmissions Using Thermal Networks-Applications to a Six-Speed Manual Gearbox," *Journal of Mechanical Design*, vol. 128, no. 3, pp. 618-625, 2005.

[10] Y. Terauchi, K. Nagamura, and K. Ikejo, "Study on Friction Loss of Internal Gear Drives : Intluence of Pinion Surface Finishing, Gear Speed and Torque," *JSME international journal. Ser. 3, Vibration, control engineering, engineering for industry*, vol. 34, no. 1, pp. 106-113, 1991.

[11] J. Cho, N. Hur, J. Choi, and J. Yoon, "Numerical simulation of oil and air two-phase flow in a planetary gear system using the overset mesh technique," in *16th International Symposium on Transport Phenomena and Dynamics of Rotating Machinery*, Honolulu, United States, 2016, https://hal.archives-ouvertes.fr/hal-01894398/document

https://hal.archives-ouvertes.fr/hal-01894398/file/408.Cho2016.pdf.

[12] V. Stavytskyy, P. Nosko, P. Fil, A. Karpov, and N. J. T. K. M. i. E. R. B. Velychko, "Load-independent power losses of gear systems: A review," vol. 10, pp. 205-213, 2010.

[13] Y. Engineer, A. Rezk, and A. K. Hossain, "Energy analysis and optimization of a small-scale axial flow turbine for Organic Rankine Cycle application," *International Journal of Thermofluids*, vol. 12, p. 100119, 2021/11/01/ 2021.

[14] S. Ahmadi, P. Hanafizadeh, M. Eraghubi, and A. J. Robinson, "Upward flow boiling of HFE-7000 in high frequency AC electric fields," *International Journal of Thermofluids*, vol. 10, p. 100076, 2021/05/01/ 2021.

[15] *Kisssoft Software Manual*. Available: https://www.kisssoft.com/en/products/technical-description/brochures/kisssoft-release-2021-user-manual

[16] *Oil Enduratex EP 150*. Available: https://lubricants.petro-canada.com/en-ae/brand/enduratex-ep#4c438c61-0a61-4851-b43d-b1bfffe8539d

[17] SKF-Bearings. (2021). Available: https://www.skf.com/africa/en/products/rolling-bearings/principles-of-rolling-bearing-selection/bearing-selection-process/operating-temperature-and-speed/bearing-friction-power-loss-and-starting-torque

[18] I. J. I. S. ISO, "TR 14179-1: 2001 (E). Gears-Thermal capacity-Part 1: Rating gear drives with thermal equilibrium at 95 C sump temperature," 2001.

[19] R. I. Elghnam, "Experimental and numerical investigation of heat transfer from a heated horizontal cylinder rotating in still air around its axis," *Ain Shams Engineering Journal*, vol. 5, no. 1, pp. 177-185, 2014/03/01/ 2014.

[20] J. Carvill, *Mechanical engineer's data handbook / J. Carvill* (no. Accessed from https://nla.gov.au/nla.cat-vn1184479). Boston: Butterworth-Heinemann, 1993.

[21] J. H. Polly, "An Experimental Investigation of Churning Power Losses of a Gearbox," Master of Science, Mechanical Engineering, The Ohio State University, 2013.

Chapter 5

Numerical Study of Electric Motors Cooling Using an Axial Air Flow

Chapter 5

Numerical Study of Electric Motors Cooling Using an Axial Air Flow

Complete Citation:

A. M. Teamah and M. S. Hamed, "Numerical Study of Electric Motors Cooling Using an Axial Air Flow," Journal of Fluid Flow, Heat and Mass Transfer (JFFHMT), vol. Vol 9, pp. 101-105, 2022-09-16 2022.

Copyright:

Relative Contributions:

Ahmed M. Teamah: Wrote the first draft of the manuscript.

Mohamed S. Hamed: Revised and edited the manuscript.

Numerical Study of Electric Motors Cooling Using an Axial Air Flow

Ahmed M. Teamah* and Mohamed S. Hamed

Thermal Processing Laboratory, Department of Mechanical Engineering,

McMaster University, Hamilton, Ontario, Canada

*Corresponding Author: teamaha@mcmaster.ca, Tel: +1 905-920-6960

Abstract

A numerical study has been carried out considering the heat transfer inside a four-pole synchronous electric motor. The computational work has been carried out using the commercial package ANSYS-CFX 2021 R1. The focus of this study is on the effect of an axial air flow passing through the gap between the stator and the rotor. The rate of cooling of the axial flow in terms of the average Nusselt number has been investigated at different rotational speeds and air flows. All surfaces were considered smooth. The source of heat generation was considered only within the rotor from the electrical windage resistance while the stator was considered insulated. The effect of the rotational speed and axial flow has been represented by a rotational and an axial Reynolds number which were varied in the ranges of 1750- 27000 and 2140- 6425, respectively. The numerical results have been validated using published experimental data with an acceptable deviation. Results showed that the average Nusselt number increases with both the rotational and the axial Reynolds numbers. However, the axial Reynolds number has a more dominant effect on the rate of cooling than the rotational Reynolds number.

Keywords: Heat transfer, Taylor Couette Poiseuille flow, Rotating concentric cylinders.

5.1 Introduction

Any electrical motor generates heat from the losses inside its electric windage. Hence, electric motors require proper cooling to avoid overheating. The cooling of a synchronous electric motor can be achieved by passing an axial air flow through the slotted gap between the rotor and the stator. Figure 5.1 shows the shape and location of such gab in a four-pole electrical motor. The flow rate of the axial air flow required to provide sufficient cooling depends on the rotational speed. Hence, the effect of the rotational speed and the rate of axial air flow on the rate of heat transfer inside the motor gap must be investigated.

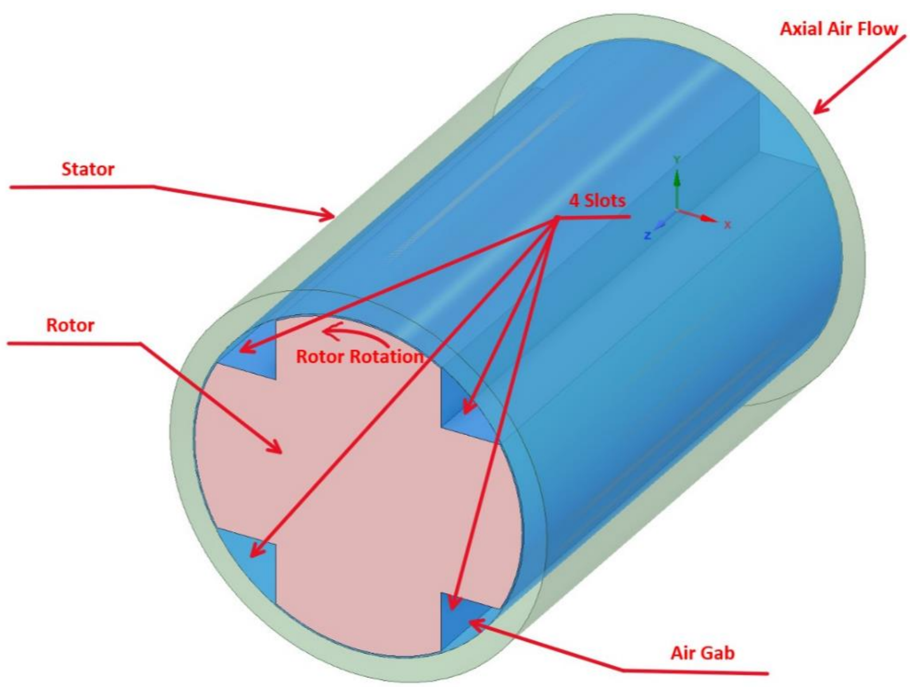

Figure 5.1 Air gap inside the synchronous motors

5.2 Literature Review

Cooling of electric motors has been studied by many researchers as it is very critical in electric motors operation. Studies like [1-4] focused on the fluid flow and heat transfer of the Taylor-Couette flow inside electric motors, which represents flow between two concentric cylinders without an axial flow.

A review of flow between concentric cylinders was carried out by [5]. The review covered the presence of an axial flow with the Taylor-Couette flow. The problem of interest which involves a Taylor-Couette flow with an axial flow has been referred to as the Taylor-Couette-Poiseuille flow. The Taylor-Couette flow might experience flow instabilities, especially if the inner cylinder is rotating at high speeds while the outer cylinder is fixed. [6] investigated Taylor-Couette flow instabilities.

Other authors studied Taylor-Couette flow (TCF) considering various configurations. [7] considered a multiphase TCF. [8] studied TCF in a narrow spherical gap. [9] considered TCF in a wider gap. [10] considered a laminar-and turbulent TCF. [11] considered a highly turbulent TCF. [12] studied a TCF between two concentric cylinders while the inner cylinder is having ribs. [13] investigated heat transfer characteristics of a TCF in a gap while the outer cylinder has a set of axially distributed slits.

[14] studied the effect of the gab entrance region on TCF with inner rotating cylinder and fixed outer cylinder. They showed that the entrance region in their case is similar to the entrance region of a pipe or a duct. [15] added a set of slots to the motor stator and investigated their effect on the rate of heat transfer of the flow within the annular gap. They showed that these slots have almost no effect on the rate of heat transfer.

To the best of the authors' knowledge, there has not been any studies that considered the effect of axial flow within a slotted rotor under operating conditions leading to a high rotational Reynolds number reaching 27000. These conditions are of prime interest in real practical applications.

5.3 Problem Definition

The problem of interest involves the cooling of a synchronous 4-pole electric motor using an axial air flow passing inside the gap between the rotor and the stator. The study resolves the flow and thermal fields inside the annular gap in the presence of the axial air flow through the rotor slots, as shown in Figure 5.2.

The inner rotating cylinder (i.e., the rotor) is subjected to a uniform heat flux of 500 W/m^2, which is the amount of heat generated due to electric losses within the motor windage. The outer cylinder (i.e., the stator) is assumed here as an insulated surface, hence no heat is being transferred to the surrounding air. All the walls were assumed smooth. Thermal radiation has been neglected. The radius ratio, (Rri/Rro), of the considered configuration is 0.65, which is similar to commercial synchronous motor available in market. The length of the rotor is 0.5 m.

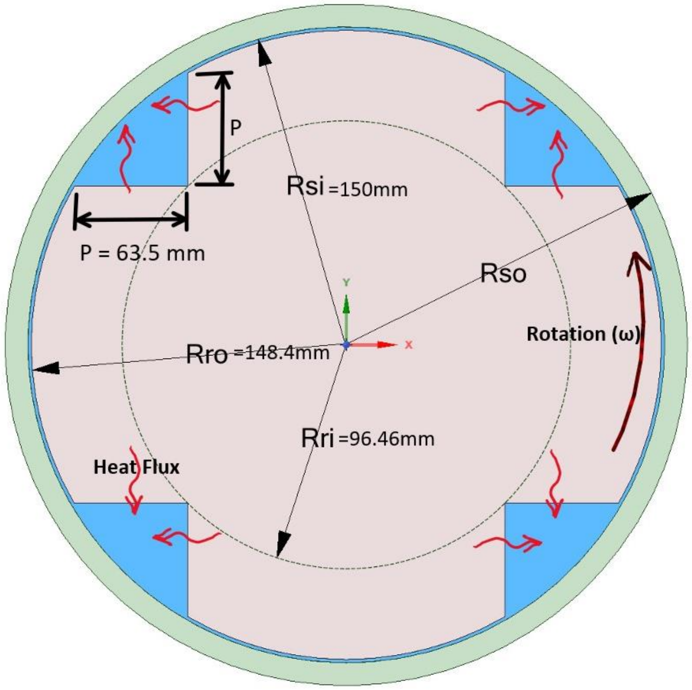

Figure 5.2 Schematic diagram of the present problem

5.4 Mathematical Model

The fluid flow and heat transfer problem has been simulated using ANSYS-CFX 2021 R1 commercial package. All the governing equations including mass, momentum and energy equations have been solved as referenced in [16].

The turbulence model used in this work is the Shear Stress Transport (SST) turbulence model to resolve the turbulence in the moving air flow. The SST turbulence model was chosen also in order to resolve the turbulent flow near the walls. The grid used in the current simulations has 10^6 elements. A grid dependence test has been carried out and the current grid has been selected so that the numerical results do not depend on the number of elements within 2%.

The boundary conditions are at the insulated fixed stator, a zero-heat flux is used. At the rotor: a fixed rotating speed (ω) is assumed. Its value was varied according to the value of the rotational Reynolds number (Re_r) considered in each simulation. The rotor surface was assumed smooth and subjected to a constant uniformly distributed heat flux of 500 W/m^2.

The air velocity at the entrance is constant and its value corresponds to the value of the axial Reynolds number (Re_a). Entering air temperature is assumed 25°C. At the exit: air pressure is equal to the atmospheric pressure.

The definitions of the axial Reynolds number (Re_a), the rotational Reynolds number (Re_r), the Nusselt number (Nu) and the hydraulic diameter (D_h) are provided in the following equations:

$$Re_a = \frac{V_a * D_h}{\nu_{air}} \tag{1}$$

$$Re_r = \frac{\omega * Rro * D_h}{\nu_{air}} \tag{2}$$

$$Nu = \frac{h * D_h}{K_{air}} \tag{3}$$

$$D_h = \frac{P}{2 + \sqrt{2}} \tag{4}$$

The axial velocity (V_a) is assumed equal to the average air velocity through the slots at the entrance. The kinematic viscosity (ν_{air}) and the thermal conductivity (K_{air}) of the air are calculated at the average fluid temperature across the gap. The heat transfer coefficient of air inside the gab is referred to by (h). The angular velocity of the rotor is identified by (ω). Gab width (P) is defined as shown in Figure 5.2.

5.4.1. Validation of The Numerical Results

Validation of the current numerical results has been carried out using experimental results published in [17]. [17] considered heat transfer from an axial air flow inside a slotted rotor of a synchronous electrical motor.

The hydraulic diameter used in [17] was 15.8 mm, the radius ratio was kept fixed at 0.75 and the value of the axial Reynolds number was 4280. The value of the rotational Reynolds number varied from 1750 to 10000. The heat generated inside the rotor is constant of 500 W/m^2. The maximum deviation between the present numerical results and the experimental data reported in [17] is about 16.8%, as illustrated in Figure 5.3.

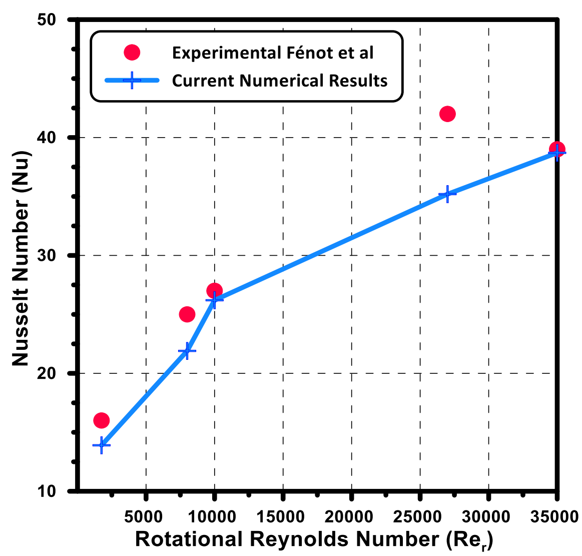

Figure 5.3 Comparison of current numerical results and experimental data reported in [17] at Re_a = 4280

5.5 Results and Discussions

The effect of the parameters investigated in the present study on the rate of heat transfer within the motor gap are: the rotational Reynolds number (Re_r) and the axial Reynolds number (Re_a) in the range of 1750 to 27000 and 2140 to 6425, respectively.

5.5.1. Effect of Re_r on Nu_{av}

Figure 5.4 shows the effect of the rotational Reynolds number on the average Nusselt number inside the motor gap. The axial Reynolds number is kept constant at 2140. Results indicated that, increasing the rotational speed enhanced the rate of heat transfer within the gap. The results showed that the rate of increase in Nusselt number decreased somewhat at Re_r about 8000. The slope in Figure 5.4 at Re_r = 8000 has decreased by about 60% compared to the slope at Re_r = 1750 (Green Line in Figure 5.4). The rate of increase in Nusselt number decreased after Re_r = 8000 due to the increase in air circulation and the formation of large eddies inside the four longitudinal slots. Figure 5.5 shows the increase in air circulations and eddies inside one of the slots at Re_r=27000 compared to that at Re_r=6000.

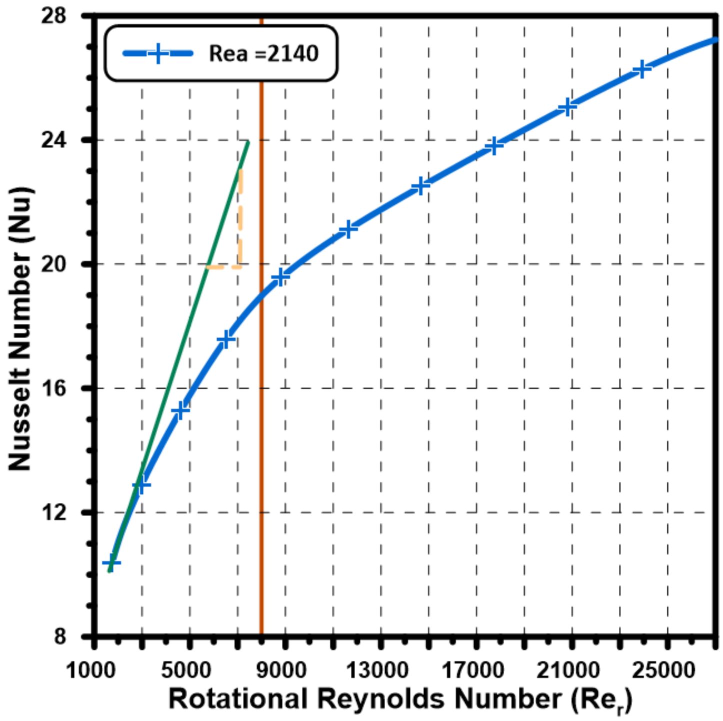

Figure 5.4 Effect of rotational Reynolds number on average Nusselt number at Re_a = 2140

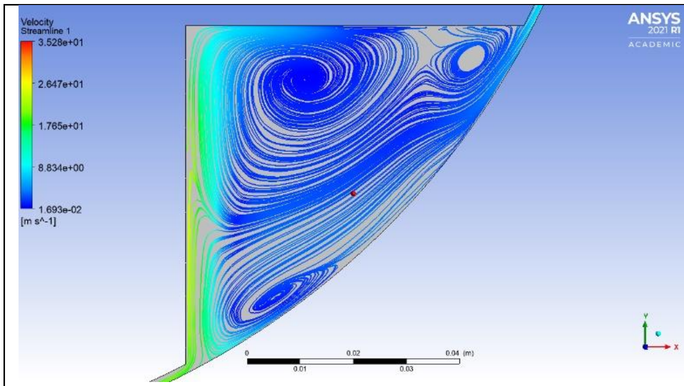

a) At Re_r=27000.

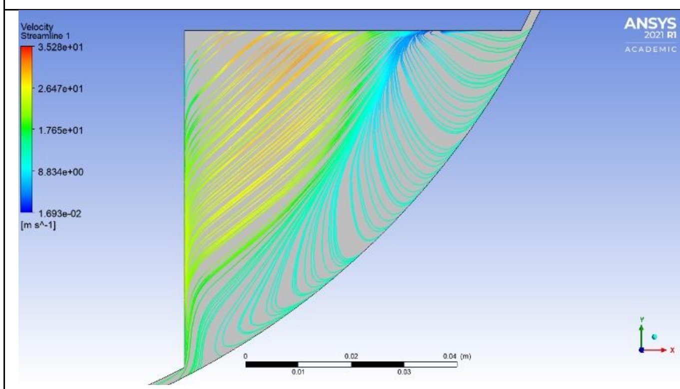

b) At Re_r=6000.

Figure 5.5 Streamlines at different Re_r at constant Re_a of 2140

5.5.2. Effect of Re_a on Nu_{av}

The effect of the axial and rotational Reynolds number on the average Nusselt number is shown in Figure 5.6. Increasing the axial Reynolds number (Re_a) from 2140 to 6425 resulted in an increase of the average Nusselt number inside the motor gap, at all values of Re_r considered in this study. Also increasing the rotational Reynolds number at any value of the axial Reynolds number resulted in improvement in the heat transfer inside the gap.

However, results showed that the effect of Re_a on the rate of heat transfer is more dominant than the effect of Re_r. Therefore, motor cooling is significantly improved by increasing the axial air velocity through the gap between the rotor and the stator. It is clear from Figure 5.6 that the rate of enhancement in Nu is reduced at Re_r equals to about 8000. Increasing Re_r above 8000 resulted in stronger eddies of hot air forming inside the gap (i.e., the slots), which decreased the rate of enhancement in Nusselt number, as shown in Figure 5.6.

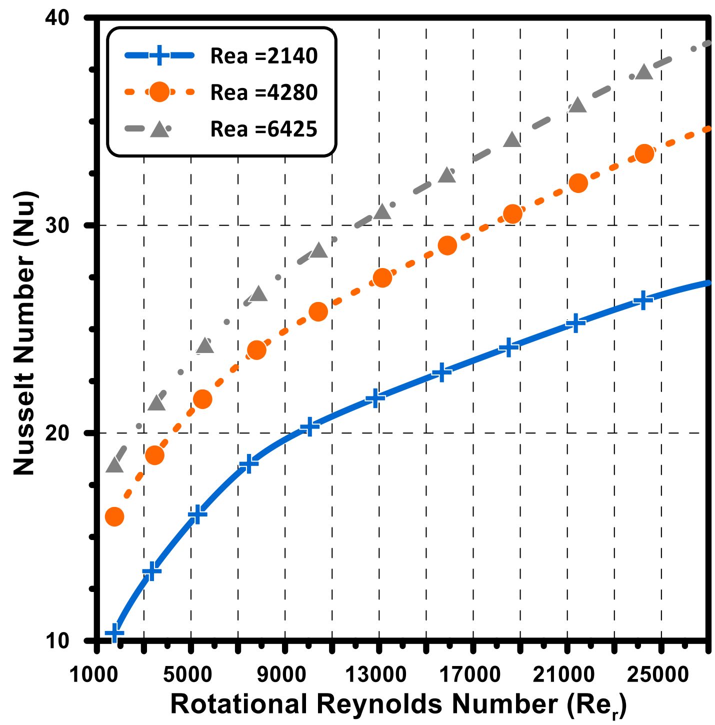

Figure 5.6 Effect of the Re_r and Re_a on Nuav

5.6 Summary and Conclusions

The rate of cooling of a slotted electric motor using an axial air flow has been investigated numerically considering the effects of the rotational and the axial Reynolds numbers. Results showed that increasing the axial air flow or the motor rotational speed improves motor cooling. However, the effect of the axial air flow is more pronounced than the effect of the rotational speed. Results also showed that better cooling is achieved when the rotational speed corresponds to a rotational Reynolds number value below 8000, as the rate of enhancement in the average Nusselt number is decreased above this value.

5.7 Acknowledgement

The authors would like to acknowledge financial support of this work received from Mathematics of Information Technology and Complex Systems (Mitacs).

5.8 References

[1] A. Fasquelle *et al.*, "Coupled electromagnetic acoustic and thermal-flow modeling of an induction motor of railway traction," *Applied Thermal Engineering,* vol. 30, pp. 2788-2795, 12/01 2010.

[2] Y. Huai, R. Melnik, and P. Thøgersen, "Computational analysis of temperature rise phenomena in electric induction motors," *Applied Thermal Engineering - APPL THERM ENG*, vol. 23, 05/01 2003.

[3] Z. Kolondzovski, A. Belahcen, and A. Arkkio, "Multiphysics thermal design of a high-speed permanent-magnet machine," *Applied Thermal Engineering - APPL THERM ENG,* vol. 29, pp. 2693-2700, 09/01 2009.

[4] C.-H. Huang and H.-C. Lo, "A three-dimensional inverse problem in estimating the internal heat flux of housing for high speed motors," *Applied Thermal Engineering - APPL THERM ENG*, vol. 26, pp. 1515-1529, 10/01 2006.

[5] M. Fénot, Y. Bertin, E. Dorignac, and G. Lalizel, "A review of heat transfer between concentric rotating cylinders with or without axial flow," *International Journal of Thermal Sciences - INT J THERM SCI*, vol. 50, pp. 1138-1155, 07/01 2011.

[6] G. I. Taylor, "Stability of Viscous Liquid Contained Between Two Rotating Cylinders," *Philosophical Transactions of the Royal Society of London,* vol. 223, pp. 289-343, 01/01 1923.

[7] A. M. Teamah and M. S. Hamed, "Investigation of transient multiphase Taylor-Couette flow," *Alexandria Engineering Journal,* vol. 61, no. 4, pp. 2723-2738, 2022/04/01/ 2022.

[8] S. Abbas and A. Shah, "Simulation of different flow regimes in a narrow-gap spherical Couette flow," *Applied Mathematics and Computation,* vol. 421, p. 126929, 2022/05/15/ 2022.

[9] N. A. Manikandan, K. Pakshirajan, and G. Pugazhenthi, "A novel rotating wide gap annular bioreactor (Taylor-Couette type flow) for polyhydroxybutyrate production by Ralstonia eutropha using carob pod extract," *Journal of Environmental Management,* vol. 299, p. 113591, 2021/12/01/ 2021.

[10] L. Jirkovsky and L. M. Bo-ot, "Laminar-turbulent transition in Taylor-Couette flow from a molecule dependent transport equation," *Physics Letters A*, vol. 408, p. 127481, 2021/08/27/ 2021.

[11] G. Luo and Z. Yao, "Decoupling tests on axial heat-transfer in highly turbulent Taylor-Couette flow using thermal waves," *Experimental Thermal and Fluid Science,* vol. 128, p. 110439, 2021/10/01/ 2021.

[12] M. Matsumoto *et al.*, "Enzymatic starch hydrolysis performance of Taylor-Couette flow reactor with ribbed inner cylinder," *Chemical Engineering Science,* vol. 231, p. 116270, 2021/02/15/ 2021.

[13] S.-l. Sun, D. Liu, Y.-Z. Wang, S. M. R. S. Naqvi, and H.-B. Kim, "Heat transfer characteristics of Taylor–Couette flow with axially distributed slits using field synergy principle and entropy generation analysis," *International Communications in Heat and Mass Transfer,* vol. 129, p. 105699, 2021/12/01/ 2021.

[14] M. Molki, K. N. Astill, and E. Leal, "Convective heat-mass transfer in the entrance region of a concentric annulus having a rotating inner cylinder," *International Journal of Heat and Fluid Flow,* vol. 11, pp. 120–128, 06/01 1990.

[15] C. Gazley, "Heat transfer characteristics of the rotational and axial flow between concentric cylinders," *Trans. ASME,* vol. 80, pp. 79-90, 01/01 1958.

[16] C. J. S. t. g. ANSYS, ANSYS, "Release 12.0 User's guide," 2009.

[17] M. Fénot, E. Dorignac, A. Giret, and G. Lalizel, "Convective heat transfer in the entry region of an annular channel with slotted rotating inner cylinder," *Applied Thermal Engineering,* vol. 54, pp. 345–358, 05/14 2013.

Chapter 6

Cooling of a Synchronous Electric Motor Using An Axial Air Flow

Chapter 6

Cooling of a Synchronous Electric Motor Using An Axial Air Flow

Relative Contributions:

Ahmed M. Teamah: Wrote the first draft of the manuscript.

Mohamed S. Hamed: Revised and edited the manuscript.

Cooling of a Synchronous Electric Motor Using An Axial Air Flow

Ahmed M. Teamah* and Mohamed S. Hamed

Thermal Processing Laboratory, Department of Mechanical Engineering,

McMaster University, Hamilton, Ontario, Canada

*Corresponding Author: teamaha@mcmaster.ca, Tel: +1 905-920-6960

Abstract

The current work investigates the rate of cooling of an axial air flow through the gap between the stator and the rotor of a four-pole synchronous electric motor. The axial air is passing though the rotor's four longitudinal slots. The stator is considered insulated. The effect of the axial air flow rate, the rotor rotational speed and the slot size on the average Nusselt number has been investigated numerically using ANSYS-CFX. These effects have been studied considering a motor radius ratio (RR) in the range of 0.65-0.85, an axial Reynolds number (Re_a) between 1750 and 40000 and a rotational Reynolds number (Re_r) of 1750 up to 35000. Numerical results have been validated using published experimental data. The maximum deviation was less than 15%. The present numerical results showed that increasing the axial air flow rate always enhances the rate of cooling. The effect of the axial Reynolds number was found to be more dominant than that of the rotational Reynolds number. Increasing the rotor rotational speed (Re_r) enhanced the rate of heat transfer up to a certain limit beyond which a revered effect was observed. Such limit was investigated and found to depend on the motor radius ratio and the relative magnitude of the axial and rotational Reynolds numbers

represented by $X = Re_a/Re_r$. The enhancement due to increasing Re_r was reversed at X = 0.35 and 0.12 when RR was at 0.85 and 0.75, respectively. A new correlation of the average Nusselt number as function of X has been developed.

Keywords: Electric Motor Cooling , Synchronous Electric Motors, Taylor-Couette-Poiseuille Flow, Rotating Concentric Cylinders.

Nomenclature

D_h	Hydraulic diameter, $D_h = \frac{P}{2+\sqrt{2}}$, m.
e	Annular gap, m.
h	Heat transfer coefficient, W/m^2.°C.
h_{tot}	Specific total enthalpy, m^2/sec^2
k	Thermal conductivity, W/m.°C.
L	Length, m.
Nu	Nusselt number, hD_h/k.
P	Slot width, m.
p	Pressure, Pa.
r	Radius, m.
Rri	Inner radius of rotor, m.
Rro	Outer radius of rotor, m.

RR	Radius Ratio of rotor, Rri/Rro.
Rsi	Inner radius of stator, m.
Rso	Outer radius of stator, m.
Re_a	Axial Reynolds number, $V_a D_h/\upsilon$.
Re_r	Rotational Reynolds number, $V_t D_h/\upsilon$.
t	Time, Second.
T	Temperature, °C.
Ta	Taylor number, $\omega^2 Rro(D_h/2)^3/\upsilon^2$
u	Fluctuating velocity component in turbulent flow, m/sec.
U	Velocity vector of velocity components (u_r, u_Θ, u_z), m/sec.
V_a	Mean axial velocity at entrance, m/sec.
V_t	Mean tangential velocity, ω*Rro, m/sec.
X	Reynolds number ratio, Re_a/Re_r

Greek symbols

α	Thermal diffusivity, m^2/sec.
λ	Turbulence kinetic energy per unit mass, J/kg.
μ	Dynamic viscosity, kg/m.s.

υ	Kinematic viscosity, m^2/s.
ρ	Density, kg/m^3
τ	Shear stress tensor, N/m^2
ω	Angular speed, rad/sec.
Ψ	Specific turbulence dissipation rate, 1/sec.

Subscript & Indexes

conv	Convective.
i	Inner surface.
o	Outer surface.
rotor	Rotor of the electric motor.
slot	Rotor slots.
Stator	Stator of the electric motor.

6.1 Introduction

Synchronous motors are widely used in the industry due to their ability to maintain a constant rotational speed regardless of the level of the applied load. The constant speed is achieved by synchronizing the rotor with the frequency of the electric alternating current connected to the motor. This kind of electric motor generates heat and needs to be cooled to avoid overheating. As their rotor contains longitudinal slots, a convenient way of cooling these electric motors is bypassing an axial cold air flow through these slots. The rate of axial air flow to avoid overheating must be determined based on the motor's operating conditions, particularly the motor's rotational speed. The configuration of these motors is shown in Figure 6.1.

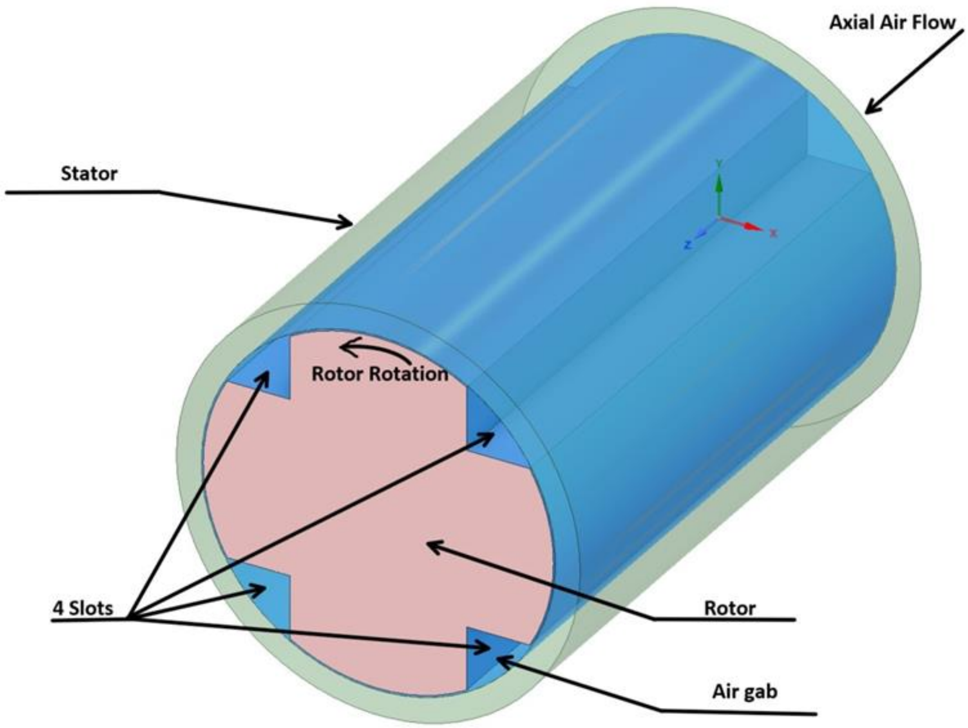

Figure 6.1 Configuration of an air gab inside a synchronous motor.

6.2 Literature Review

Many researchers have studied the rate of heat transfer and fluid flow inside electric motors considering many industrial applications. Fasquelle, et al. [1] have studied numerically and experimentally the rate of heat transfer and fluid flow within an induction motor used in railway traction. Their model solved the electromagnetics to find the losses in the motor. The thermal part was solved by a thermal resistance network of a similar model. They studied the effect of the rotational speed on the motor losses and the internal flow structure inside the motor gap. The rotational speed varied from 1500 to 4000 rpm. They found that increasing the rotational speed always increased the mechanical losses generated within the motor. However, the iron losses in the motor decreased with the increase in the rotational speed.

Humphreys, et al. [2] studied the effect of an axial turbulent air flow inside a rotating circular duct. The duct is rotating to a horizontal axis parallel to it and shifted by a fixed distance from its axis. Their study was carried out experimentally. They considered an axial Reynolds number in the range of 5000 to 20000 and varied the motor rotational speed between 0 and 500 rpm. They considered uniform heat flux and uniform temperature distribution conditions. Their results showed that increasing the axial Reynolds number or the rotational speed would enhance the rate of heat transfer.

Huai, et al. [3] carried out a study to estimate the losses from an induction motor. An experimental model was constructed to validate their numerical temperature distributions obtained at various operating conditions using FEMLAB. They considered a 1.5 KW squirrel cage induction motor. A SIMULINK model was developed to predict the temperature rise inside the model. They found that the highest temperature was located at the two ends of the windings.

A numerical study by Kolondzovski, et al. [4] was carried out for a high speed permanent magnet motor. The motor had an axial air flow cooling through the circular gap between the rotor and the stator. They used the COMSOL Multiphysics software. They considered a very high rotational speed of 31,500 rpm and a power of 130 KW. They obtained the temperature distribution inside the solid rotor and the air gap. They found that the highest temperature rise for the cooling air was at the air exit. The maximum temperature of the rotor shaft was at the middle of the shaft.

Huang and Lo [5] focused on the transient heat generation inside high-speed electric motors using inverse heat conduction techniques. The electrical motor housing had a spiral cooling passage. Transient heat fluxes inside the rotor and the stator were studied using inverse heat conduction. When the heat flux value was determined, a 3D model using ANSYS-CFX was used to find the detailed temperature distribution within the motor housing. They found that the estimated heat flux within the cooling passages was not accurate due to the complexity of the geometry of the cooling channels inside the motor housing. However, using the method of effective heat flux improved the accuracy by taking the average heat flux over the surface.

The flow within the annular space between the motor rotor and stator can be considered a Taylor-Couette flow. A comprehensive review of flow between concentric cylinders was carried out by Fénot, et al. [6]. They considered Taylor-Couette flows with and without axial air flows. The review covered the effect of the rotational speed, axial ratio (L/(Rsi – Rro)) and gap thickness on the rate of heat transfer and fluid flow. They concluded that the rate of heat transfer can be enhanced by increasing the rotational speed or by narrowing the gap (i.e., larger RR) or by adding slots to the rotor or to the stator or to both.

Becker and Kaye [7] studied the Taylor-Couette flow at very low Taylor numbers for a laminar steady flow. They found that the heat transfer mechanism was dominated by conduction. Taylor [8] investigated flow instabilities that occur within flows between rotating cylinders. He defined a critical Taylor number of approximately 1700 at which the flow became unstable, forming what he called Taylor vortices.

Gollub and Swinney [9] and Serre, et al. [10] studied the Taylor-Couette flow at high Taylor numbers at which cases increasing the rotational speed led to the development of complex flow regimes having many vortices and the flow became highly turbulent. Other researchers, e.g., Nijaguna and Mathiprakasam [11] and Bouafia, et al. [12] have studied heat transfer of the Taylor-Couette flow at high Taylor numbers. They have found that increasing the Taylor number enhanced the rate of heat transfer due to the increased turbulence. The increase in the rate of heat transfer was found to be proportional to the value of Taylor number raised to the power of quarter (i.e., $Ta^{1/4}$).

Taylor-Couette-Poiseuille flow includes the superposition of an axial flow to a rotational flow. Kaye [13] studied this type of flow and identified four flow regimes: laminar, turbulent, laminar with Taylor vortices and turbulent with Taylor vortices. This flow is dependent on both the rotational speed and the axial flow speed. Molki, et al. [14] studied the effect of the gab entrance region and showed that it is similar to the entrance region of a pipe or a duct. Tachibama, et al. [15] studied experimentally the axial flow between two concentric cylinders. The inner cylinder was heated and rotating, while the outer was stationary. They found that increasing the rotational speed or the axial flow rate enhanced the heat transfer. Poncet, et al. [16] also studied the Taylor-Couette-Poiseuille flow numerically in a narrow gap of radius ratio = 0.961. Correlations have been developed for the average Nusselt number for both cylinders.

In the case of cooling electric motors using an axial flow, due to the presence of slots with different sizes over the rotor surface, the flow in this case is not just a Taylor-Couette-Poiseuille flow inside the annular gap. The flow problem is much more complex.

Very few investigations related to this complicated case can be found in the literature. Gazley [17] studied the effect of adding slots to the motor rotor or to the stator or both on the rate of heat transfer to the flow within the annular gap. The slots introduced by Gazley [17] were rectangular and considered to be insulated. The radius ratio taken into consideration about 0.975. They concluded that these slots had almost no effect on the rate of heat transfer within the gap in comparison with the regular case without slots.

Yanagida and Kawasaki [18] studied the Taylor-Couette-Poiseuille flow in the gap between the rotor and the stator. They had 60 rectangular slots in the stator. The radius ratio considered in this study was 0.99. The rotational Reynolds number was varied from 500 to 64,000. The axial Reynolds number was varied from 4400 to 17,000. They found that the rate of heat transfer was increased when the slots were added compared to the plain stator case.Their results showed that Nusselt number was increased by increasing the axial or the rotational Reynolds numbers.

Jeng, et al. [19] investigated experimentally the effect of adding a set of longitudinal ribs on the outer surface of the rotating inner cylinder. The radius ratio used in their study was 0.95. The outer cylinder was kept stationary. An air axial flow was superimposed within the gap. The axial Reynolds and the rotational Reynolds numbers varied in the ranges of 30 – 1200 and 0 – 2922, respectively. The use of the longitudinal ribs enhanced the rate of heat transfer by about 140% compared to the case of no ribs at $Re_r = 2000$ and $Re_a = 600$.

Nouri-Borujerdi and Nakhchi [20], studied the effect of adding grooves over the inner surface of a stationary outer cylinder while keeping the surface of the inner rotating cylinder unchanged. They included an axial air flow in the gap. The number of grooves, their aspect ratio, the values of the axial Reynolds number, the Taylor number and the outer cylinder surface temperature were varied in the range of 0 - 20, 0 - 1.5, 4440 - 14,300 , 0 - 8.36×10^6, and 50 - 90 °C, respectively. They found that increasing the number of grooves, the rotational speed, the axial Reynolds number and the groove aspect ratio enhanced the rate of heat transfer. The groove aspect ratio of 1.5 gave the highest enhancement of 115% compared to the case with no grooves.

The previous literature review indicates that many investigations have been carried out on the Taylor-Couette flow and the Taylor-Couette-Poiseuille flows without slots. A limited number of studies considered the effect of rectangular slots on the rate of heat transfer within a Taylor-Couette-Poiseuille flow. To the best of the authors' knowledge, there has not been any studies that covered the case of a Taylor-Couette-Poiseuille flow with triangular slots except the authors' previous study reported in Teamah and Hamed [21] and the work of Fénot, et al. [22] which considered constant values of the radius ratio at 0.65 and 0.72, respectively. The different configurations and dimensions of the added slots have not been assessed before. The novelty of the current work is that it provides a comprehensive analysis of the axial air flow within the annular space (gap) between the stator and a slotted rotor, taking into account the effect of slot size, the axial and the rotational Reynolds numbers on the cooling of a synchronous electric motor. The main objective of this study is to develop a new correlation that can be used to achieve proper cooling strategies for these electric motors.

6.3 Problem Definition

The problem of interest involves investigating the fluid flow and heat transfer within an annular space between an outer stationary cylinder (stator) and an inner slotted rotating cylinder (the rotor), as shown in Figure 6.2. An axial air flow is passing through the slots. The inner cylinder is subjected to a constant heat flux of 500 W/m^2 that represents the rate of heat generated within the motor. The axial air temperature that has been used at the entrance is of ambient air at 25°C. The axial air velocity has varied between 1.8 and 76 m/s which corresponds to an axial Reynolds number in the range of 1.75×10^3 to 4×10^4.

Figure 6.2 shows the problem dimensions for the case of radius ratio, RR = 0.65. The value of RR was varied between 0.65 to 0.85 by varying the slot dimension P between 29.5 and 63.5 mm which represents the typical range used in synchronous electric motors [23]. The motor length, normal to the page in Figure 6.2, is 0.55 m.

The rotor speed has been varied between 100 and 3600 rpm corresponding to a rotational Reynolds number in the range of 1.75×10^3 to 3.5×10^4. This wide range of rotor speed has been chosen to cover motors with high number of poles like big salient pole in hydro generators and ordinary 2-pole motor which is common in many applications. All surfaces are considered smooth, and the effect of radiation heat transfer was neglected due to typical low temperatures

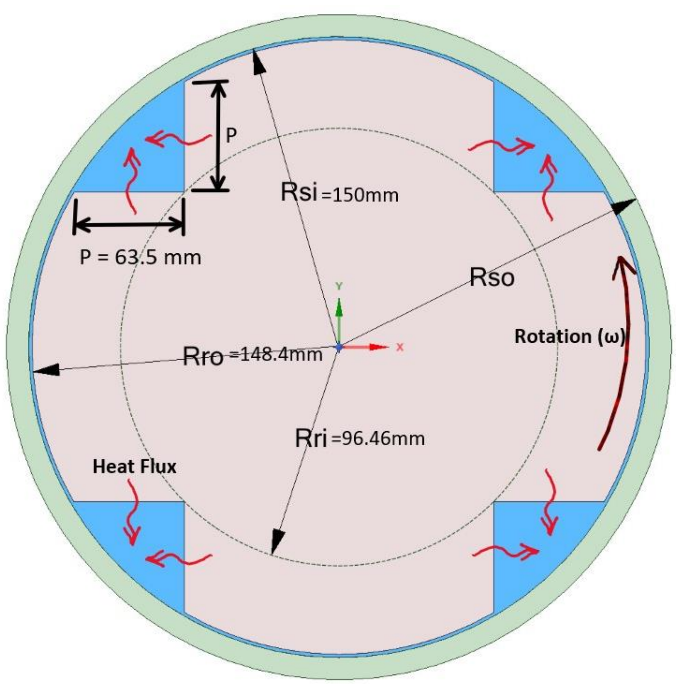

Figure 6.2 Schematic diagram of the present Problem at RR=0.65

6.4 Mathematical Model

6.4.1. Governing Equations for the Problem

A numerical model was developed for the current problem using ANSYS-CFX. The governing equations for the solver are from ANSYS [24] as follows:

$$\frac{\partial \rho}{\partial t} + \nabla \cdot (\rho U) = 0.0 \tag{1}$$

$$\frac{\partial (\rho U)}{\partial t} + \nabla \cdot (\rho U \otimes U) = -\nabla p + \nabla \cdot \tau \tag{2}$$

$$\frac{\partial (\rho h_{tot})}{\partial t} - \frac{\partial p}{\partial t} + \nabla \cdot (\rho U h_{tot}) = \nabla \cdot (k \nabla T) + \nabla \cdot (U \cdot \tau) \tag{3}$$

Where the shear stress tensor and total enthalpy are defined in equations(4) and (5).

$$\tau = \mu \left(\nabla U + (\nabla U)^T - \frac{2}{3} \delta \nabla \cdot U \right) \tag{4}$$

$$h_{tot} = enthalpy + \frac{1}{2} U^2 \tag{5}$$

The Shear Stress Transport (SST) turbulence model has been used in the simulations to accurately solve the near-walls and the air circulation regions. The SST model equations are:

$$\frac{\partial (\rho k)}{\partial t} + \frac{\partial (\rho u_j k)}{\partial x_j} = P - \beta^* \rho \Psi k + \frac{\partial}{\partial x_j} [(\mu + \sigma_k \mu_t) \frac{\partial k}{\partial x_j}] \tag{6}$$

$$\frac{\partial (\rho \Psi)}{\partial t} + \frac{\partial (\rho u_j \Psi)}{\partial x_j} = \frac{\gamma}{\nu_t} P - \beta \rho \Psi^2 + \frac{\partial}{\partial x_j} [(\mu + \sigma_\omega \mu_t) \frac{\partial \Psi}{\partial x_j}] + 2(1 - F_1) \frac{\rho \sigma_{\omega 2}}{\Psi} \frac{\partial k}{\partial x_j} \frac{\partial \Psi}{\partial x_j} \tag{7}$$

The variables in the SST turbulence model are defined as follows:

$$P = \tau_{ij} \frac{\partial u_i}{\partial x_j} \tag{8}$$

$$\tau_{ij} = \mu_t (2S_{ij} - \frac{2}{3} \frac{\partial u_k}{\partial x_k} \delta_{ij}) - \frac{2}{3} \rho k \delta_{ij} \tag{9}$$

$$S_{ij} = \frac{1}{2} (\frac{\partial u_i}{\partial x_j} + \frac{\partial u_j}{\partial x_i}) \tag{10}$$

$$\mu_t = \frac{\rho a_1 k}{max(a_1 \Psi, \Omega F_2)} \tag{11}$$

$$\phi = F_1 \phi_1 + (1 - F_1) \phi_2 \tag{12}$$

$$F_1 = \tanh\,(\arg_1^4) \tag{13}$$

$$\arg_1 = min[max(\frac{\sqrt{k}}{\beta^* \Psi d}, \frac{500\nu}{d^2 \Psi}), \frac{4\rho \sigma_{\omega 2} k}{\mathrm{CD}_{k\omega} d^2}] \tag{14}$$

$$\mathrm{CD}_{k\omega} = max(2\rho \sigma_{\omega 2} \frac{1}{\Psi} \frac{\partial k}{\partial x_j} \frac{\partial \Psi}{\partial x_j}, 10^{-20}) \tag{15}$$

$$F_2 = \tanh\,(\arg_2^2) \tag{16}$$

$$\arg_2 = max(2 \frac{\sqrt{k}}{\beta^* \Psi d}, \frac{500\nu}{d^2 \Psi}) \tag{17}$$

6.4.2. Boundary conditions

The boundary conditions of the given problem shown in Figure 6.2 are as follows:

i. At entrance (z=0):

Constant axial inlet velocity: $u_z = V_a$, $u_r = u_\Theta = 0$ and $T_i = 25$℃ (18)

ii. At exit (z=0.55m):

An outlet fully developed axial air flow: $\frac{\partial \beta}{\partial z}_{at\ z=0.55m} = 0$ (19)

Where, β is a symbol for any parameter, e.g., temperature, pressure, velocity component, etc.

iii. At stator walls ($r=R_{si}$):

A stationary insulated wall: $u_r = u_\Theta = u_z = 0$ and $q''_{at\ r=Rsi} = 0$ (20)

iv. At rotor and slot surfaces ($r=R_{ro}$):

$u_\Theta = \omega r, u_r = u_z = 0$ and $q'' = 500\ W/m^2$ (21)

The definition of the axial Reynolds number (Re_a), the rotational Reynolds number (Re_r), the Nusselt number (Nu), the hydraulic diameter (D_h) and the Reynolds number ratio (X) are provided in equations from (22) - (26):

$$Re_a = \frac{V_a * D_h}{\nu_{air}} \tag{22}$$

$$Re_r = \frac{\omega * Rro * D_h}{\nu_{air}} \tag{23}$$

$$Nu = \frac{h * D_h}{k_{air}} \tag{24}$$

$$D_h = \frac{P}{2 + \sqrt{2}} \tag{25}$$

$$X = \frac{Re_a}{Re_r} \tag{26}$$

6.4.3. Solution Procedure

The CFX-Solver is based on the a finite-volume method. Convergence was considered when the Root Mean Square (RMS) of all governing equations residuals reached a value less than 10^{-6}.

i. Grid Independence test

A grid independence test has been conducted. The number of elements varied from 120 to 10^7. The effect of the number of elements on the average rotor temperature was examined. As shown in in Figure 6.3, the mesh with 1.44×10^6 elements was found adequate for the present study. The mesh was locally refined to accurately resolve the boundary layer. Mesh statistics were examined. The average skewness was 0.24 and the mesh aspect ratio was 7.4.

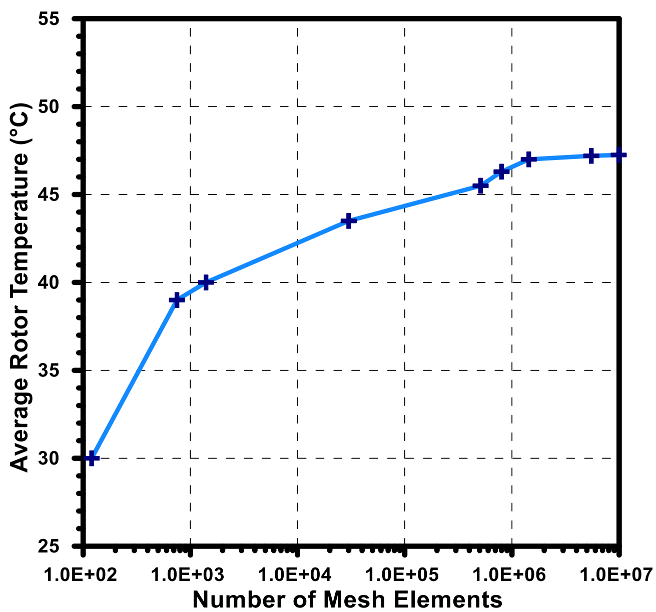

Figure 6.3 Grid independence test

6.4.4. Validation

The numerical model validation was performed by comparing the present numerical results with the experimental data reported in Fénot, et al. [22]. They studied flow and heat transfer within a synchronous motor. The rotor had four longitudinal slots. The stator was insulated. The rotor was subjected to a constant heat flux and a constant rotational speed. The radius ratio was kept constant at 0.72 using a slot size P of 53.5 mm. The length of the motor was 0.5 m. The hydraulic diameter was 15.8 mm. They considered three values of the axial Reynolds number at 2140, 4280 and 6425. For each value of the axial Reynolds number, the rotational Reynolds number was changed from 1750 to 35000. Accordingly, the Reynolds number ratio, X, varied from 0.061 to 3.67. Figure 6.4 shows a comparison of the variation of Nusselt number as function of Re_r obtained from the present numerical results and from Fénot, et al. [22] for the three values of Re_a considered in [22]. It is worth noting that [22] did not include error bars. The maximum deviation, considering all points shown in Figure 6.4, is less than 15%.

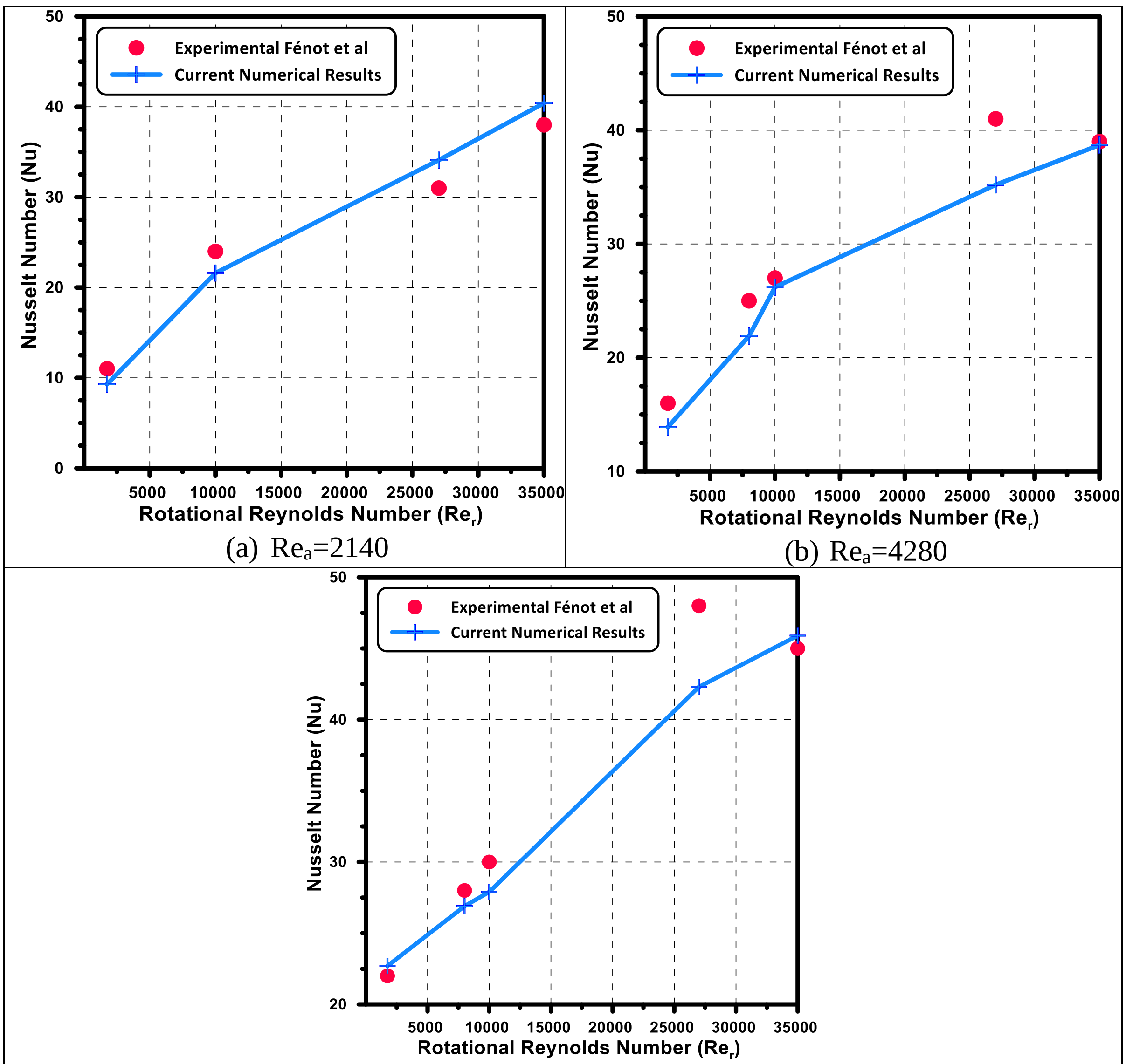

(a) Re_a=2140 (b) Re_a=4280 (c) Re_a=6425

Figure 6.4 Numerical model validation with experimental data reported in Fénot, et al. [22]

6.5 Results and Discussion

The current study investigates the effect of the axial and rotational Reynolds numbers, Re_a and Re_r, and the motor radius ratio (RR) considering the following ranges: $Re_a = 1.75x10^3 - 4x10^4$, $Re_r = 1.75x10^3 - 3.5x10^4$ and RR = 0.65 - 0.85. Accordingly, the Reynolds number ratio, X, considered in this study varied from 0.05 to 23. It is worth noting that all the results presented in this paper have a Taylor number (Ta) of values greater than $2x10^4$ which is higher that the critical Ta of 10^4 determined by Gardiner and Sabersky [25]. Hence, Taylor vortices are present in all configurations. The results are discussed here in two sections, according to the value of the Reynolds number ratio (X), less than or greater than 1.

6.5.1. Results obtained with Reynolds number ratio ($X \geq 1$):

In this case, the value of the axial Reynolds number was greater than the value of the rotational Reynolds number. The rotational Reynolds number was kept constant at 1750 while the axial Reynolds number was changed from 1750 to 40000, resulting in a value of X between 1 and 23. Also, the effect of the slot size by varying the radius ratio is taken into consideration. The effect of radius ratio was investigated by varying the values of slot size P of 63.5, 47.1, and 29.5 mm, corresponding to RR values of 0.65, 0.75 and 0.85.

Figure 6.5 shows the effect of X on the average Nusselt number at constant RR of 0.65. One can clearly notice that increasing X tends to increase the average Nusselt number. The average Nusselt number increases due to the increase in the heat transfer by convection associated with the increase in the axial air flow rate. However, the rate of increase is higher at X < 7 and tapers off as X increases beyond 7. Figure 6.5 shows the slope of the curve at X = 1 and X = 23. It is clear that the rate has been reduced by about 83%.

The streamlines inside the slot at RR = 0.65 for different values of X are shown in Figure 6.6. Figure 6.6a shows the streamlines inside the slot at X = 1. It is noticeable that there is circulation near the wall of the slot in Figure 6.6a. However, at X = 7 in Figure 6.6b, this circulation is dramatically reduced due to the powerful axial air stream. Figure 6.6c at X = 23, this circulation is almost diminished. The circulation of air inside the heated slot increases its temperature.

The bulk temperature of the cooling air depends on the inlet and exit air temperatures. For all cases, the air inlet temperature was kept constant at 25 ℃. However, the air outlet temperature depends on the rate of heat transfer inside the gap. Figure 6.7 shows the effect of X on the outlet air temperature at RR = 0.65. At low values of X, the slight increase in the axial air flow reduced the bulk air temperature dramatically which resulted in an enhanced cooling rate. The rate of enhancement is reduced when X increases further as the bulk air temperature is slightly reduced at high Re_a as shown in Figure 6.7.

The results in Figure 6.8 shows clearly that the radius ratio is not a factor in enhancing the heat transfer in case of having Reynolds number ratio greater than one. Changing the radius ratio from 0.65 up to 0.85 does not have a significant effect on the average Nusselt number if the axial Reynolds number is greater than the rotational Reynolds number.

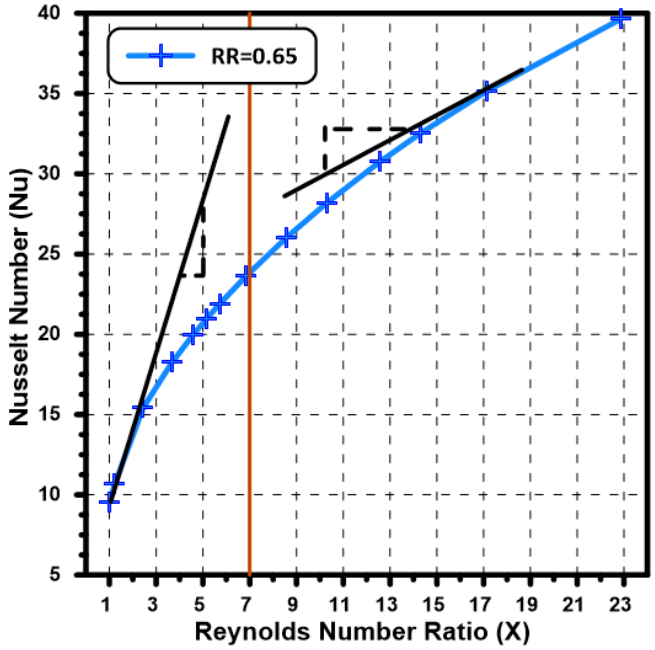

Figure 6.5 Effect of Reynolds number ratio on average Nusselt number at X ≥ 1 and RR = 0.65

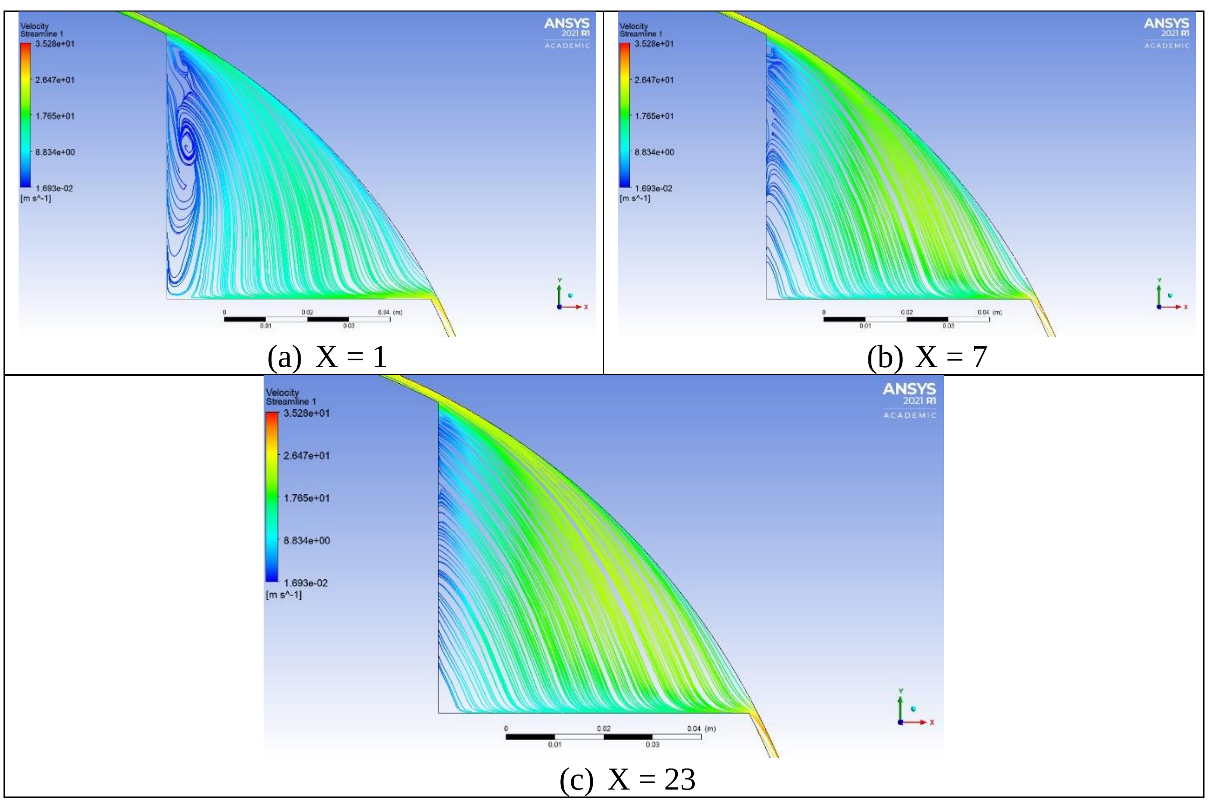

Figure 6.6 Effect of Reynolds number ratio on the streamlines at X ≥ 1 and RR = 0.65

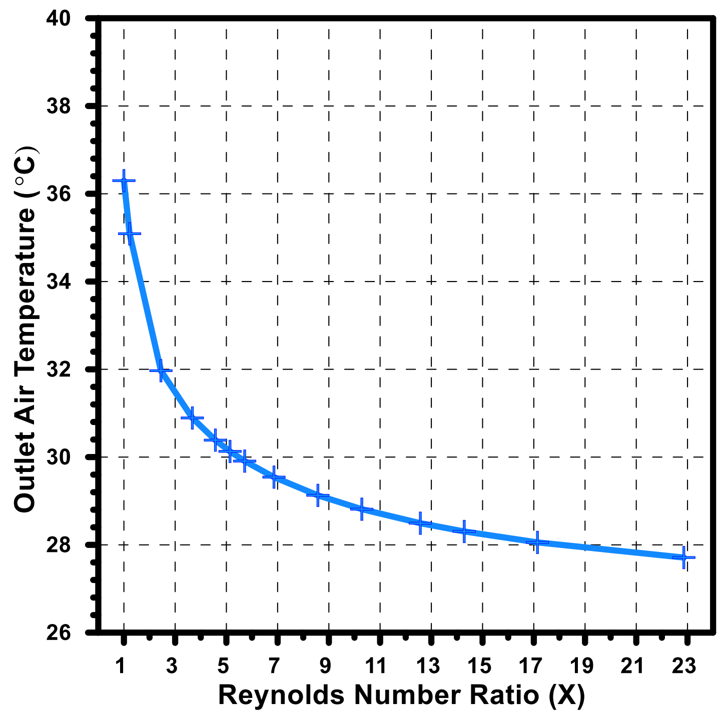

Figure 6.7 Effect of Reynolds number ratio on outlet air temperature at X ≥ 1 and RR = 0.65

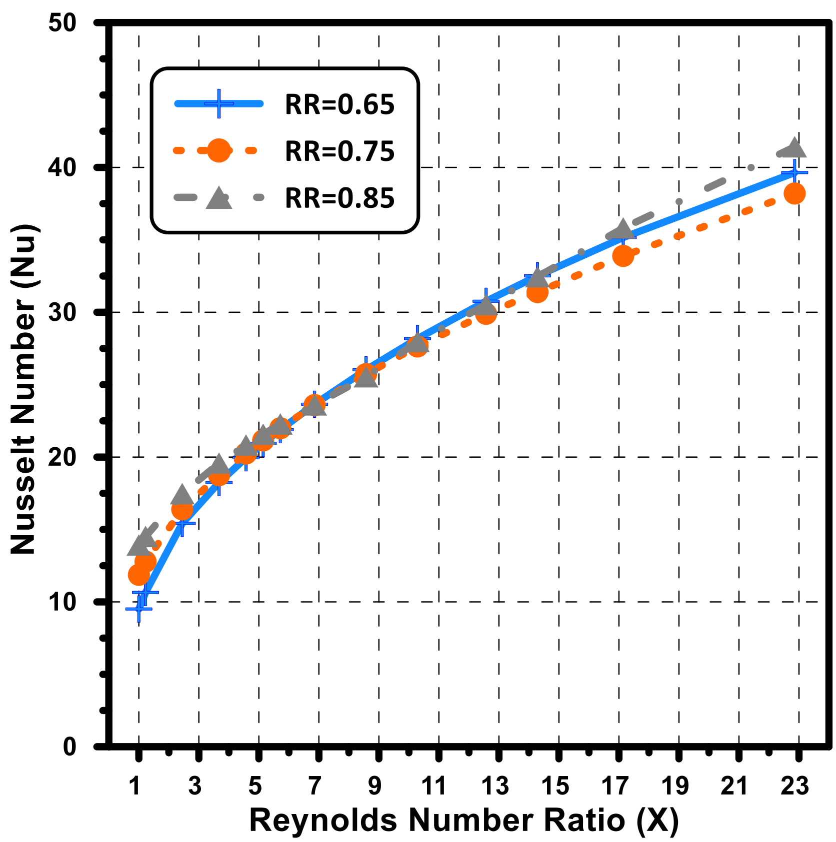

Figure 6.8 Effect of Reynolds number ratio and radius ratio on average Nusselt number at X≥1

6.5.2. Results obtained with Reynolds number ratio ($X \leq 1$):

In this section, The cases considered in the current subsection is for $X \leq 1$. This means that the value of the rotational Reynolds number is higher than the value of the axial Reynolds number. The axial Reynolds number was kept constant at 2000. The rotational Reynolds number varies from 2000 to 35000. The effect of RR has been taken into consideration in addition to the effect of decreasing the value of X from 1 to 0.057.

Figure 6.9 shows the effect of the RR and X on the average Nusselt number. At RR = 0.85, the increase in the rotational Reynolds number or the reduction in X value seems to have two different trends before and after X = 0.35. At $0.35 \leq X \leq 1$, the decrease in X slightly increases the average Nusselt number. However, at $0.057 \leq X \leq 0.35$, the decrease in X decreases the average Nusselt number. Figure 6.10 shows clearly the effect of X on the streamlines within the slot. The circulations at X = 1 is very weak as shown in Figure 6.10a while at X = 0.33, the circulation becomes bigger within the slot as in Figure 6.10b. As the rotor rotational speed is increased further, the circulation becomes stronger and spreads all over the slot with two eddies as clear in Figure 6.10c.

Similarly at RR = 0.75, the reduction in X value seems to have two different trends before and after X = 0.12 as shown in Figure 6.9. At $0.12 \leq X \leq 1$, the decrease in X slightly increases the average Nusselt number. However, at $0.057 \leq X \leq 0.12$, the decrease in X decreases the average Nusselt number. Figure 6.11 shows clearly the effect of X on the streamlines within the slot at RR = 0.75. The circulations at X = 1 is weak as shown in Figure 6.11a but at X = 0.12, the circulation becomes bigger within the slot as in Figure 6.11b. As the rotational Reynolds number is increased further, the eddies spread in the entire slot with a strong big eddy as clear in Figure 6.11c.

At RR = 0.65, the decrease in X has just one trend in the entire studied range on the average Nusselt number as clear in Figure 6.9. As X decreases, the average Nusselt number increases. The flow streamlines within the slot at RR = 0.65 are shown in Figure 6.12. The reduction in the value of X from 1 to 0.057 does not significantly increase the circulation within the slot, unlike the cases of RR = 0.75 and 0.85.

Figure 6.9 shows the relation between Reynolds number ratio and average Nusselt number. At small Reynolds number ratio, the average Nusselt number is directly proportional to rotational Reynolds number. However, at a certain point the average Nusselt number decreases with increasing rotational Reynolds number beyond this point.

This point, where the trend changes, is a critical point which is dependent on two factors: the radius ratio of the geometry and the Reynolds number ratio (X) for this flow. For large value of radius ratio like (RR=0.85), this point comes very early at almost X=0.35. On the other hand, for RR=0.75, this point is delayed as the curve started to flatten below X=0.12. For the case of RR=0.65, at any value of X between 1 and 0.057, the average Nusselt number is always increasing without this point which actually present but became shifted further below X=0.057. The change in the critical point value happens as the hydraulic diameter is decreased with the increase in RR. So, the rotor rotational speed is increased for the same rotational Reynolds number as clear from equation (23). This means that the flow of air will take much more time in the same cross-section due to the air circulation. Hence, the air temperature is increased faster, so the cooling rate is decreased with increasing the radius ratio.

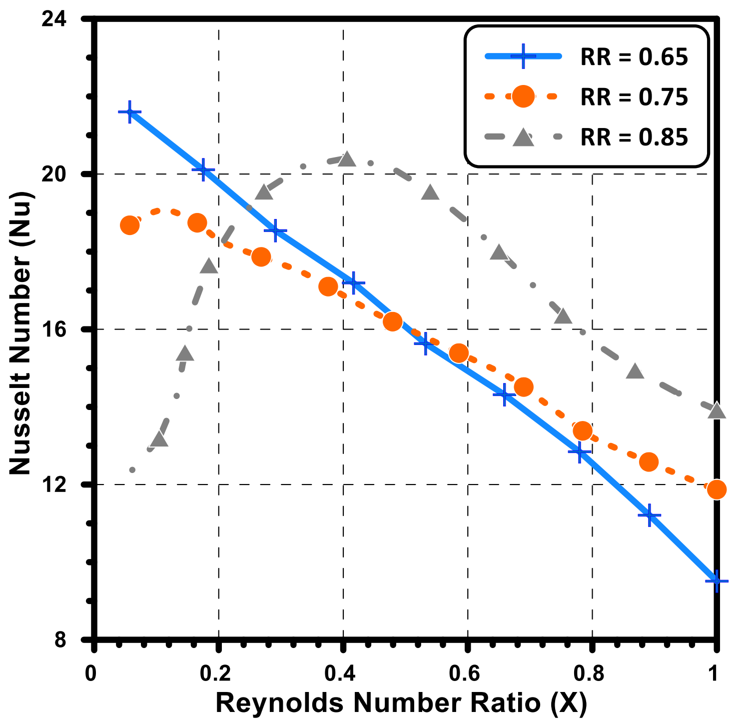

Figure 6.9 Effect of Reynolds number ratio and radius ratio on average Nusselt number at X≤1

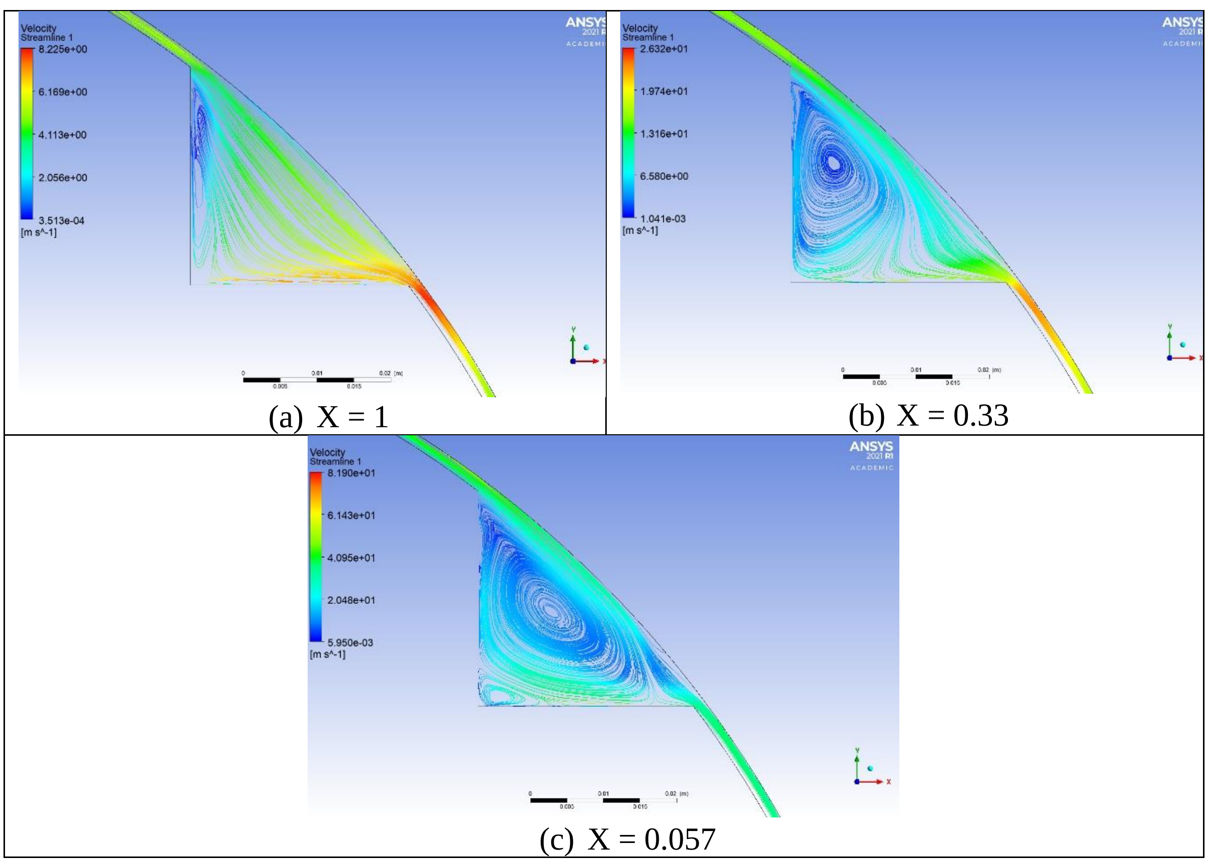

Figure 6.10 Effect of Reynolds number ratio on the streamlines at X ≤ 1 and RR = 0.85

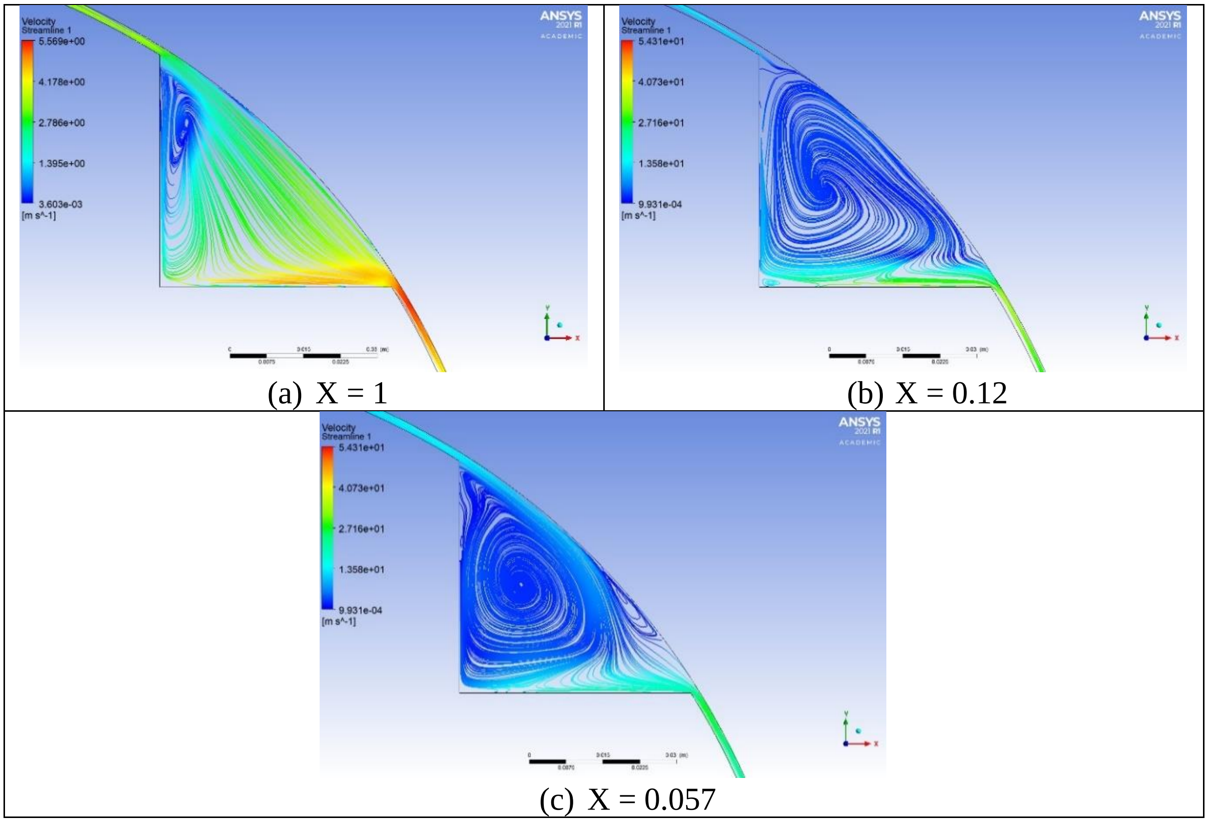

(a) X = 1 (b) X = 0.12

(c) X = 0.057

Figure 6.11 Effect of Reynolds number ratio on the streamlines at X ≤ 1 and RR = 0.75

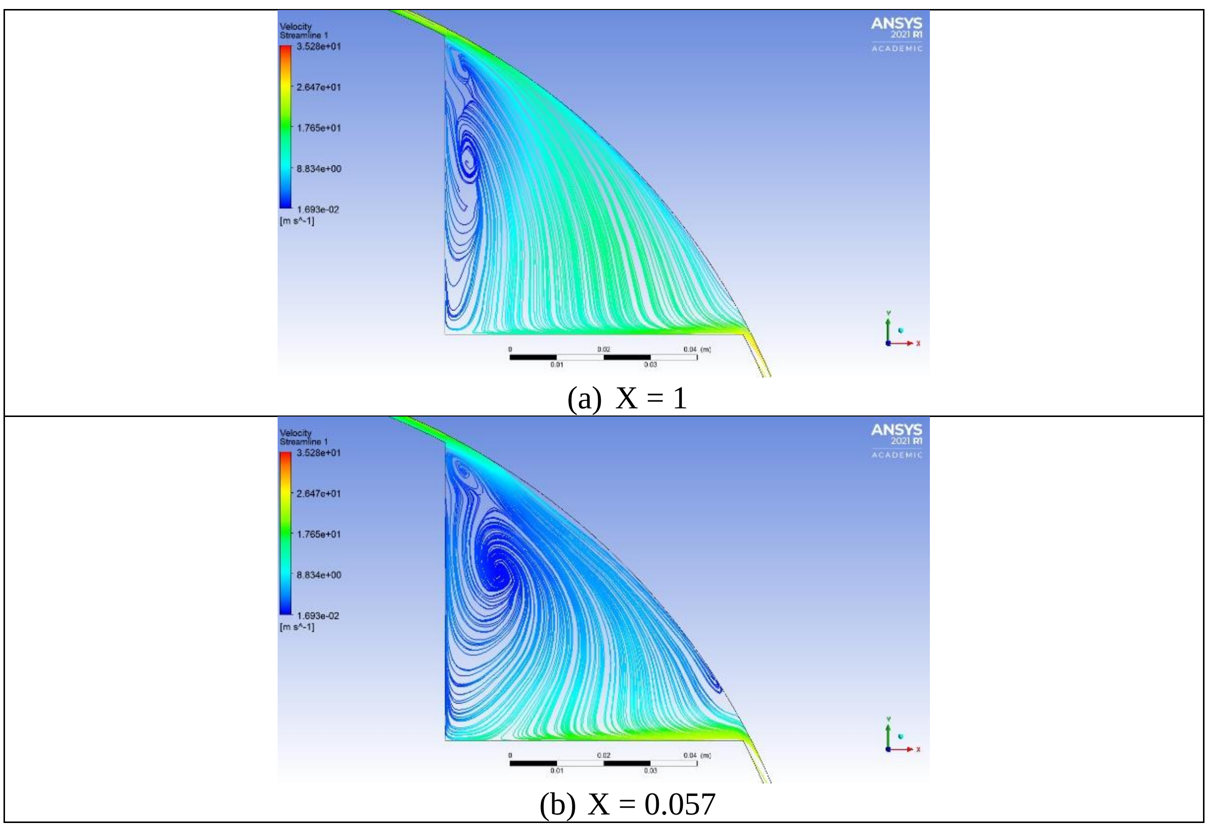

(a) X = 1

(b) X = 0.057

Figure 6.12 Effect of Reynolds number ratio on the streamlines at X ≤ 1 and RR = 0.65

6.6 Correlation

The present work has provided a comprehensive analysis of motor cooling with an axial flow through longitudinal slots. The variation of the slot geometry, axial, and rotational Reynolds number were considered. The Nusselt number was found to be a strong function of the ratio between axial and radial Reynolds number. A novel correlation has been concluded to estimate the average Nusselt number according to the ratio of Reynolds number ($X=Re_a/Re_r$) as given in equation (26):

$$Nu = 11.1735 * (X)^{0.397} \tag{26}$$

The above correlation is valid for $1 \leq X \leq 23$ and $0.65 \leq RR \leq 0.85$ with a maximum error of 13%. The fluid properties considered in the equation are calculated at the average temperature.

6.7 Conclusion

The current work has investigated the axial cooling of synchronous motor with axial air flow through longitudinal slots. The study has been conducted numerically using ANSYS-CFX. It was validated against experimental data. The simulations have included the variation of radius ratio, axial, and radial Reynolds numbers. The results show that increasing the axial or rotational Reynolds numbers will enhance the heat transfer. However, increasing the axial Reynolds number is more preferable as it always enhances the cooling of the electric motor. On the other hand, increasing the rotational Reynolds number isn't always a good way as at certain limit the Nusselt number will decrease. This happens due to the increase of air circulations inside the slots which in return rises the air temperature, so the cooling is deteriorated. Also, at any configuration, the rotational Reynolds number effect on enhancing the heat transfer is of less impact compared to the axial Reynolds number. A novel correlation is developed to estimate the value of the average Nusselt number according to the value of Reynolds number ratio up to 23 times. This correlation is valid under any considered radius ratio from 0.65 up to 0.85.

6.8 References

[1] A. Fasquelle *et al.*, "Coupled electromagnetic acoustic and thermal-flow modeling of an induction motor of railway traction," *Applied Thermal Engineering,* vol. 30, pp. 2788-2795, 12/01 2010.

[2] J. Humphreys, W. D. Morris, and H. Barrow, "Convection heat transfer in the entry region of a tube which revolves about an axis parallel to itself," *International Journal of Heat and Mass Transfer - INT J HEAT MASS TRANSFER,* vol. 10, pp. 333-340, 03/01 1967.

[3] Y. Huai, R. Melnik, and P. Thøgersen, "Computational analysis of temperature rise phenomena in electric induction motors," *Applied Thermal Engineering - APPL THERM ENG,* vol. 23, 05/01 2003.

[4] Z. Kolondzovski, A. Belahcen, and A. Arkkio, "Multiphysics thermal design of a high-speed permanent-magnet machine," *Applied Thermal Engineering - APPL THERM ENG,* vol. 29, pp. 2693-2700, 09/01 2009.

[5] C.-H. Huang and H.-C. Lo, "A three-dimensional inverse problem in estimating the internal heat flux of housing for high speed motors," *Applied Thermal Engineering - APPL THERM ENG,* vol. 26, pp. 1515-1529, 10/01 2006.

[6] M. Fénot, Y. Bertin, E. Dorignac, and G. Lalizel, "A review of heat transfer between concentric rotating cylinders with or without axial flow," *International Journal of Thermal Sciences - INT J THERM SCI*, vol. 50, pp. 1138-1155, 07/01 2011.

[7] K. M. Becker and J. Kaye, "Measurements of Diabatic Flow in an Annulus With an Inner Rotating Cylinder," *Journal of Heat Transfer (U.S.),* vol. Vol: 84, 05/01 1962.

[8] G. I. Taylor, "Stability of Viscous Liquid Contained Between Two Rotating Cylinders," *Philosophical Transactions of the Royal Society of London,* vol. 223, pp. 289-343, 01/01 1923.

[9] J. P. Gollub and H. L. Swinney, "Onset of Turbulence in a Rotating Fluid," *Physical Review Letters,* vol. 35, no. 14, pp. 927-930, 10/06/ 1975.

[10] E. Serre, M. Sprague, and R. Lueptow, "Stability of Taylor-Couette flow with radial throughflow," *Physics of Fluids - PHYS FLUIDS,* vol. 20, 03/01 2008.

[11] B. T. Nijaguna and B. Mathiprakasam, "HEAT TRANSFER IN AN ANNULUS WITH SPIRAL FLOWS," 1982.

[12] M. Bouafia, Y. Bertin, J. B. Saulnier, and P. Ropert, "Analyse expérimentale des transferts de chaleur en espace annulaire étroit et rainuré avec cylindre intérieur tournant," *International Journal of Heat and Mass Transfer,* vol. 41, no. 10, pp. 1279-1291, 1998/05/01/ 1998.

[13] J. E. E. C. Kaye, *Modes of adiabatic and diabatic fluid flow in an annulus with an inner rotating cylinder*. Cambridge, Mass.: M.I.T. Research Laboratory of Heat Transfer in Electronics, 1957.

[14] M. Molki, K. N. Astill, and E. Leal, "Convective heat-mass transfer in the entrance region of a concentric annulus having a rotating inner cylinder," *International Journal of Heat and Fluid Flow,* vol. 11, pp. 120–128, 06/01 1990.

[15] F. Tachibama, S. Fukui, and H. Mitsumura, "Convective Heat Transfer of the Rotational and Axial Flow between Two Concentric Cylinders," *Transactions of the Japan Society of Mechanical Engineers,* vol. 29, pp. 1360-1366, 01/01 1963.

[16] S. Poncet, S. Haddadi, and S. Viazzo, "Numerical modeling of fluid flow and heat transfer in a narrow Taylor–Couette–Poiseuille system," *International Journal of Heat and Fluid Flow,* vol. 32, pp. 128-144, 03/01 2011.

[17] C. Gazley, "Heat transfer characteristics of the rotational and axial flow between concentric cylinders," *Trans. ASME,* vol. 80, pp. 79-90, 01/01 1958.

[18] Yanagida and N. Kawasaki, "Pressure drop and heat transfer characteristics of axial air flow through an annulus with a deep-slotted outer cylinder and a rotating inner cylinder. 2nd Report. ; Heat transfer characteristics. Gaito ni slot wo yushi, naito ga kaitensuru kanjo ryuro no atsuryoku sonshitsu oyobi netsu dentatsu. Dai niho. ; Netsu dentatsu tokusei," *Nippon Kikai Gakkai Ronbunshu, B Hen (Transactions of the Japan Society of Mechanical Engineers, Part B); (Japan),* vol. 57:538, 1991/6 1991.

[19] T.-M. Jeng, S.-C. Tzeng, and C.-H. Lin, "Heat transfer enhancement of Taylor–Couette–Poiseuille flow in an annulus by mounting longitudinal ribs on the rotating inner cylinder," *International Journal of Heat and Mass Transfer,* vol. 50, no. 1, pp. 381-390, 2007/01/01/ 2007.

[20] A. Nouri-Borujerdi and M. E. Nakhchi, "Heat transfer enhancement in annular flow with outer grooved cylinder and rotating inner cylinder: Review and experiments," *Applied Thermal Engineering,* vol. 120, pp. 257-268, 2017/06/25/ 2017.

[21] A. M. Teamah and M. S. Hamed, "Numerical Study of Electric Motors Cooling Using an Axial Air Flow," *Journal of Fluid Flow, Heat and Mass Transfer (JFFHMT),* vol. 9, pp. 101-105, 2022-09-16 2022.

[22] M. Fénot, E. Dorignac, A. Giret, and G. Lalizel, "Convective heat transfer in the entry region of an annular channel with slotted rotating inner cylinder," *Applied Thermal Engineering,* vol. 54, pp. 345–358, 05/14 2013.

[23] *Synchronous Motors Catalogues*. Available: https://www.electromate.com/

[24] C. J. S. t. g. ANSYS, ANSYS, "Release 12.0 User's guide," 2009.

[25] S. R. M. Gardiner and R. H. Sabersky, "Heat transfer in an annular gap," *International Journal of Heat and Mass Transfer,* vol. 21, no. 12, pp. 1459-1466, 1978/12/01/ 1978.

Chapter 7

Digital Twin

7.1 Introduction to The Digital Twin (DT)

The digital twin (DT) is an analytical model with a user-friendly interface that can be used to size and check the thermal performance of the SCDMDS. The DT has been constructed using Visual Basics and Microsoft Excel. The DT has been developed using the thermal resistance network discussed in chapter 3. Correlations from chapters 2 and 3 have been implemented inside the DT. The DT has been validated using experimental data. The DT has also been validated using a list of about 100 overheated SCDMDS cases provided by the industrial partner. In addition, a number of blind cases have been provided by the industrial partner and tested using the DT. Significant agreement has been found between the DT results and the tested case studies with a maximum deviation in estimated temperatures of 10%.

7.2 Digital Twin Inputs

The DT inputs have been classified into geometrical inputs and operational inputs. The geometrical inputs include all the dimensional features of the SCDMDS. The operational inputs include the operating parameters.

7.2.1. Geometrical Inputs of the DT

i. The Drum Diameter [Do] (mm or inch).

ii. The Face Width of the Drum [L] (mm or inch).

iii. The Electric Motor Casing Outer Diameter [do] (mm or inch).

iv. Number of Poles for the Electric Motor [n] & Sealing Condition.

v. The Gearbox type (Planetary or Internal Gear Train).

vi. The Shell Emissivity according to material and surface finish.

vii. The Lagging Thickness [th_lag] (mm or inch).

viii. Internal Motor Dimensions (mm or inch).

7.2.2. Operational Inputs of the DT

i. The Drum Rotational Speed [N] (rpm) or Belt Linear Speed [Vb] (ft/min).

ii. The Oil Volume Percentage [OV] (%).

iii. The Oil Enduratex Type for Oil Properties.

iv. The Belt Pull [BP] (N or lbf) to calculate torque required over the drum.

v. The Target Maximum Temperature Over Motor Casing [Tmax] (℃).

vi. The Surrounding Temperature [Tamb] (℃).

vii. The Thermal Conductivity of Lagging [K_lag] (W/m.K).

7.3 DT Types of Analysis and Outputs

7.3.1. Analysis Types inside the DT

The program has two different types or methods of analysis:

i. The Optimized Thermal Rating (OPTR) Method:

This rating method uses the maximum allowable motor temperature to find the corresponding maximum possible motor power input and the corresponding temperature distribution in order to achieve a safe to operate, i.e., with no overheating.

ii. The Thermal Rating based on The User-Inputs (TRUI) Method:

This rating method uses the actual motor power input supplied by the user and determines the corresponding temperature distribution within the SCDMDS.

7.3.2. Outputs of the DT

i. The temperature distribution with lagging.

ii. The temperature distribution without lagging of the same problem.

iii. The heat generation from the electric motor and viscous dissipation in (W).

iv. The gearbox heat losses in (W).

v. The heat dissipation from the flanges and from the drum (W).

vi. Estimation of whether overheating is occurring or safe to operate.

vii. If overheating is occurring, the program suggests solving the overheating problem by some possible modifications.

7.4 Digital Twin Mathematical Model and Solution Technique

The mathematical model of the DT is based on thermal resistance network as shown in **Figure 7.1** for the case without lagging and **Figure 7.2** for the case with lagging. For each resistance inside the thermal resistance network, there is a developed correlation to predict the heat transfer coefficients as mentioned in Chapters 2 and 3. The DT has two different solution methods as discussed before. The flowchart shown in **Figure 7.3** describes the way used to solve each method.

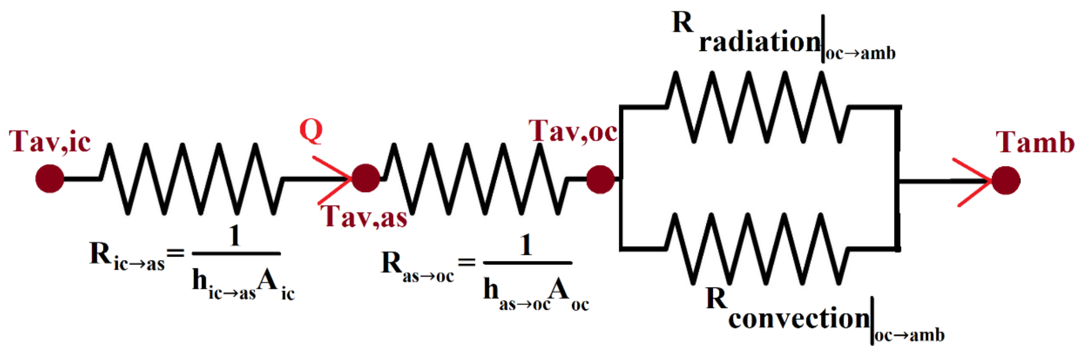

Figure 7.1 Thermal resistance network without lagging

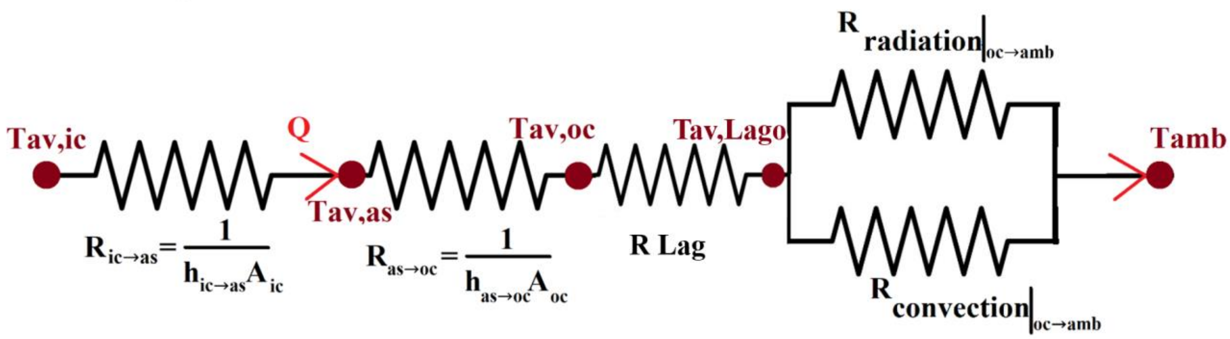

Figure 7.2 Thermal resistance network with lagging

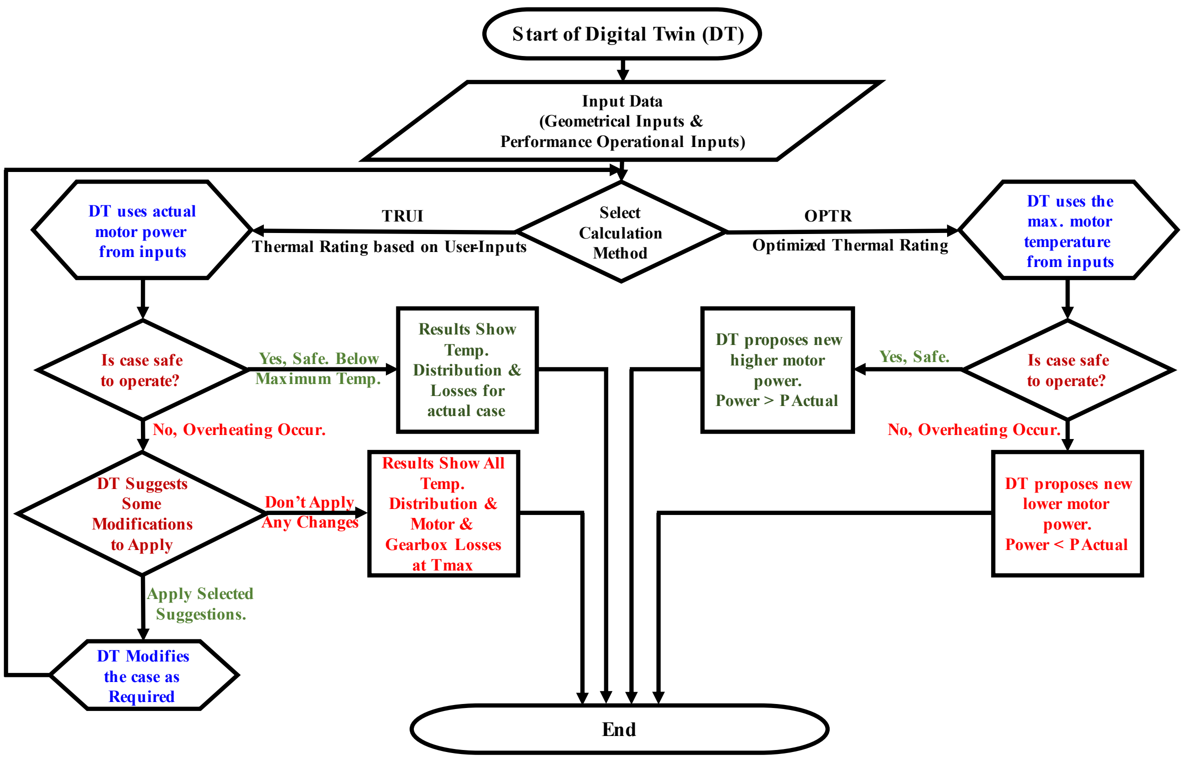

Figure 7.3 Digital Twin bird's-eye view flowchart

The DT has a solution technique to solve for each method of OPTR and TRUI. The following sections discuss in deep detail how the DT deals within each solving method.

7.4.1. Optimized Thermal Rating (OPTR) solution technique

In the OPTR, the motor temperature is already defined and kept at the maximum temperature specified by the user. The unknown values are the amount of heat generated from all sources, oil temperature, drum temperature and lagging temperature if lagging material is present. In order to solve for these unknowns, the DT is programmed to move in the steps shown in Figure 7.4.

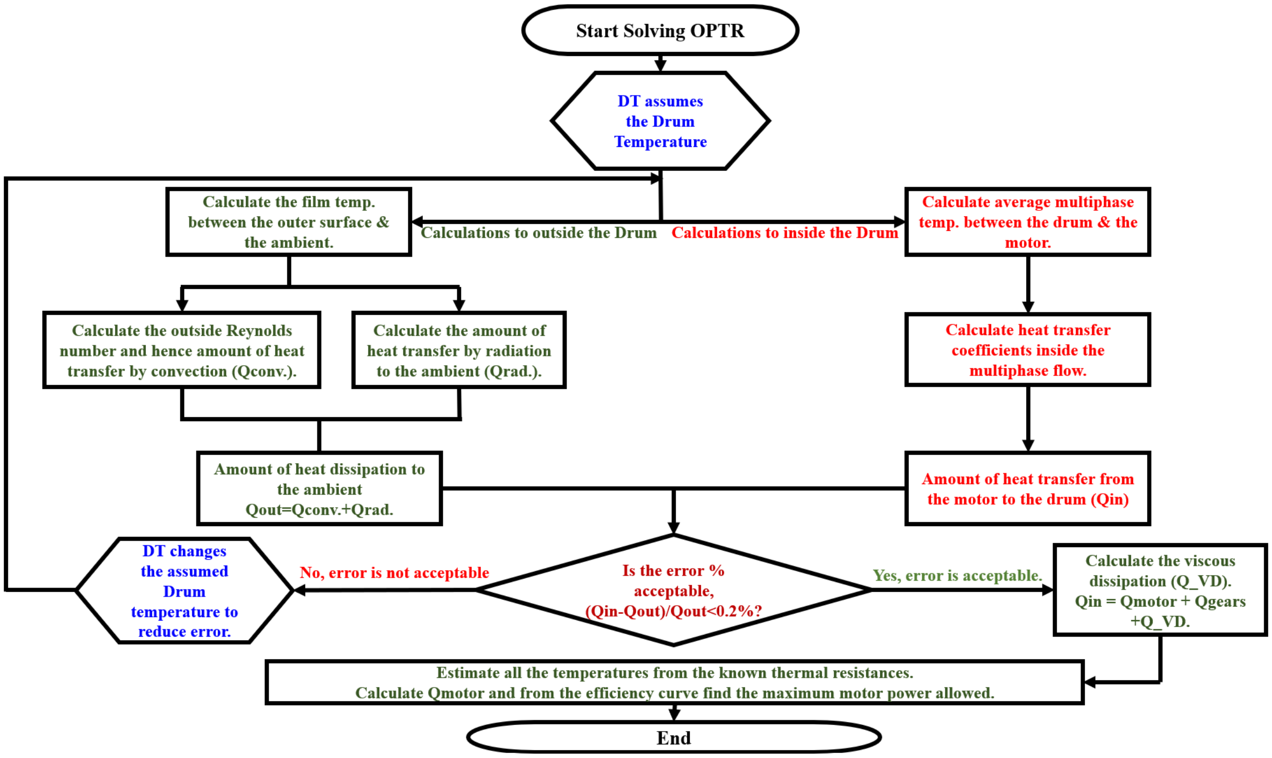

Figure 7.4 OPTR solution technique flowchart

7.4.2. Thermal Rating based on User-Inputs (TRUI) solution technique

When the user selects to solve TRUI, the program starts at first by solving the OPTR in order to check for the maximum allowed motor power. In the case of TRUI, the DT uses the actual motor power supplied and compares it with the maximum allowed motor power. If the actual motor power supplied by the user is higher than the maximum allowed motor power calculated from the OPTR, the case is considered overheating. When a case is reported by the DT as overheated, the program shows multiple signs of warnings and alerts to the user and notifies him of the maximum allowed motor capacity that can be used without problems. The DT at this point will show some proposed modifications to solve the overheating issue based on what is inserted in the inputs. The user can select one or more from the options and the DT will try to resolve again with the modified case.

On the other hand, if the actual motor power supplied by the user is lower than the maximum allowed motor power calculated from the OPTR, the case is considered safe to operate. This time, the motor temperature is unknown. However, the motor power is given which in return from the efficiency curve gives the amount of heat dissipated from the motor. By doing an iterative method as dealt with the OPTR case until reaching an acceptable error. The results from this type of solving will be the temperature distribution in each part of the system besides the heat generated from each component.

7.5 Validation of DT

The DT has been validated with experimental SCDMDS with the presence of belt. **Figure 7.5** shows the comparison of the DT results with the experimental data of SCDMDS with the presence of belt and lagging. There is great agreement between the DT results and the experimental data with a maximum deviation of 8%.

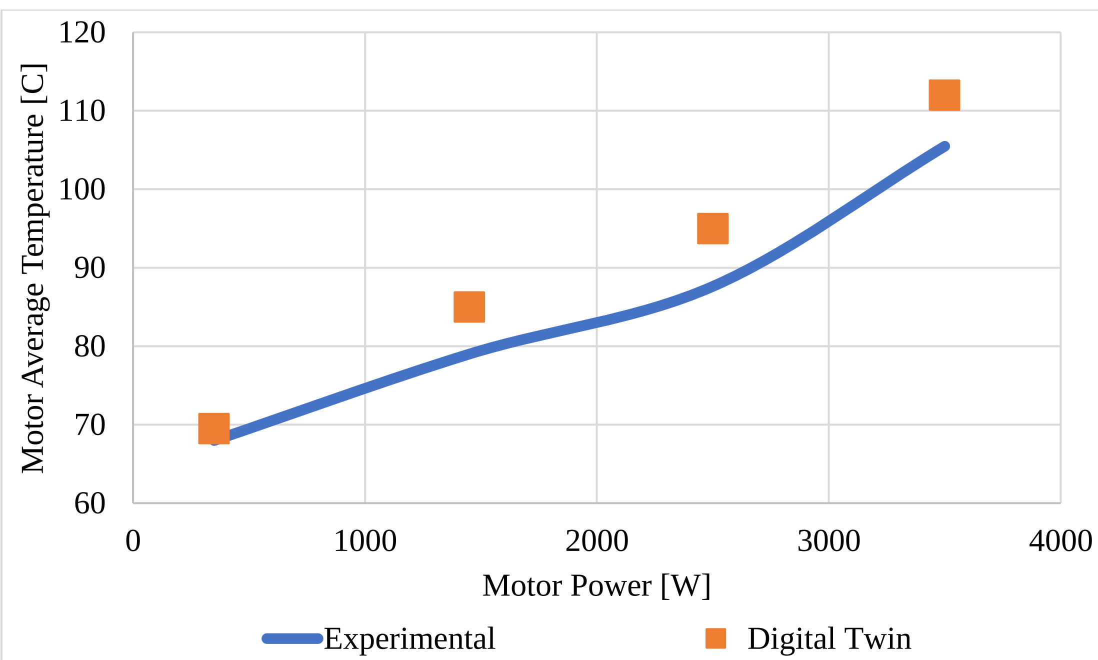

Figure 7.5 Validation of Digital Twin with experimental data

7.6 Digital Twin Interface

The interface of the DT has three sheets. The first one is the main sheet which contains the inputs and the outputs of the DT. **Figure 7.6** shows all the geometrical and operational inputs of the DT. The outputs of the DT for the two-analysis types are shown in **Figure 7.7**. The second sheet includes the motor efficiency curve and the motor internal dimensions as shown in **Figure 7.8**. The third sheet is a user-guide for the whole DT as shown in **Figure 7.9**.

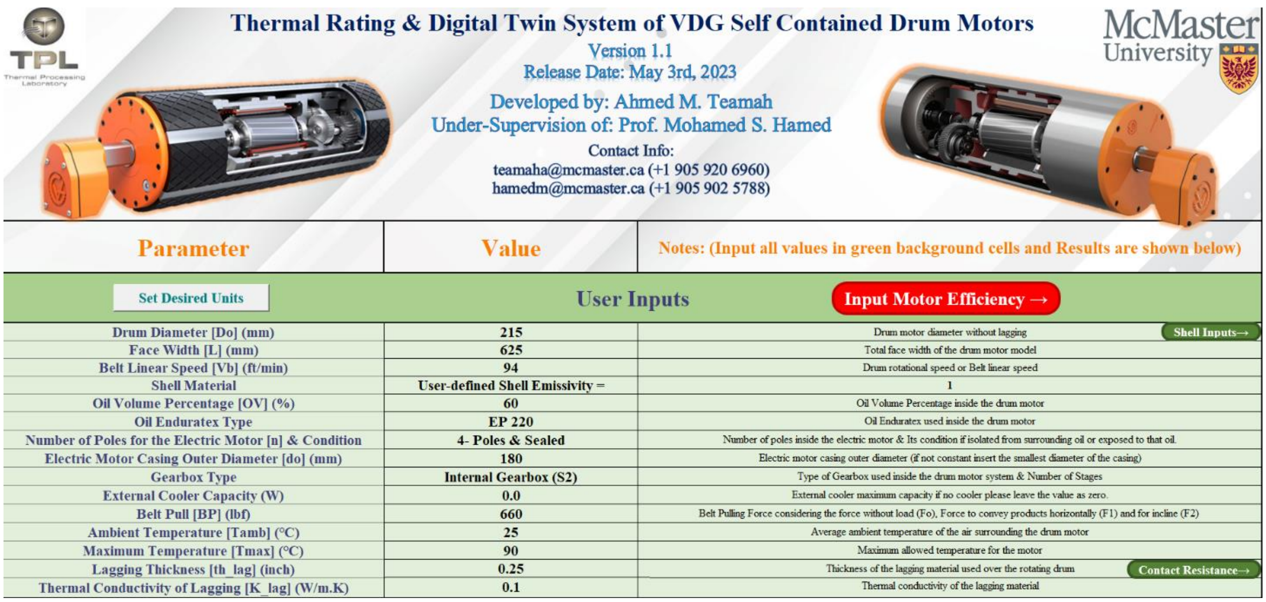

Figure 7.6 DT user-interface of the inputs

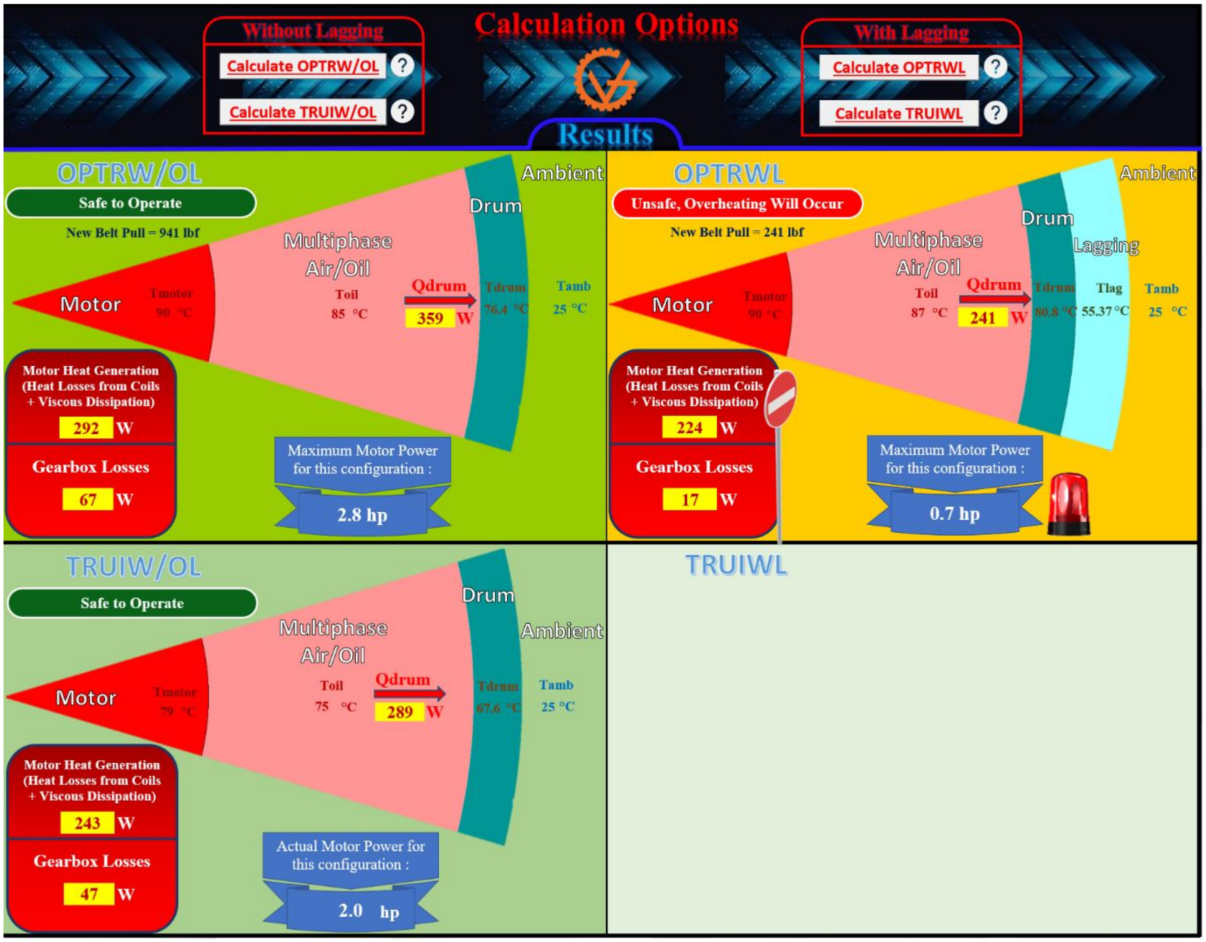

Figure 7.7 DT user-interface of the outputs for all calculation methods

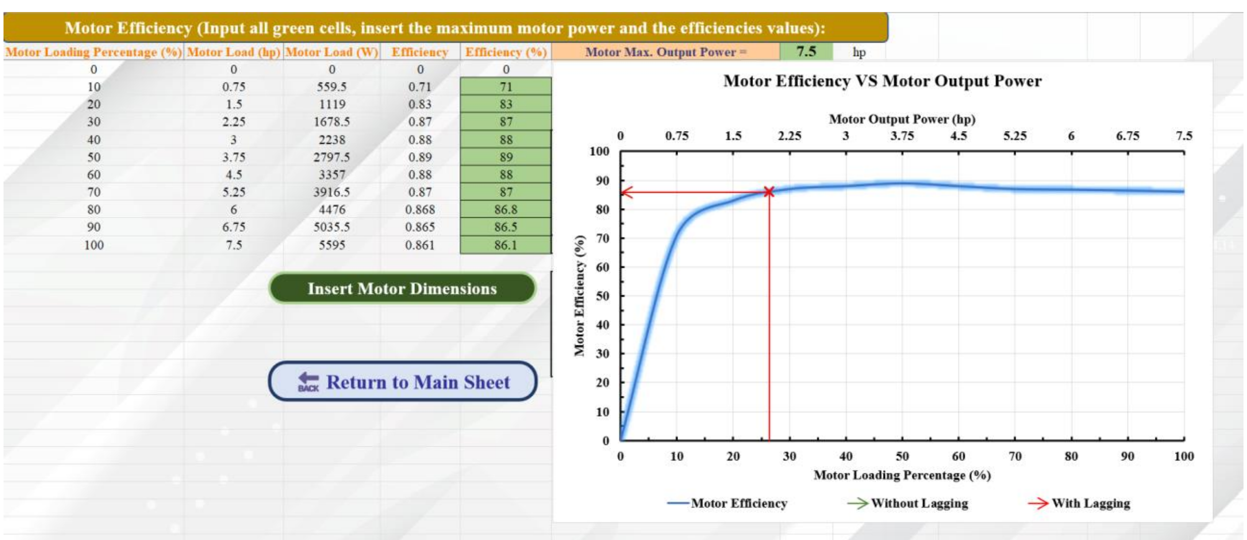

Motor Loading Percentage (%)	Motor Load (hp)	Motor Load (W)	Efficiency	Efficiency (%)
0	0	0	0	0
10	0.75	559.5	0.71	71
20	1.5	1119	0.83	83
30	2.25	1678.5	0.87	87
40	3	2238	0.88	88
50	3.75	2797.5	0.89	89
60	4.5	3357	0.88	88
70	5.25	3916.5	0.87	87
80	6	4476	0.868	86.8
90	6.75	5035.5	0.865	86.5
100	7.5	5595	0.861	86.1

Figure 7.8 Motor Efficiency Data inside the DT

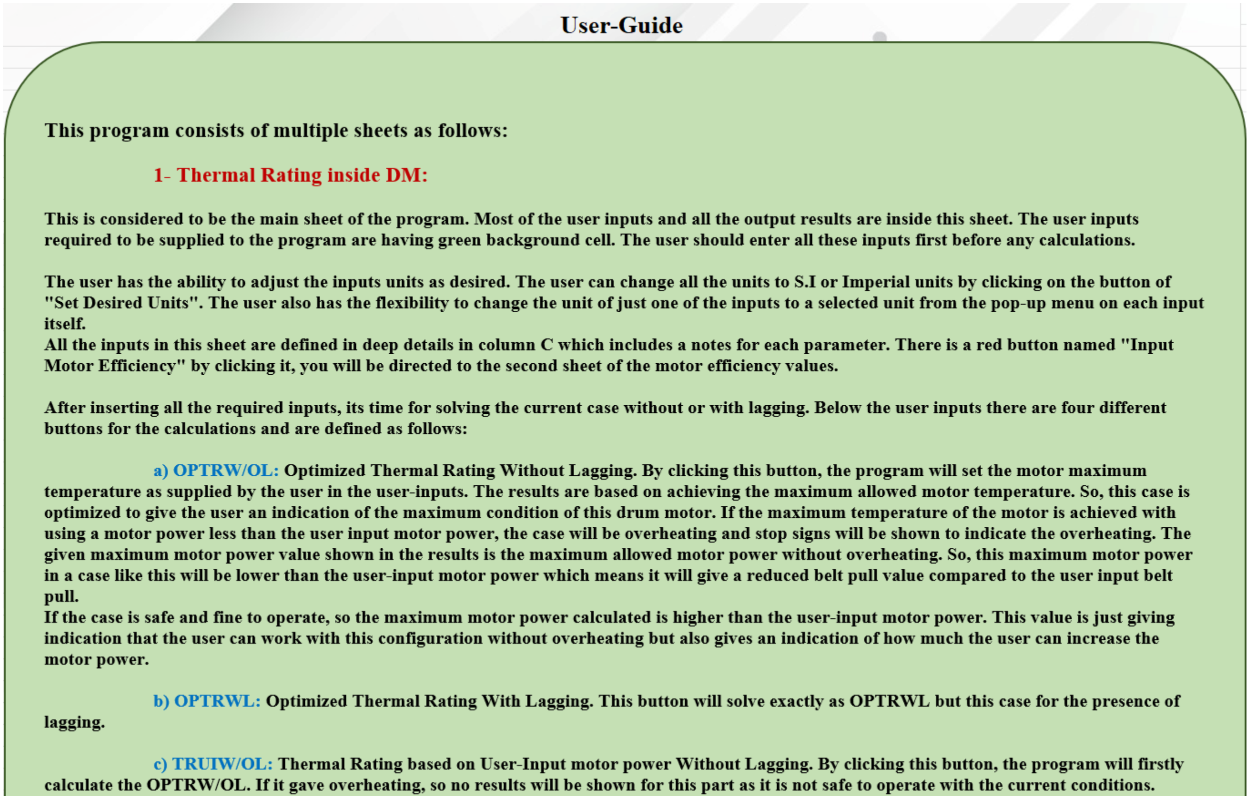

User-Guide

This program consists of multiple sheets as follows:

1- Thermal Rating inside DM:

This is considered to be the main sheet of the program. Most of the user inputs and all the output results are inside this sheet. The user inputs required to be supplied to the program are having green background cell. The user should enter all these inputs first before any calculations.

The user has the ability to adjust the inputs units as desired. The user can change all the units to S.I or Imperial units by clicking on the button of "Set Desired Units". The user also has the flexibility to change the unit of just one of the inputs to a selected unit from the pop-up menu on each input itself.
All the inputs in this sheet are defined in deep details in column C which includes a notes for each parameter. There is a red button named "Input Motor Efficiency" by clicking it, you will be directed to the second sheet of the motor efficiency values.

After inserting all the required inputs, its time for solving the current case without or with lagging. Below the user inputs there are four different buttons for the calculations and are defined as follows:

a) OPTRW/OL: Optimized Thermal Rating Without Lagging. By clicking this button, the program will set the motor maximum temperature as supplied by the user in the user-inputs. The results are based on achieving the maximum allowed motor temperature. So, this case is optimized to give the user an indication of the maximum condition of this drum motor. If the maximum temperature of the motor is achieved with using a motor power less than the user input motor power, the case will be overheating and stop signs will be shown to indicate the overheating. The given maximum motor power value shown in the results is the maximum allowed motor power without overheating. So, this maximum motor power in a case like this will be lower than the user-input motor power which means it will give a reduced belt pull value compared to the user input belt pull.
If the case is safe and fine to operate, so the maximum motor power calculated is higher than the user-input motor power. This value is just giving indication that the user can work with this configuration without overheating but also gives an indication of how much the user can increase the motor power.

b) OPTRWL: Optimized Thermal Rating With Lagging. This button will solve exactly as OPTRWL but this case for the presence of lagging.

c) TRUIW/OL: Thermal Rating based on User-Input motor power Without Lagging. By clicking this button, the program will firstly calculate the OPTRW/OL. If it gave overheating, so no results will be shown for this part as it is not safe to operate with the current conditions.

Figure 7.9 User-guide inside the DT

7.7 Case study

A case has been shared by our industrial partner VDG that was reported as overheated by multiple customers. This case of 2 hp motor has the following specifications:

i. TM-215 Drum Motor series of outer diameter = 215 mm.

ii. Face width (L) = 425 mm.

iii. Belt linear speed = 94 ft/min.

iv. Shell Material: Mild Steel.

v. Oil level = 45%.

vi. Number of Poles = 4 and unsealed.

vii. Internal Gearbox 2 stages.

viii. Belt Pull = 660 lbf.

ix. ¼” lagging material standard black nitrile.

All the inputs and the motor efficiency of this case have been supplied to the DT. When trying to solve the case both with and without lagging, the case is overheating. The maximum motor power that can be used without overheating inside this SCDMDS with the current dimensions is just 0.3 hp instead of the 2 hp as shown in **Figure 7.10**. This SCDMDS has reached 134 °C at the motor surface if the 2 hp motor is fully loaded as shown in **Figure 7.11**. This high temperature reduces the life span of this drum motor dramatically as the temperature should not increase above 90 °C.

Figure 7.10 Case study results for a maximum motor temperature of 90°C.

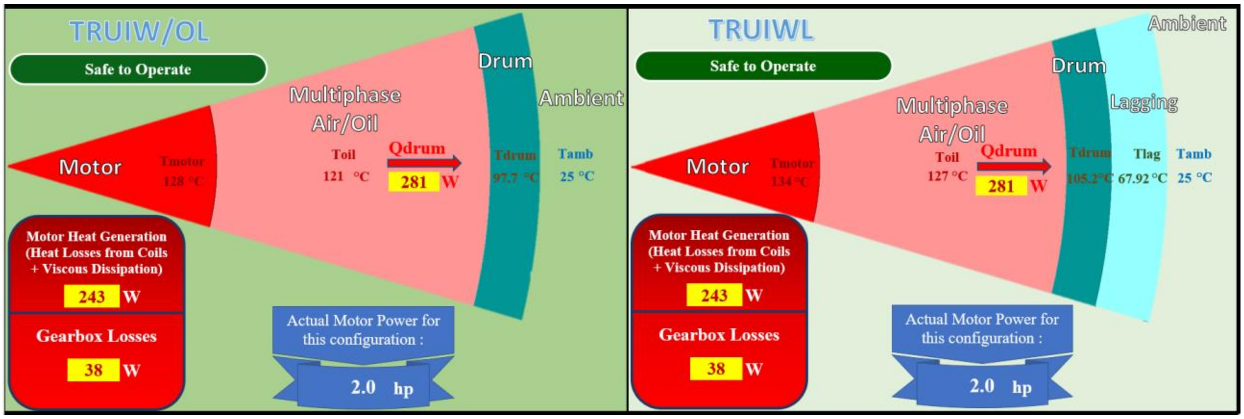

Figure 7.11 Case study results if fully loaded by 2 hp.

When the case is reported as overheating inside the DT, the program suggests some modifications to avoid this overheating issue as shown in **Figure 7.12**. The user is able to select one or multiple options as desired. The DT will automatically adjust the case with the applied changes selected and resolve again. The overheating issue has been solved by increasing the face width of the drum motor to 625 mm instead of 425 mm and coating the shell surface to improve the surface emissivity besides raising the oil level to 60%. After applying the previous changes as shown in **Figure 7.13**, the motor temperature became below 90 °C in the full load case.

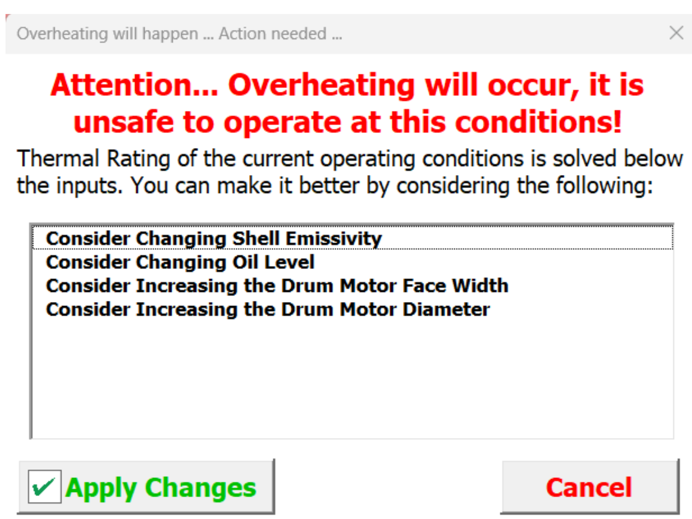

Figure 7.12 Proposed changes in order to avoid the overheating issue.

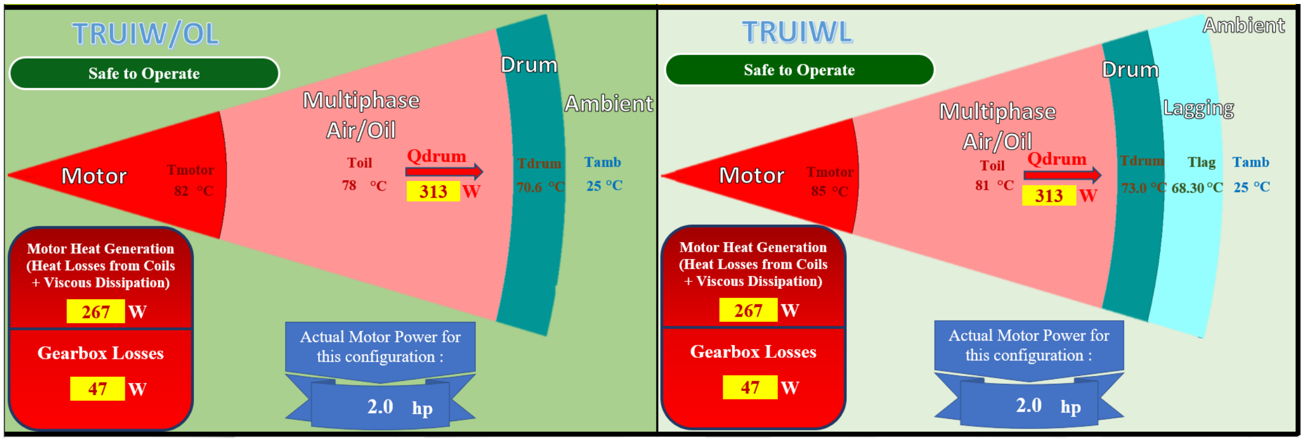

Figure 7.13 Case study results after applying the proposed changes to avoid the overheating issue.

Chapter 8

Summary, Conclusions and Recommendations For Future Work

8.1 Summary and Conclusions

This research investigated the thermal performance of a Self-Contained Drum Motor Drive System (SCDMDS). The SCDMDS is susceptible to overheating due to the significant amount of heat generated inside and the limited heat dissipation. The thesis investigated the overall thermal performance of the SCDMDS. The interplay of all components has been addressed in great details by implementing a thermal resistance network of the entire system. This research has been carried out in collaboration with a Canadian industrial partner.

The flow and heat transfer of the multiphase oil/air flow within the SCDMDS has been investigated numerically and experimentally. Multiple parameters have been studied in this section considering the effect of drum rotational speed (N), oil level (OV) and radius ratio (RR). Results of the single-phase cases considering 100% air and 100% oil have been discussed. The single-phase cases results indicated that increasing drum rotational speed would have a significantly negative effect on the thermal performance of SCDMDS having a small radius ratio like 0.21. Since in this case, the cooling of the inner cylinder is primarily due to natural convection, increasing drum rotational speed causes a thicker boundary layer to develop over the inner surface of the rotating cylinder. So, increasing the rotational speed in the single-phase cases causes a deterioration of heat transfer around the inner cylinder if the RR is small like 0.21. On the other hand, if the RR is large like 0.85, the increase in N would improve the heat transfer inside the gap. The case of 100% oil is significantly better than 100% air, due to the higher thermal conductivity of oil.

Results of the multiphase cases indicated that, the thermal performance of the SCDMDS would significantly deteriorate if the annular space was completely filled with oil compared to a multiphase case. Also, increasing drum rotational speed enhances heat transfer inside the annular space by improving the oil splashing over the inner cylinder. The increase in the RR improves dramatically the heat transfer in the gap between the two cylinders. The best thermal performance of the SCDMDS can be achieved by maintaining oil at an optimum oil level of about 65% to ensure proper oil distribution for cooling the motor. The Nusselt number within the system has been correlated as a function of Reynolds number, radius ratio and oil level. The proposed correlations can be used as a design tool to optimize the system thermal performance by determining the optimum operating conditions and also to assess a current case of a SCDMDS.

The lagging material effect has been studied and can be dealt simply as an added insulation over the drum surface. In some models, the lagging material can be beneficial as it increases the surface emmisivity and enhances the heat transfer coefficient to the ambient. This is attributed to the larger outer diameter and area of heat dissipation. However, this is not always the case as in other models it acts like insulation over the outer drum and prevents the heat from transmitting to the surrounding air. The optimum thickness of the lagging can be determined by estimating the critical thickness of insulation to avoid high resistance to heat transfer.

The effect of the shell emissivity has been investigated. Increasing the outer surface emissivity enhances the heat transfer to the ambient and hence reduces the temperatures inside the annular gap and over the motor surface. It is better to add black dull coating over the outer drum instead of the reflective shiny polished stainless steel used in the current design.

The heat losses from an internal and a planetary gear train have been investigted numerically. The effect of drum or casing rotational speed (N), torque (ζ) and oil volume percentage (OV) were considered. In addition, a comparison has been made between two cases including static or rotating casing over the gearbox. Increasing the casing rotational speed (N) increases the heat losses from the gear train. The effect of rotational speed becomes more significant when the oil level is high as the churning losses will rise it dramatically. The increase in the torque (ζ) leads to an increase in the losses from the gear train whatever the value of the casing rotational speed or the oil volume percentage. The load just affects the meshing and bearing losses as they are the dependent on load losses.

The increase in the oil volume percentage increases the churning losses up to certain level then becomes constant. This specific oil level is determined by the height of oil required to submerge the pinion gear. After that level, increasing the oil level will not affect the heat losses from the internal gear train. However, when dealing with planetary gear train, the increase in the oil level will always increase the churning losses as there are planet gears rotating in the whole casing.

A rotating casing shows a positive impact on the performance of the gear train compared to a static casing. The rotational speed of the rotating casing improves the heat transfer to the surrounding air which in return improves the performance of the gear train by reducing the losses.

In order to solve overheating problem in the SCDMDS, some modifications to the current design have been proposed. One of them is by cooling the electrical motor by passing axial air flow between the motor stator and rotor.

The cooling of synchronous motor with axial air flow through longitudinal slots between the motor rotor and the stator has been investigated. The study has been conducted numerically using ANSYS-CFX. The simulations have included the variation of radius ratio, axial, and radial Reynolds numbers. The results showed that increasing the axial or rotational Reynolds numbers will enhance the heat transfer. However, increasing the axial Reynolds number is more preferable as it always enhances the cooling of the electric motor.

On the other hand, increasing the rotational Reynolds number isn't always a good way as at certain limit the Nusselt number will decrease. This happens due to the increase of air circulations inside the slots which in return rises the air temperature, so the cooling is deteriorated. Also, at any configuration, the rotational Reynolds number effect on enhancing the heat transfer is of less impact compared to the axial Reynolds number. A novel correlation has been developed to estimate the value of the average Nusselt number according to the value of Reynolds number ratio up to 23 times. This correlation is valid under any considered radius ratio.

All the correlations developed for each part in the SCDMDS have been implemented in the Digital Twin (DT). The DT has been programmed on Visual Basics in Excel. The DT is a user-friendly interface that can assess the thermal performance of the SCDMDS according to the user-inputs. The DT has the ability to detect whether overheating is going to occur or not in the solved SCDMDS case. If the case is predicted as overheating, the DT will be able to propose some modifications in order to solve the overheating issue. The DT has the ability to optimize the case and find the maximum motor power that can be used inside the SCDMDS without overheating. The DT is a powerful tool to size and assess the thermal performance of the SCDMDS for wide range of geometerical and operational inputs.

8.2 Recommendations for Future Work

Investigating the thermal performance of the SCDMDS and proposing modifications to the current design to solve the overheating issue is challenging. Although the contributions made by the research in this thesis address the whole thermal performance and proposed some modifications to the SCDMDS, there remain several avenues for future research to build upon the current work, including:

1. Investigate current design modifications to accommodate an axial air flow through the tight space within a SCDMDS without adding any external components. Such flow can lead to significant heat dissipation capability.
2. Consider large SCDMDS which have more than one motor inside the rotating drum.
3. Explore the ability to increase traction between the drive drum and the belt without adding lagging material possibly by some surface modifications in order to avoid the deterioration of the thermal performance associated with the use of the lagging.
4. Extend the current study to cover different drum profiles and more belt types.
5. Extend the current two-dimensional numerical work to three-dimensional which would allow investigating the effect of oil distribution of the temperature distribution in the axial direction.
6. Consider oil thermal conductivity change with temperature in all numerical simulations.